G.N. BULANIK DURMUŞ

DEVELOPMENT OF A HIGH-PERFORMANCE ELECTROCHEMICAL HYDROGEN COMPRESSOR THROUGH EXPERIMENTAL STUDIES

THE GRADUATE SCHOOL OF NATURAL AND APPLIED SCIENCES
OF
ATILIM UNIVERSITY

GİZEM NUR BULANIK DURMUŞ

DOCTOR OF PHILOSOPHY THESIS
IN
THE DEPARTMENT OF MECHANICAL ENGINEERING

JUNE 2023

ATILIM UNIVERSITY 2023

DEVELOPMENT OF A HIGH-PERFORMANCE ELECTROCHEMICAL HYDROGEN COMPRESSOR THROUGH EXPERIMENTAL STUDIES

A THESIS SUBMITTED TO
THE GRADUATE SCHOOL OF NATURAL AND APPLIED SCIENCES
OF
ATILIM UNIVERSITY

BY

GİZEM NUR BULANIK DURMUŞ

IN PARTIAL FULFILLMENT OF THE REQUIREMENTS
FOR
THE DEGREE OF DOCTOR OF PHILOSOPHY
IN
THE DEPARTMENT OF MECHANICAL ENGINEERING

JUNE 2023

Approval of the Graduate School of Natural and Applied Sciences, Atilim University.

_____

Prof. Dr. Ender Keskinkılıç
Director

I certify that this thesis satisfies all the requirements as a thesis for the degree of **Doctor of Philosophy in Mechanical Engineering, Atilim University**.

_____

Prof. Dr. Sadık Engin Kılıç
Head of Department

This is to certify that we have read the thesis **DEVELOPMENT OF A HIGH-PERFORMANCE ELECTROCHEMICAL HYDROGEN COMPRESSOR THROUGH EXPERIMENTAL STUDIES** submitted by GİZEM NUR BULANIK DURMUŞ and that in our opinion it is fully adequate, in scope and quality, as a thesis for the degree of Doctor of Philosophy.

_____	_____
Prof. Dr. Can Özgür Çolpan Co-Supervisor	Prof. Dr. Yılser Devrim Supervisor

Examining Committee Members:

Prof. Dr. A. Necati Özkan
Polymer Science and Technology, METU _____

Prof. Dr. Yılser Devrim
Energy Systems Engineering, Atilim University _____

Prof. Dr. Ayhan Albostan
Energy Systems Engineering, Atilim University _____

Prof. Dr. A. Hakan Argeşo
Aerospace Engineering, Atilim University _____

Doç Dr. Hadi Genceli,
Mechanical Engineering, Yıldız Technical University _____

Date: *16.06.2023*

I hereby declare that all information in this document has been obtained and presented in accordance with academic rules and ethical conduct. I also declare that, as required by these rules and conduct, I have fully cited and referenced all material and results that are not original to this work.

Name, Last Name : Gizem Nur BULANIK DURMUŞ

Signature :

ABSTRACT

DEVELOPMENT OF A HIGH-PERFORMANCE ELECTROCHEMICAL HYDROGEN COMPRESSOR THROUGH EXPERIMENTAL STUDIES

Bulanık Durmuş, Gizem Nur
PhD., Department of Mechanical Engineering
Supervisor: Prof. Dr. Yılser DEVRİM
Co-Supervisor: Prof. Dr. Can Özgür ÇOLPAN

June 2023, 114 pages

Energy in the world goes beyond fossil fuels and moves towards green solutions and clean energy is of great importance for a sustainable future. Hydrogen, which is an important clean energy alternative, needs to be purified and compressed effectively in order to become a common energy carrier. Hydrogen compressors, which are widely used industrially today, are mechanical, pneumatic and electrically operated compressors, and their most important disadvantages are vibration and noise caused by their moving parts. However, electrochemical hydrogen compressors allow both electrochemical hydrogen purification from various gas mixtures and compression in a single step with high energy efficiency. In addition, they are quiet as they contain no moving parts. Because of these advantages, they have lower capital costs, longer service life and less maintenance.

Electrochemical hydrogen (H_2) compression (ECHC) technology has recently attracted attention because it is promising for H_2 compression and purification in a single step. Currently, the most common and cheapest method for producing H_2 is steam reforming of hydrocarbons. In other words, natural gas and coal are the most

affordable sources of H_2. However, this method has the drawback of emitting some impurities like carbon monoxide (CO) and carbon dioxide (CO_2).

Within the scope of this thesis, a high-temperature electrochemical H_2 compressor (HT-ECHC) has been developed. An experimental method has been used for studies on the purification and compression of H_2. One of the biggest problems encountered in ECHC systems is the poisoning of the catalyst due to CO. This makes the catalyst unusable, and catalyst costs arise. Therefore, this study aimed to develop an HT-ECHC with a high CO tolerance, operating between 140-180 °C, and consuming low power. In this study, the H_2 purification and compression performance of a Poly [2,2'-(m-phenylene)-5,5'-bibenzimidazole] (PBI) membrane-based HT-ECHC was investigated using reformed gases containing different molar ratios of H_2, CO_2 and CO. In the performance tests, it was emphasized that the effect of temperature on HT-ECHC performance was one of the most critical factors. It was observed that the performance of the HT-ECHC decreased with the increase in the molar ratio of CO. The results of the gas chromatography (GC) analysis indicate that >99.99% H_2 purity was achieved at 160 °C. According to the results, H_2 was successfully compressed from atmospheric pressure to 60 bar with a 1.5V constant voltage.

Keywords: Electrochemical Hydrogen Compression, Electrochemical Hydrogen Purification, PBI Membrane

ÖZ

YÜKSEK PERFORMANSLI ELEKTROKİMYASAL HİDROJEN KOMPRESÖRÜN DENEYSEL ÇALIŞMALAR İLE GELİŞTİRİLMESİ

Bulanık Durmuş, Gizem Nur
Doktora, Makine Mühendisliği Bölümü
Tez Yöneticisi : Prof. Dr. Yılser DEVRİM
Ortak Tez Yöneticisi : Prof. Dr. Can Özgür ÇOLPAN

Haziran 2023, 114 sayfa

Elektrokimyasal hidrojen (H_2) sıkıştırma (ECHC) teknolojisi, H_2'nin tek bir adımda sıkıştırılması ve saflaştırılması için umut vaat etmesi nedeniyle son zamanlarda dikkatleri üzerine çekmiştir. Şu anda, H_2 üretmenin en yaygın ve en ucuz yöntemi, hidrokarbonların buharla reformasyonudur. Diğer bir deyişle, doğal gaz ve kömür H_2'nin en uygun kaynaklarıdır. Bununla birlikte, bu yöntemin dezavantajı, karbon monoksit (CO) ve karbon dioksit (CO_2) gibi bazı safsızlıklar yaymasıdır.

Bu tez kapsamında yüksek sıcaklık elektrokimyasal H_2 kompresörü (HT-ECHC) geliştirilmiştir. H_2'nin saflaştırılması ve sıkıştırılması ile ilgili çalışmalarda deneysel bir yöntem kullanılmıştır. ECHC sistemlerinde karşılaşılan en büyük sorunlardan biri katalizörün CO nedeniyle zehirlenmesidir. Bu durum katalizörü kullanılamaz hale getirmekte ve katalizör maliyetleri ortaya çıkmaktadır. Bu nedenle bu çalışma, CO toleransı yüksek, 140-180 °C arasında çalışan ve düşük güç tüketen bir HT-ECHC geliştirmeyi amaçlamıştır. Bu çalışmada, farklı molar oranlarda H_2, CO_2 ve CO içeren reformat gazlar kullanılarak PBI membran bazlı HT-ECHC'nin H_2 saflaştırma ve sıkıştırma performansı incelenmiştir. Performans testlerinde sıcaklığın HT-ECHC performansı üzerindeki etkisinin en kritik faktörlerden biri olduğu vurgulanmıştır. HT-ECHC'nin performansının CO'nun molar oranının artmasıyla düştüğü gözlenmiştir. Gaz kromatografisi (GC) sonuçları, 160 °C'de >%99,99 H_2 saflığının elde edildiğini

göstermiştir. Sonuçlara göre H_2, 1.5V sabit voltaj ile atmosferik basınçtan 60 bara başarıyla sıkıştırılmıştır.

Anahtar Kelimeler: Elektrokimyasal Hidrojen Sıkıştırma, Elektrokimyasal Hidrojen Saflaştırma, PBI Membranı

To my family

ACKNOWLEDGMENTS

Many people gave me support, inspiration, and encouragement during my Ph.D. studies, which I proudly left behind, and I would like to express my gratitude to each one of them for being with me during this challenging process.

First, I would like to acknowledge my mentor, guide, and supervisor Prof. Dr. Yılser Devrim who made this work possible. Her guidance and advice enlightened me through all phases of this thesis. She supported me during this unique Ph.D. process with her endless energy and inexhaustible determination. She included me in a very valuable project and helped me meet Hydrogen. I am grateful for all the laboratory facilities she has provided me. The values she taught and added to me by dedicating her precious time to all my academic studies and organizing meticulously are invaluable. I would also like to thank her for making all the negativities easier for me and enabling me to go through the most productive doctorate period possible, even if it coincides with the pandemic process. The completion of this study could not have been possible without her expertise, support, and motivation.

I also would like to present my gratitude to my co-supervisor Prof. Dr. Can Özgür Çolpan for his guidance and support. His knowledge and experience are very valuable. His advice, continuous support, and patience carried me through all the stages.

I would like to give my special thanks to Hüseyin Devrim and Teksis Company. I feel very lucky that he shared his time, valuable knowledge and all the possibilities of his company with me. Without the opportunities he offered me, a part of my doctoral studies would be incomplete.

I would like to express my sincere gratitude to Deniz Durdağ and Evren Tuncer who have all the skills and abilities of a good engineer and do not hesitate to share them with me, for sparing their valuable time. I learned a lot from them, and I feel very lucky to know them.

I would like to thank the Gamze Çakır Kabakcı and Barkın Şenel, for every minute they spared me and for all the good times we had.

Words are not enough for the existence of İrem Bulanık Özdemir, my dear sister, mentor, friend, and one of my biggest supporters, who has never left me alone in this period as well as throughout my life. We spent our undergraduate, graduate and Ph.D. education periods together, as we did our whole lives, and I am very happy to have such a natural companion. The existence of someone like her in my life is priceless.

The biggest and endless thanks go to my parents Firuzan Bulanık and Erol Bulanık for their unconditional love and support. They have been my biggest supporters throughout my life, giving me the love, courage, and support I needed. I would not have made it this far without them. I would like to thank my second mother and father, Kamuran Durmuş and Cemal Durmuş, who supported me in the warmest and most sincere way, believed in me, and made me feel very lucky.

Finally, I would like to thank my dearest husband, Caner Durmuş, with all my heart and sincerest feelings. He stood by me with his perfect heart in all circumstances. I would like to express my gratitude to him for sharing all his inspiration, energy, possibilities, and endless love with me without a second thought. Without his patience, wisdom, and support, I wouldn't have been able to achieve this process. He will always be in my heart and mind.

This study was supported by The Scientific and Technological Research Council of Turkey (TUBITAK) 1001 (Grant number: 219M333) Project.

TABLE OF CONTENTS

ABSTRACT iii
ÖZ v
ACKNOWLEDGMENTS viii
TABLE OF CONTENTS x
LIST OF TABLES xiii
LIST OF FIGURES xiv
LIST OF SYMBOLS/ABBREVIATIONS xvi
CHAPTER 1 1
INTRODUCTION 1
1.1. Motivation of the Thesis 1
1.2. Aim of the Thesis 2
1.3. Thesis Outline 3
CHAPTER 2 4
HYDROGEN ENERGY 4
2.1. Properties of H_2 4
2.2. H_2 Production 5
2.3. H_2 Purification, Compression and Storage Methods 8
2.3.1. H_2 Purification Methods 9
2.3.1.1. Pressure Swing Adsorption (PSA) 10
2.3.1.2. Membrane Based Purification 11
2.3.1.3. Cryogenic 11
2.3.1.4. Metal Hydrides 12
2.3.2. H_2 Compression Methods 12
2.3.2.1. Mechanical Compressors 13
2.3.2.1.1. Reciprocating Compressor 14
2.3.2.1.2. Diaphragm Compressors 15
2.3.2.1.3. Ionic Liquid Compressors 16
2.3.2.1.4. Linear Compressors 16
2.3.2.2. Non-mechanical Compressors 17
2.3.2.2.1 Cryogenic Compressors 17

2.3.2.2.2 Metal Hydride Compressors 18
2.3.2.2.3 Adsorption Compressors 19
2.3.3. H_2 Storage Methods 20
CHAPTER 3 22
ELECTROCHEMICAL HYDROGEN COMPRESSORS 22
3.1. Reaction Mechanism and Overpotentials in ECHC 23
3.2. Literature Survey on ECHC 27
3.3. Components of ECHC 31
3.3.1 Membrane Electrode Assembly 32
3.3.1.1. ECHC Membranes 33
3.3.1.1.1. Low-Temperature ECHC Membranes 33
3.3.1.1.2. High-Temperature ECHC Membranes 34
3.3.1.2. Catalyst Layer 37
3.3.2 Gas Diffusion Layer 38
3.3.3 Bipolar Plates 39
3.3.4 Sealing and O-rings 41
3.3.5 End Plates 42
3.4. Effects of Operating Parameters on ECHC Performance 44
3.5. Importance of High-Temperature ECHC 46
CHAPTER 4 48
EXPERIMENTAL STUDIES 48
4.1. Materials 48
4.2. MEA Preparation 48
4.1.1. Membrane Preparation 48
4.1.2. Gas Diffusion Electrode Preparation 50
4.3. HT-ECHC Single Cell and Stack 51
4.4. HT-ECHC Test System 57
CHAPTER 5 62
RESULTS AND DISCUSSION 62
5.1. Bipolar Plate Design and Flow Analysis Results 62
5.2. HT-ECHC Purification Test Results 68
5.2.1. Pure H_2 Experiments 68

5.2.2. H_2 Separation from Reformate Gas Mixture 70
5.3. Compression Results 80
CHAPTER 6 84
CONCLUSIONS 84
REFERENCES 86
APPENDICES 106
A. TYPICAL GC CHROMATOGRAM FOR PURE H_2 106
B. TYPICAL GC CHROMATOGRAM FOR CO_2 107
C. TYPICAL GC CHROMATOGRAM FOR CO 108
D. TYPICAL GC CHROMATOGRAM FOR RG-1 109
E. TYPICAL GC CHROMATOGRAM FOR RG-2 110
F. TYPICAL GC CHROMATOGRAM FOR RG-3 111
G. TYPICAL GC CHROMATOGRAM FOR RG-4 112
H. TYPICAL GC CHROMATOGRAM FOR RG-5 113
I. TYPICAL GC CHROMATOGRAM FOR RG-6 114

LIST OF TABLES

Table 2.1 H_2 properties at room temperature and atmospheric pressure [15] 5
Table 2.2 Comparison of some studies on different H_2 purification methods [48].... 10
Table 2.3 Some studies on H_2 compression methods [48] 13
Table 3.1 The patents for ECHC technology [48] 30
Table 3.2 Literature studies for ECHC studies 31
Table 3.3 Literature survey on ECHC components 43
Table 4.1 Properties of the undoped and PA-doped PBI (Modified from Ref. [215])..49
Table 4.2 Gas compositions for HT-ECHC purification experiments..... 60
Table 5.1 Purification grades of H_2 purified from reformate gas mixture 76

LIST OF FIGURES

Figure 2.1 The H_2 production methods 6
Figure 2.2 H_2 production, purification, and compression methods 9
Figure 2.3 Reciprocating piston compressor 15
Figure 2.4 Diaphragm compressor 15
Figure 2.5 Ionic liquid compressor 16
Figure 2.6 Linear compressor 17
Figure 2.7 Cryogenic compressor 18
Figure 2.8 Metal hydride compressor 19
Figure 2.9 Adsorption compressor 20
Figure 3.1 Components of the ECHC 24
Figure 3.2 The working principle of the ECHC 25
Figure 3.3 Components of 3-layer, 5-layer and 7-layer MEAs 32
Figure 3.4 Chemical structure of PBI 35
Figure 3.5 Proton conductivity mechanism of PA-doped PBI membrane 35
Figure 3.6 Bipolar plate materials (based on Ref. [202]) 40
Figure 3.7 Bipolar plate flow geometries with inlet (green) and exit (red) directions of the reactant 41
Figure 3.8 a) Kapton seal and b) Viton o-rings 42
Figure 3.9 CO poisoning of the bare Pt surface a) terminal site, b) bridging site, c) three-fold hollow site (modified from Ref. [214]) 47
Figure 4.1 PBI membrane preparation steps 49
Figure 4.2 GDE preparation steps 51
Figure 4.3 MEA preparation steps 51
Figure 4.4 a) Anode end plate, b) cathode end plate 53
Figure 4.5 Single-cell HT-ECHC 54
Figure 4.6 HT-ECHC stack with 5 cells 54
Figure 4.7 Assembled render view for (a) single cell and (b) stack 55
Figure 4.8 HT-ECHC cell preparation 56
Figure 4.9 Assembled HT-ECHC single cell and stack 57
Figure 4.10 Diagram of HT-ECHC test station 58

Figure 4.11 HT-ECHC test station 59
Figure 4.12 Typical GC chromatogram for RG-3……...61
Figure 5.1 Bipolar plates of square flow geometries 63
Figure 5.2 Bipolar plates of circular flow geometries..... 64
Figure 5.3 Pressure analysis of the bipolar plates 65
Figure 5.4 a) Flow plate of HT-ECHC cell, b) pressure analysis of flow plate..... 67
Figure 5.5 Polarization curves for pure H_2 at 160 °C with different H_2 inlet flow rates 68
Figure 5.6 Polarization curves of HT-ECHC with pure H_2 at different operating temperatures 69
Figure 5.7 Polarization curves of HT-ECHC with RG-1 at different temperatures... 71
Figure 5.8 Polarization curves of HT-ECHC with RG-2 at different temperatures... 73
Figure 5.9 Polarization curves of HT-ECHC with RG-3 at different temperatures... 73
Figure 5.10 Polarization curves of HT-ECHC with RG-4 at different temperatures. 74
Figure 5.11 Polarization curves of HT-ECHC with RG-5 at different temperatures. 74
Figure 5.12 Polarization curves of HT-ECHC with RG-6 at different temperatures. 75
Figure 5.13 Separation efficiencies of HT-ECHC with RG-1 at different operating temperatures 77
Figure 5.14 Separation efficiencies of HT-ECHC with RG-2 at different operating temperatures 78
Figure 5.15 Separation efficiencies of HT-ECHC with RG-3 at different operating temperatures 78
Figure 5.16 Separation efficiencies of HT-ECHC with RG-4 at different operating temperatures 79
Figure 5.17 Separation efficiencies of HT-ECHC with RG-5 at different operating temperatures 79
Figure 5.18 Separation efficiencies of HT-ECHC with RG-6 at different operating temperatures 80
Figure 5.19 HT-ECHC polarization curves at 160 °C for open cathode 82
Figure 5.20 The change of cathode pressure of HT-ECHC at 160°C 83

LIST OF SYMBOLS/ABBREVIATIONS

ECHC	Electrochemical hydrogen compressor
PEMFC	Proton exchange membrane fuel cell
MEA	Membrane electrode assembly
GDL	Gas diffusion layer
CCM	Catalyst coated membrane
PSA	Pressure swing adsorption
SMR	Steam methane reforming
CCS	Carbon capture and storage
HTS	High-temperature shift
LTS	Low-temperature shift
RWGS	Reverse water gas shift reaction
LP	Low pressure
HP	High pressure
PFSA	Perfluorosulfonic acid
SPEEK	Sulphonated poly ether-ether ketone
CrPSSA	Cross-linked poly styrene sulfonic acid
O-CNT	Oxidized carbon nanotubes
PBI	Poly [2,2'-(m-phenylene)-5,5'-bibenzimidazole]
H_2SO_4	Sulfuric acid
H_3PO_4	Phosphoric acid
HNO_3	Nitric acid
HCl	Hydrochloric acid
SiO_2	Silicon dioxide
N_2	Dinitrogen
CO	Carbon monoxide
CO_2	Carbon dioxide
Pt	Platinum
Pd	Palladium
Ru	Ruthenium
Ti	Titanium

Al	Aluminum
Mg	Magnesium
Si	Silicon
MOF	Metal-organic framework
E°	Standard potential of a hydrogen reaction
R	Universal gas constant (8.314 J/mol·K)
T	Temperature (K)
j	Current density (A/cm^2)
A	Area (cm^2)
I	Current (A)
F	Faraday's constant (96,485 C/mol)
MW	Molecular weight (g/mol)
$P_{cathode}$	Cathode pressure (bar)
P_{anode}	Anode pressure (bar)
E_{cell}	Cell voltage (V)
E_{Nernst}	Nernst voltage (V)
$\eta_{voltage}$	Voltage efficiency
$\eta_{current}$	Current efficiency
η_{total}	Overall efficiency
σ_{UT}	Ultimate strength (MPa)
E	The Young's modulus (GPa)

CHAPTER 1

INTRODUCTION

One of the most critical issues that scientists are currently focusing on is the energy problem and global warming. This issue has forced governments and other organizations to consider reducing negative environmental impacts and fuel costs. Today, many innovative and attractive technologies are being researched to solve the energy problem. Among these technologies, H_2 is predicted to become a more critical component in meeting the world's energy needs, as it has the potential to decarbonize the transportation and stationary energy industries. Effective H_2 storage and H_2 production technologies are very important for the widespread use of H_2 in daily life and the development of the H_2 economy. ECHC systems are particularly promising systems for H_2 purification, storage and transmission. ECHCs are single-stage, highly efficient, low-maintenance and quiet systems that purify high-pressure H_2 isothermally without moving components or mechanical losses. Therefore, this innovative technology can be used in critical applications such as stationary, residential, military and aerospace due to its mobility, scalability, quiet and vibration-free operation.

1.1. Motivation of the Thesis

Most of the world's energy needs are met by fossil fuels. However, alternative energy sources are increasingly important, especially considering climate change and the depletion of fossil fuel resources. H_2, which has a high energy density among alternative energy resources, is gaining more importance day by day. Today, the use of H_2 has become widespread, but some non-technical factors such as economic and logistics prevent further use of H_2 systems in daily life. In addition, difficulties with H_2 compression, purification, storage and transportation cause the cost of H_2 supply to increase significantly. For this reason, supporting R&D and infrastructure studies

related to H_2 energy, which is accepted as the energy of the future, seems to be a necessity for all countries of the world.

In order for the H_2 economy to become widespread, high-purity H_2 must be produced and stored in low volumes. The need for H_2 purification and pressurization technologies has led to a greater focus on technologies that can obtain compressed and high-purity H_2, such as ECHCs. One of the most important difficulties encountered in ECHC systems is the poisoning of the catalyst used in the system and the cost of the catalyst. In low temperature (60-80 ^oC) ECHC applications (LT-ECHC), the use of different gas mixtures obtained from alternative fuels, especially in mixtures containing CO and CO_2, is not efficient because catalyst poisoning is encountered. In these systems, impurities are adsorbed on the catalyst surface and reduce the electrochemical activity of the catalyst. Despite the disadvantages of LT-ECHC systems, HT-ECHC systems are particularly promising for contaminant tolerance. However, there are not many studies in the literature on HT-ECHC systems. Therefore, it is important to develop promising HT-ECHC systems.

1.2. Aim of the Thesis

The significance of HT-ECHC is emphasized in this study because the current methods utilize separate units to purify and compress H_2. This work offers the HT-ECHC's operation with unique components, performance and an overview of research on HT-ECHC technology. The aims of the thesis are as follows:

- To separare H_2 from gas mixtures at different temperatures: The best method to increase impurity tolerance in ECHC systems is to use high operating temperatures (140-200 ^oC). In contrast to the low CO tolerance of LT-ECHCs, operating in the 140-200 ^oC range will increase the impurity tolerance. While the tolerance for CO is <100 ppm at 80 ^oC, this value rises to 3% (30000 ppm) in the 160-200 ^oC temperature range. It is aimed to develop HT-ECHC prepared with unique components that can separate H_2 from gas mixtures with different molar ratios of H_2:CO_2:CO, H_2:CO_2, and H_2:CO through commercial PBI membrane in a temperature range of 140-180 °C.

- To investigate the effect of temperature and HT-ECHC performance using voltage-current characteristics is aimed.

- To compress H_2 as well as H_2 purification with HT-PEMFC. Although H_2 pressurization technologies appear to be mature and meet the requirements, there is still a search for critical applications such as military, aerospace, stationary and residential applications. HT-ECHC is a quiet, vibration-free and efficient compression technology that can meet the requirement compared to conventional technologies.

1.3. Thesis Outline

The second chapter consists of information that covers the properties of H_2, its production, purification, compression, and storage methods. A comprehensive literature review on H_2, including recent studies, is also given in this section.

The third chapter is devoted to ECHC technology. Reaction mechanism and overpotentials in ECHC, a literature survey, its components and properties, the influence of operating parameters on ECHC performance and finally the importance of high-temperature applications are emphasized based on the studies done so far.

The fourth chapter is about the preparation process for the experiment. In this section, the materials used in the experiments, the components prepared using these materials, all the elements in the test station, the properties of single and stack cells and the procedure followed in the performance tests are explained in detail.

In the fifth chapter, the properties of the geometry with the new flow channel, the results of the purification tests and the compression tests are discussed and interpreted.

In the sixth section, a comprehensive summary of all the results is given. Suggestions for new studies are also included in this section.

CHAPTER 2

HYDROGEN ENERGY

Due to growing populations and technological advancements, the demand for primary energy has been increasing globally, and it is predicted that this need will rise sharply in the coming decades [1], [2]. H_2 is an exciting energy option that could help with the world's energy and environmental concerns. Among all available fuels, H_2 has the most considerable calorific content [3] and is considered an alternative to carbon-based fuels. The systems in which H_2 is used are fuel cell-based applications like automobiles, stationary and military, and other industrial areas like chemistry, glass, and electronics [4]. Over the next five years, it is anticipated that the demand for H_2 will rise 4-5% yearly [5].

The concept of using H_2 as a form of energy is not new. In the 1960s, H_2 was used as a component of a mixture of gases for streetlamps and heating [6]. After the 1970s oil crises, an H_2-based energy system was first proposed. A renewed interest in H_2, particularly regarding the transportation sector, was spurred by advances in fuel cell technology in the late 1990s [7]. Today, H_2-based systems are technologies that have been studied commonly and commercialized in many applications. However, some non-technical factors, such as economics and logistics, prevent these systems from becoming more widespread. Difficulties with H_2 pressurization, storage, and shipping cause the cost of H_2 supply to rise considerably. For the H_2 economy to become widespread, H_2 must be produced, purified, and stored in low volumes since H_2 is the lightest gas and is challenging to store as a gas.

2.1. Properties of H_2

H_2 is present in the universe in the greatest amount, which is a colorless, odorless, combustible gas that is primarily found in water and organic materials [8], [9]. H_2 has an atomic weight of 1.00794 atomic mass units [10]. The energy content of H_2 is 141.8 MJ/kg at 25 °C for its higher heating value, and 120 MJ/kg at 25 °C for its lower

heating value [10]. These values are considerably higher than the commonly used fuel gasoline which has a heating value of 44 MJ/kg at 25 °C [11]. In contrast, the density of liquid H_2 is only 8 MJ/L, while that of gasoline is 32 MJ/L [12]. This implies that significantly less energy can be stored in each volume of liquid H_2. H_2 must be stored in a tank because it has a lower energy density when measured in terms of volume compared to hydrocarbons but a higher energy density when measured in terms of weight [13], [14]. H_2 properties at room temperature and atmospheric pressure are given in Table 2.1.

Table 2.1 H_2 properties at room temperature and atmospheric pressure [15]

Properties	**Value**
Atomic number	1
Atomic weight	1.008
Molar weight (MW)	2.016 kg/kmol
Specific gravity (air = 1)	0.0696
Density	0.08375 kg/m^3
Gas constant	4.124 $kJ\ kg^{-1}\ K^{-1}$
Specific Heat at Constant Pressure	14.307 $_{@300\ K}$ $kJ\ kg^{-1}\ K^{-1}$
Specific Heat at Constant Volume	10.183 $_{@300\ K}$ $kJ\ kg^{-1}\ K^{-1}$
Specific Heat Ratio, k = Cp/Cv	1.405 $_{@300\ K}$
Boiling point	−253 °C
Melting point	−259 °C

2.2. H_2 Production

There are numerous ways to produce H_2, but H_2 is mostly produced from steam reforming of natural gas [16], [17]. According to the International Energy Agency, Global Hydrogen Review 2022 report, 62% of the total 94 million tons of H_2 produced in 2021 was produced from natural gas[18]. Other environmentally friendly and sustainable ways to produce H_2 are thermochemical (such as coal gasification),

biological (such as bio photolysis), and electrochemical (such as water electrolysis) processes [19]. While there are numerous techniques to produce H_2, the gas still has some pollutants and needs to be purified before it can be used in storage or other devices like cars or fuel cells.

According to the new perspective on the literature, H_2 production is symbolized by colors according to the primary source and the progress used. This new trend has very different color coding, however, grey, brown/black, blue, and green H_2 seem more pioneer. Figure 2.1 shows the classification of H_2 methods according to the colors.

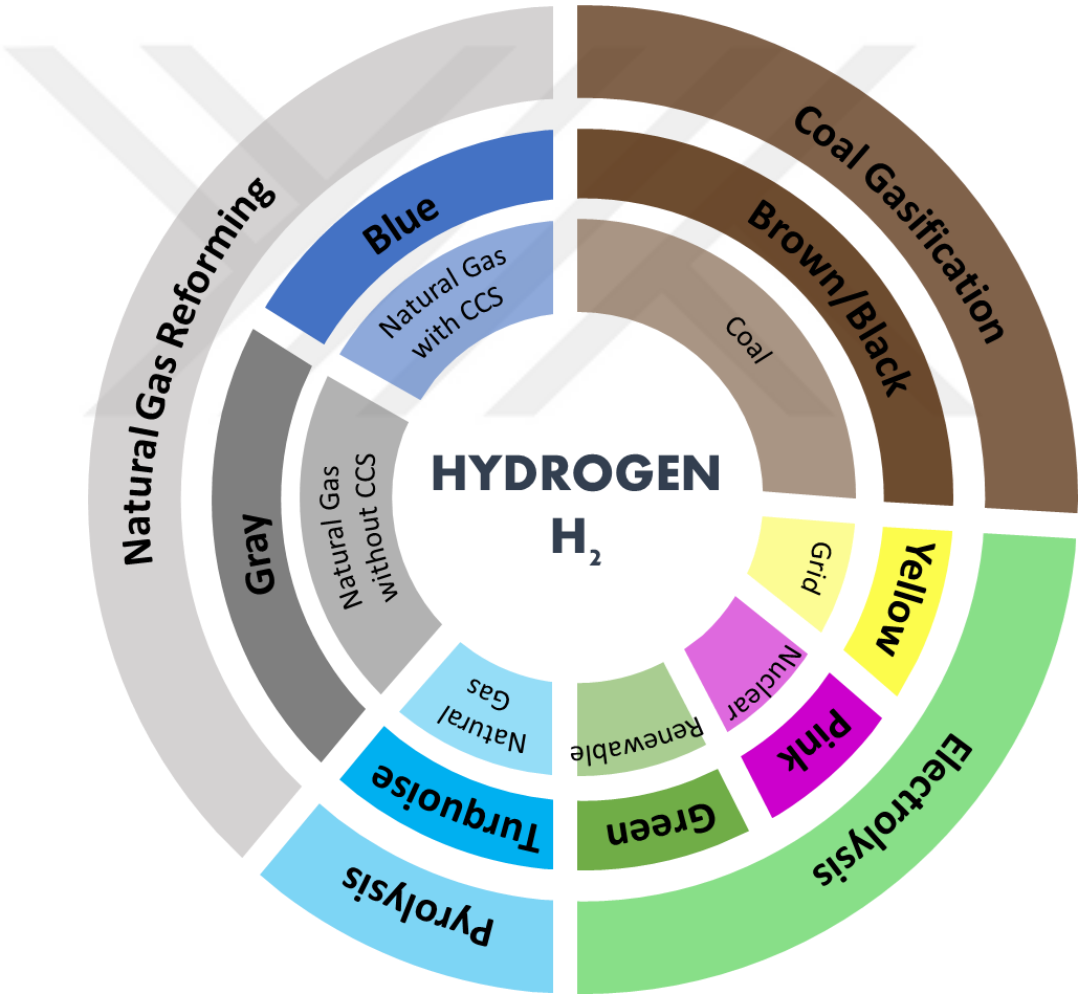

Figure 2.1 The H_2 production methods

Grey H_2 currently forms most of the H_2 [20] through the SMR. In this process, H_2 is produced from natural gas, which is an easily accessible and inexpensive resource. The

75-99% molar fraction of natural gas consists of methane (CH_4) [21]. This hydrocarbon decomposes to CO and H_2 in the presence of steam (H_2O) [22]. For this reason, this process is called "SMR" [23]. SMR is frequently used with a Water Gas Shift (WGS) reaction to oxidize CO to CO_2 and produce more H_2. SMR involves the following sets of reactions [24] :

$$CH_4 + H_2O \rightarrow CO + 3H_2 \qquad \Delta H = \frac{206\ kJ}{mol} \tag{1}$$

$$CH_4 + 2H_2O \rightarrow CO_2 + 4H_2 \qquad \Delta H = \frac{164.9\ kJ}{mol} \tag{2}$$

$$CO + H_2O \rightarrow CO_2 + H_2 \qquad \Delta H = \frac{-41\ kJ}{mol} \tag{3}$$

Equations (1) and (2) are endothermic reactions. Two steps are required to complete these reactions: The first step is reforming (Equation (1) and (2)) to produce synthesis gases at 750–800°C. WGS is considered the second step (Equation (3)) and is an exothermic reaction. WGS involves high-temperature shift (HTS) at 350 °C and low-temperature shift (LTS) at 190-210 °C [25]. Precious metals such as nickel (Ni), and ruthenium (Ru) are used as the catalysts in SMR process [26]. However, in the grey H_2 process, carbon capture and storage (CCS) is not done. Therefore, the main drawback of grey H_2 is the significant CO_2 emission [27]. The production of ammonia and the petrochemical industry are the two main uses of grey H_2 [28].

Gasification-extracted brown or black H_2 from coal is also a widely used production technique since the planet has huge coal reserves [29]. Coal gasification is a fully developed technology with a 74-85 % process efficiency [10]. It appears to be an important process to produce more cost-effective energy and other chemical products [30]. In addition to H_2, some other impurities like CO, CH_4, ash, H_2S, NH_3, HCl and HCN are released in the coal gasification process [31]. However, carbon capture is the main problem like the grey H_2.

Green H_2 is a promising solution to a decarbonized energy system [32]. Green H_2 is generated from water electrolysis using electricity generated from renewable sources like wind or solar, with no carbon emissions [33]. There are currently three main

electrolysis technologies: solid oxide electrolyzer cell, polymer electrolyte membrane, and alkaline water electrolysis [34].

Yellow H_2 is a result of electrolysis with electricity inputs from the grid [35] and is strongly correlated with natural gas prices as grid electricity depends on natural gas in many areas.

Turquoise H_2 is obtained from the high-temperature pyrolysis of methane [36]. The main advantage of turquoise H_2 is that it is thermodynamically significantly less energy-intensive compared to water electrolysis [37] and SMR and takes advantage of existing natural gas infrastructure [38]. While the production of purple/pink H_2 from nuclear energy-based electricity is not heavily emphasized in European H_2 strategies, it may become a workable substitute in other parts of the world, such as China and Russia [39], [40].

Aqua and white H_2 are two brand-new tones mentioned in the literature. Aqua H_2 is a production method that comes from oil fields with no carbon emissions [41]. The color is chosen because it is between blue and green, is created using fossil fuels (blue), but does not emit carbon (green). The direct splitting of water molecules using concentrated solar energy is considered white H_2 [42]. However, both suggested colors are still in the early stages of research [43].

2.3. H_2 Purification, Compression and Storage Methods

Current H_2 compression and purification techniques are briefly discussed in this work, along with their benefits and drawbacks. Figure 2.2 shows the H_2 production, purification, and compression methods.

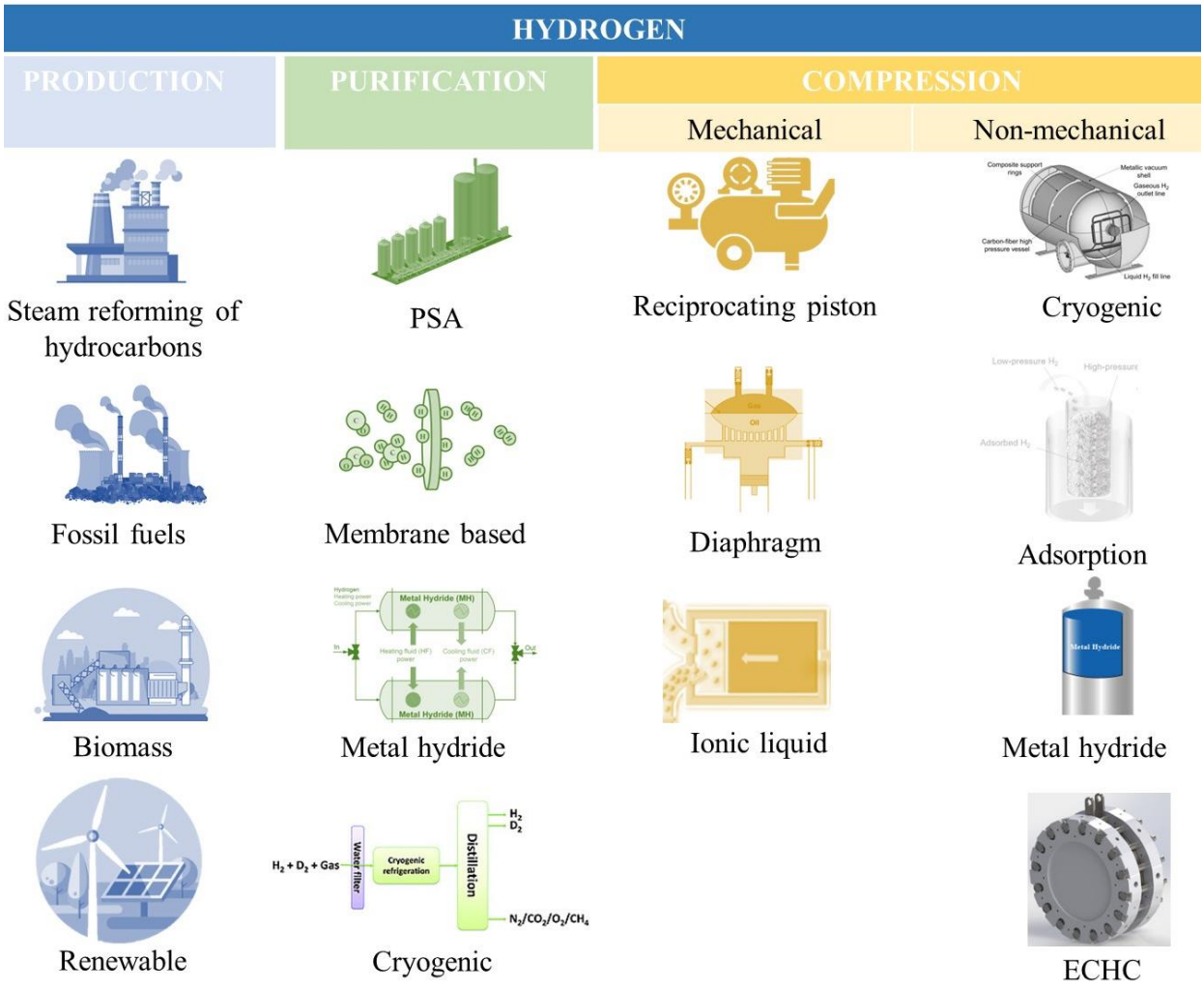

Figure 2.2 H_2 production, purification, and compression methods

2.3.1. H_2 Purification Methods

Since H_2 production is mainly obtained by SMR through fossil resources [44], [45] and H_2 is usually produced with other gases such as CO, and CO_2. Therefore, H_2 needs to be separated, purified, and stored safely to be used efficiently. Researchers have spent many years on H_2 separation and purification methods [46], [47]. Different H_2 purification methods are shown in Table 2.2, with the purification level at operating temperature and pressure.

Table 2.2 Comparison of some studies on different H_2 purification methods [48]

Purification Method	**Purification (%)**	**Temperature (°C)**	**Pressure (bar)**	**Ref.**
Pressure Swing Adsorption	99.95	N/A	25–60	[49]
Pressure Swing Adsorption	99.999	N/A	N/A	[50]
Pressure Swing Adsorption	99.97	20	9	[51]
Pressure Swing Adsorption	99.9296	30	7	[52]
Pressure Swing Adsorption	99.990	30	3.5	[53]
Vacuum Pressure Swing Adsorption	99.170	30	5	[54]
Cryogenic Adsorption	>99	-213.15	20.6-206.8	[55]
Cryogenic Adsorption	90-98	-213.15	N/A	[56]
Pd based membranes	>99.999	400	N/A	[57]
Carbon molecular sieve membrane	N/A	30-50	0.1	[45]
Carbon membrane	>95	1^{st} stage – 120 2^{nd} stage – 20	20	[58]
PdCu alloy membrane	N/A	30	N/A	[59]
Pd/NaY/PSS membrane	N/A	450	N/A	[60]
$Pd/Nb_{40}Ti_{30}Ni_{30}$/Pd/porous nickel support membrane	N/A	300 to 400	1.5 to 2	[61]
Pd/bcc membrane	N/A	500	0.5	[62]
Graphenylene–1 membrane	N/A	27	N/A	[63]

2.3.1.1. Pressure Swing Adsorption (PSA)

The most common method used to separate H_2 from other impurities is the pressure swing adsorption (PSA) method [64]. In the PSA process, an air/ozone mixture is first produced from the air. The preheated methane/air mixture combines with the air/ozone mixture and is sucked into the engine. The engine produces syngas containing heating water and product gas. The WGS is utilized to increase the mole fraction of H_2. As the gradually cooled product gas is exhausted, the purified H_2 is compressed and finally

cooled [65]. This method usually uses zeolite material because it offers a large surface area. In addition, PSA provides up to 99.999% H_2 purification [50], [66]. Using PSA, Tao et al. [54] separated 99.17% pure H_2 from a mixture of N_2, CO, CO_2, CH_4, and H_2. Yánez et al. [51] used a PSA process with various design parameters (e.g., purge-to-feed ratio and cycle duration) to produce H_2 stream with purities of 99.25% and 99.97% at 9 bar. Xiao et al.'s [52] study found a 99.9296% H_2 purity level at 7 bar adsorption pressure. Ye et al. [53] reached 99.99% purity on the Cu-BTC bed with 3.5 bar pressure.

2.3.1.2. Membrane Based Purification

Although the PSA method is widely used, the membrane-based can also be used for H_2 purification. Depending on the gas mixture's variety and proportion of gases, the membrane-based separation method may be more efficient than the PSA method in some cases [67]. Polymeric membranes, porous membranes such as ceramic, carbon, dense metal membranes and ion conductive membranes are commonly used for membrane based H_2 purification methods [68]. Among these methods, the most advanced ones are polymeric membranes and dense metal membranes [69]. H_2 separation with the palladium membrane is very similar to the PSA method since a pressure gradient is used in this method [65]. These membrane systems can achieve a moderate H_2 purity of 90-95% [70]. High temperatures (>573 K) can be employed with palladium (Pd) membranes [59]. High-purity H_2 can be produced using ultra-high permeability CMS-700, CMS-800, and CMS-900 membranes that are manufactured at 700, 800, and 900 °C, respectively [45]. The use of composite membranes, such as Pd/NaY/PSS composite membrane [60], Pd/Nb40Ti30Ni30/Pd/porous nickel support membrane [61], and Pd/BCC metal composite membrane [62], in the purification process has also been the subject of various investigations [71]. Pure H_2 was separated from gaseous mixtures containing CO_2, N_2, and CH_4 using a membrane made of graphenylene [63].

2.3.1.3. Cryogenic

The cryogenic separation method is an alternative H_2 purification method. In this process, partial condensation of other impurities is done to separate H_2 [69]. Since H_2

can be stored directly in liquid form with the cryogenic separation method, it is more suitable for extensive facilities [72]. The main disadvantage of this method is that it cannot achieve the high purity levels obtained with PSA and its high cooling requirements [73].

2.3.1.4. Metal Hydrides

Metal hydrides can be used for H_2 purification [74]. When the gas mixture containing H_2 encounters the hydride material bed, and the H_2 partial pressure of the gas is higher than the equilibrium pressure of the hydride material, the material will selectively react with H_2 to form a metal hydride [75]. Metal hydrides may be contaminated due to the toxic effects of some substances such as H_2S, CO, and CO_2, or the absorption reaction of H_2 may be slowed down due to additives such as N_2 [76], [77]. $La(Ni, Co, Al, Mn)_5$ was investigated by Modibane et al. [78] to separate H_2 from CO_2/CO mixtures. $La(Ni, Co, , Mn)_5$ material produced good H_2 absorption from the CO and CO_2 gas mixture with hard degradation.

2.3.2. H_2 Compression Methods

Compression of the gas in appropriate tanks is a practical approach for transportation [79]. However, H_2 has a low density, it must be stored in huge tanks. The cost of manufacturing and shipping these tanks will be high. According to Sheffield et al. [80], although compressed H_2 has a lower density than liquid H_2, compression, uses only a third of the energy required for liquefaction. Recent research indicates that higher H_2 concentrations can be stored at a lower pressure. For instance, Liu et al. [81] reported using a Ti-Mn alloy to create a gaseous and solid hybrid H_2 storage system that can compress H_2 at a pressure of 5 MPa and a density of 40.07 kg/m^3.

In recent years, researchers have spent much effort on cost-effective and efficient compression methods. For this purpose, mechanical compressors and non-mechanical compressors are frequently utilized [79]. Table 2.3 shows some of the most used H_2 compression methods in the literature.

Table 2.3 Some studies on H_2 compression methods [48]

Compression Method	Inlet Pressure (MPa)	Outlet Pressure (MPa)	H_2 Production	Ref.
Mechanical	35	85	N/A	[82]
Mechanical	0.6	70	N/A	[83]
Mechanical	1.8	28.1	581 Nm^3/h	[84]
Mechanical/ reciprocating	0.4	25.5	N/A	[85]
Mechanical/ linear	2	86-95	10 kg/h	[86]
Mechanical/ ionic piston	0.5	100	370 Nm^3/h	[87]
Cryo-compressors	0.1	34.5	100 kg/h	[88]
Nonmechanical/ metal hydride	0.3	15	10 m^3/h	[89]
Nonmechanical/ thermally driven	8	70	N/A	[90]
Nonmechanical/ adsorption	0.1	10	9.5×10^{-4} m^3/s	[91]

2.3.2.1. Mechanical Compressors

Today, the industry uses mechanical compressors widely [57]. In these systems, mechanical energy is used to compress the gases by decreasing the volume through pneumatic and electrically powered compressors. Mechanical compressors come in various designs, such as linear compressors, liquid compressors, reciprocating compressors, and diaphragm compressors. In dynamic types, the gas is accelerated by spinning parts. H_2 compression has been completed by HydroPac Inc. [82] with an inlet pressure of 35 MPa and an exit pressure of 85 MPa. Other investigations have used mechanical compression to compress H_2 at pressures ranging from 0.4 MPa to 25.5 MPa [85], 0.6 MPa to 70 MPa [83], and 1.8 MPa to 28.1 MPa [84]. H_2 with a 2 MPa intake pressure was compressed to 86–95 MPa after three stages [86] by a linear compressor. From 5 bar to 1000 bar of H_2 compression was achieved by Markus-Mayer et al. [87] using an ionic piston compressor.

Mechanical compressors have lower efficiency compared to isothermal compression under the same compression ratios. Adiabatic compression, commonly used in mechanical compressors, consumes more energy and is less efficient. The moving parts have potential of failure [92]. Suermann et al. [93] determined that electrochemical compression efficiency increased with increasing current density and reached 99% electrochemical compression efficiency at 100 MPa compression and 3 A/cm^2.

2.3.2.1.1. Reciprocating Compressor

One of the positive displacement types of compressors is the reciprocating compressor, which uses pistons that move back and forth to increase the volume. Piston compressors can operate with or without oil and are preferred in conditions where the expected pressure is higher than 3 MPa. Its working principle is based on two piston-cylinder systems, one for suction and one for discharge. The linear motion, known as reciprocating motion [94], is due to the rotational motion of the moving units. The power required for compression is supplied externally by an electrical or thermal device. Multistage reciprocating compressors are used to obtain higher pressure H_2 [95]. At each stage, the H_2 pressure rises more and reaches the desired value. To limit the stress that arises in these compressors, it is recommended to reduce the speed. The definition of speed was made by the number of cycles per unit of time [79]. Embrittlement is also a disadvantage in piston compressors due to their moving parts, as in other mechanical compressors. Although compressors using mineral oils are still used today, oil-free compressors that offer high-purity gas compression are preferred [96]. Another subject that is still being studied is the prevention of H_2 leaks.

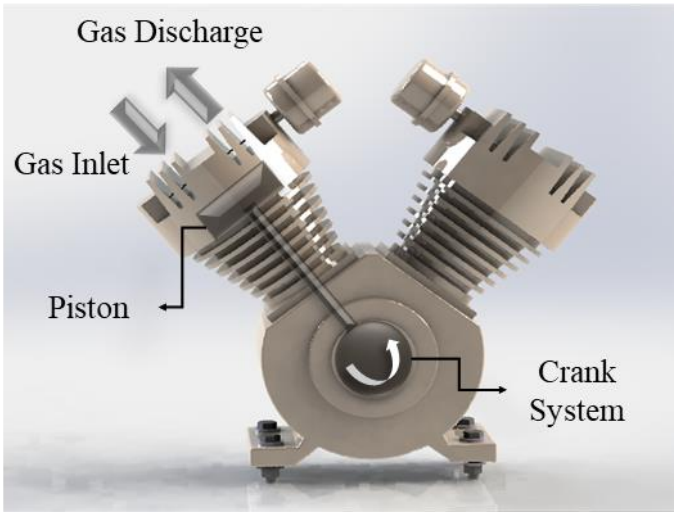

Figure 2.3 Reciprocating piston compressor

2.3.2.1.2. Diaphragm Compressors

As one of the positive displacement types, diaphragm compressors are used. Since the gas is completely isolated from the piston in diaphragm compressors, the contact between the gas and the piston is prevented and it is widely used for pressurizing high-purity gases [79]. Besides, it consumes low power and has high efficiency. Metal membranes are called diaphragms to reduce the volume and increase the gas pressure. Since these metal membranes are in contact with H_2 on one side and oil on the other, the material should be chosen as stainless steel, nickel steel alloy, or copper alloy [97].

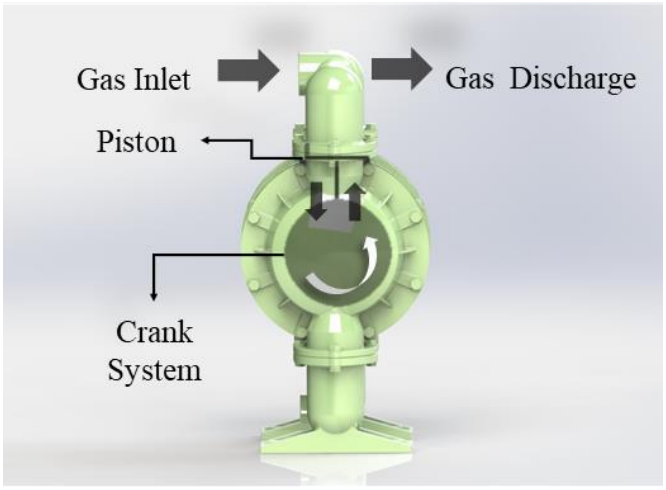

Figure 2.4 Diaphragm compressor

2.3.2.1.3. Ionic Liquid Compressors

Ionic liquid compressors were created especially for H_2 applications and are based on the material characteristics of ionic liquids [98]. These salts have low melting points, high ionic conductivity, good thermal and chemical stability, flame resistance, and moderate viscosity [99], [100]. Ionic liquids can perform exceptionally well in compression applications when solid pistons are substituted in positive displacement devices and rotary configurations. It is possible to achieve high volumetric yields and high compression ratios. Ionic liquids are used to compress H_2, which guarantees low energy usage, long service life, affordable materials, and low noise emissions. However, the risk of corrosion is still very high, which lowers component material strength and raises the chance of contamination with corrosion products, lowering overall efficiency [79].

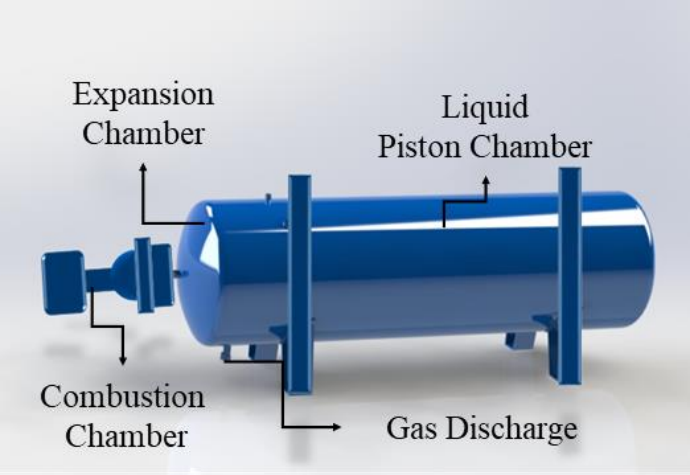

Figure 2.5 Ionic liquid compressor

2.3.2.1.4. Linear Compressors

Linear compressors are formed by the direct coupling of a resonant spring system to a linear motor, which has fewer moving parts. Since the number of moving components is less than in other compressors, it saves significantly on maintenance and repair costs [101]. However, because it is an innovative method, it is used less frequently.

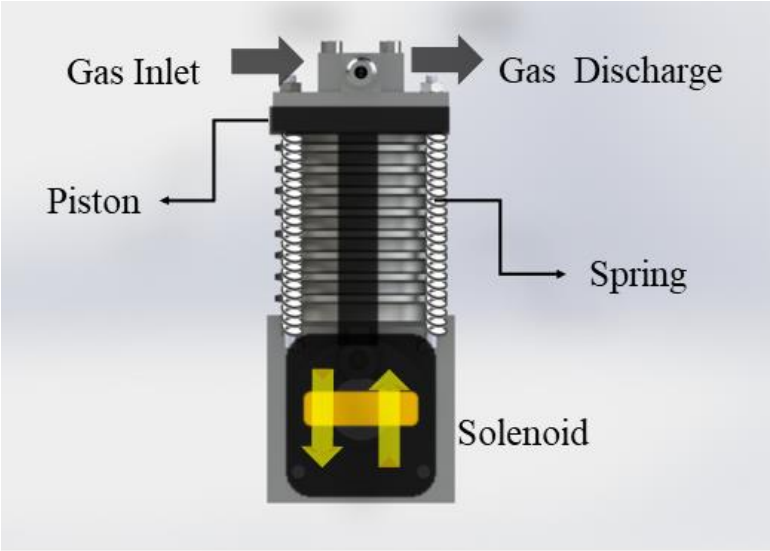

Figure 2.6 Linear compressor

Despite being often employed for compression, mechanical compressors have several drawbacks such as a significant amount of power being consumed during the compression process [102]. Mechanical compressors produce noise and vibration due to their moving parts; it is not practical to utilize them in strategic applications like the defense industry [57], [103], particularly in reformer-integrated studies. Although the efficiency of these compressors is comparable, the significant expenses associated with their installation and repair make these systems expensive [57]. As a result of oil and moving parts used in conventional compressor systems, H_2 can be contaminated during pressurization.

2.3.2.2. Non-mechanical Compressors

Alternatives and non-mechanical compressors to reduce the high cost of the widespread use of H_2 are presented in this section. According to some studies, non-mechanical compressors can compete with mechanical compressors in some markets [104]. Metal hydride compressors, cryo-compression (which operates between -243.15 °C and -173.15 °C), adsorption compressors, and electrochemical H_2 compressors are a few alternatives to traditional techniques of compressing H_2.

2.3.2.2.1 Cryogenic Compressors

One of the innovative non-mechanical compressor types is cryo-compressors. The idea behind cryo-compression is to pressurize H_2 at very low temperatures (between

-243.15 °C and -173.15 °C). Systems using cryo-compression are twice as efficient in terms of volume than mechanical systems [105]. The system's thermal insulation must be constantly monitored due to the low temperatures. The main technological challenge is controlling vacuum stability which increased system complexity [106], [107]. The geometry of the pressure vessel and the materials used have a direct impact on the system's performance.

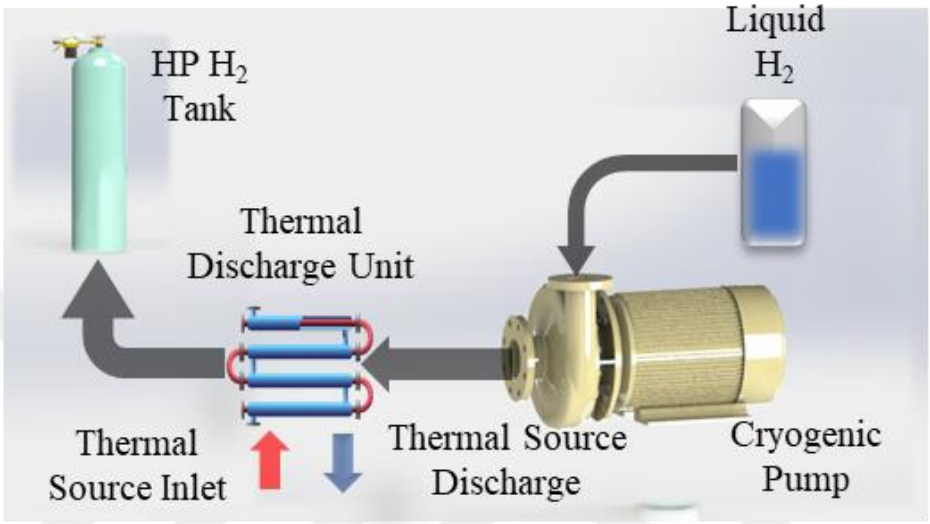

Figure 2.7 Cryogenic compressor

2.3.2.2.2 Metal Hydride Compressors

In the metal hydride technique, H_2 can be kept at a moderate temperature and pressure by joining with specific metals or alloys. Since the metals' natural absorbing and desorbing abilities, metal hydride compressors are also known as “thermally powered compressors” [108]. Metals react with H_2 reversibly (Eq. (4)):

$$M_s + \frac{x}{2} H_2(g) \leftrightarrow MH_x(s) + Q \tag{4}$$

H_2 absorption is an exothermic reaction and H_2 desorption is an endothermic reaction [109]. Low-pressure H_2 diffuses in the metal hydride bed and H_2 exothermic absorption occurs when it is added to the metal hydride tank. Absorption continues until the equilibrium pressure and supply pressure are equal. Once the equilibrium pressure has been reached, H_2 desorption can be carried out by applying heat to the metal hydride. Thus, thermally driven compression can be carried out without the use

of moving parts or noise. The production cost significantly impacts whether pressurizing H_2 using metal hydrides will be commercially successful. However, surface poisoning is one of the most significant issues with metal hydride materials. Lototskyy et al. [110] increased pressure from 100 bar to 5000 bar in their metal hydride compressor study.

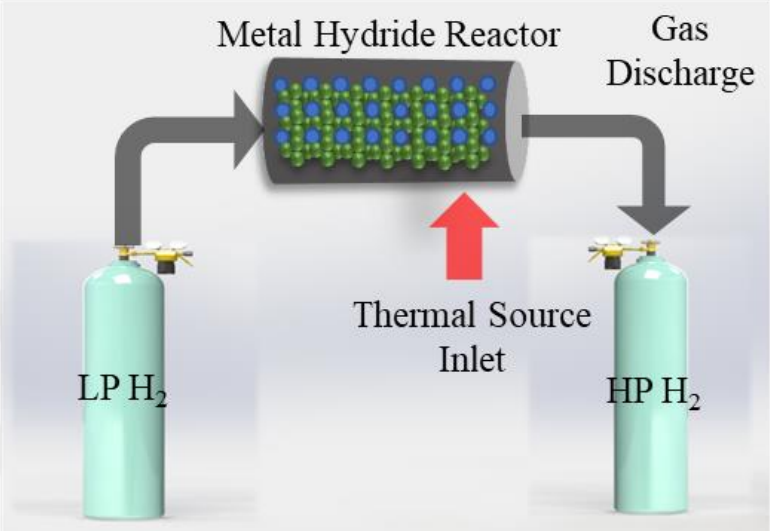

Figure 2.8 Metal hydride compressor

2.3.2.2.3 Adsorption Compressors

In the H_2 compression technology based on adsorption, H_2 is fed to a closed tank filled with a solid bed of porous material with a high surface area and consequently high adsorption potential. Adsorption only occurs on the surface of the porous material at specific temperatures and pressures. Heat is added to the system after adsorption, which raises the temperature and results in H_2 desorption. As a result, high-pressure H_2 is produced [111].

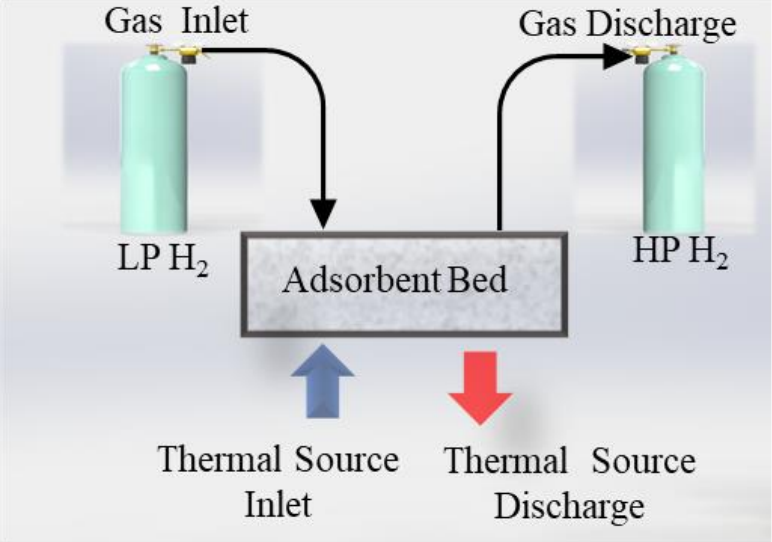

Figure 2.9 Adsorption compressor

The choice of the H_2 compression technique is influenced by various operational factors, including cost, the temperature ranges that can be used, and the pressure restrictions. Therefore, the application determines which H_2 compression technique to use.

2.3.3. H_2 Storage Methods

Storage of H_2 in compressed gas form is currently the most popular approach, although solid storage of H_2 is safer than liquid or gaseous since the safety concerns and volumetric storage capacity [3], [112], [113]. Physical techniques include cryo-compressed storage, liquid storage, or compressed gas storage. Materials-based H_2 storage techniques include storing H_2 in metal hydrides, glass microspheres, liquid organic carriers, activated carbons as H_2 storage materials, and metal-organic frameworks [114]–[117]. Cryo-compressed H_2 storage could be used to achieve high volumetric energy density. However, this approach is only favored for specific applications due to the cost of cooling and compressing H_2 and the difficulty of designing a storage system that can hold cryogenic liquid for an extended period [80]. The use of well-insulated tanks is recommended for liquid-state storage. The liquefaction process is costly and consumes a lot of energy. Since H_2 has a low boiling point, if there is a leak in a tank that is not adequately insulated, the H_2 will shift from a liquid to a gas and begin to boil locally. This would build pressure, which could lead to a dangerous condition in the storage. The zero-boil-off concepts are being worked

on by a select few institutions, including NASA [118]. There have been many different H_2 absorption materials investigated for H_2 storage. However, none of the materials have achieved the desired high volumetric energy storage density, and the best designs for large-scale H_2 storage systems have not yet been established [119]. The need for efficient and affordable H_2 storage in small volumes hinders commercialization.

CHAPTER 3

ELECTROCHEMICAL HYDROGEN COMPRESSORS

Researchers claim that since the first antecedents of Nafion® films were created for fuel cells, electrochemical H_2 transport over a membrane employing an ionic transport mechanism has been recognized [120]. Although H_2 evolution or oxidation is used in fuel cells and electrolyzers, both processes are significantly different from compressing H_2 because, except for a slight overvoltage at each electrode, the net chemical reaction neither produces nor consumes energy [121]. However, electrochemical H_2 transport offers other advantages, including purification, compression, and silent operation.

ECHCs can be used for pressurization, purification of H_2 or both purification and pressurization [122]. ECHCs and PEM fuel cells appear to be quite similar in terms of components. A membrane electrode assembly (MEA), gas diffusion layers, bipolar plates, current distribution plates, and end plates are the main component of a single-cell ECHC (Figure 3.1). Membrane is the key component between the anode and cathode side electrodes. Bipolar plates' gas flow channels deliver reactants uniformly to the gas diffusion layer. The anode and cathode catalyst layers are in contact with the porous gas diffusion layer. They are essential for managing heat and water. Mechanically robust end plates keep all these parts together. Fasteners (such as nuts and screws) are used, and gaskets are used to prevent leakage [57], [123]–[125].

ECHC has a high efficiency and pressurization capacity and become a viable alternative to conventional H_2 compressors [57]. The idea of electrochemical H_2 compression has been around for a while, and it has recently accomplished compression in the ECHC technology with a high level of efficiency [126]. Both capital expenditure and O&M expenses for ECHC are cheaper than mechanical compressors, particularly for low-pressure applications (<10 MPa) [79]. ECHC systems have other additional benefits over traditional approaches. These systems do

not have moving parts; therefore, there is less chance of a malfunction, less noise during compression, and lower maintenance and repair costs. The humidification of the membrane is crucial for the proper operation of ECHC at low temperatures. Similarly, acid doping is vital for high-temperature applications. The membrane may become damaged under specific working conditions if adequate humidification/acid doping is not provided. Since ECHC is a power-consuming technology, the operation should aim for low power density. Since ECHC is a more recent technology, new challenges might arise when the theoretical studies are translated into experiments.

3.1. Reaction Mechanism and Overpotentials in ECHC

A Pt-based catalyst assists in the oxidation of H_2 (given in Eq. (5)) into protons (H^+) and electrons (e^-) when it encounters the anode electrode [127]. Theoretically, only protons are allowed to pass through the membrane, and the membrane behaves as a kind of barrier for gases other than H_2. H^+ passing through the membrane combine with e^- from the external circuit at the cathode to form H_2 (Eq. (6)).

Anode side [H_2 oxidation reaction (HOR)]: $H_2(LP) \rightarrow 2H^+ + 2e^-$ (5)

Cathode side [H_2 evolution reaction (HER)]: $2H^+ + 2e^- \rightarrow H_2\ (HP)$ (6)

Overall cell reaction: $H_2(LP) \rightarrow H_2(HP)$ (7)

The gas flow channels on the bipolar plates transmit the reactants homogeneously to the gas diffusion layer. The porous gas diffusion layer is in contact with the anode and cathode catalyst layers. Since ECHC systems are also employed as compressors, large pressure differences occur between the anode and cathode sides, and this pressure can damage the MEA. Therefore, materials such as ti mesh or felt are often used to prevent the high pressure on the cathode side from damaging the MEA. All these components are sandwiched using a mechanically resistant end plate. Gaskets are used to prevent leakage, and fasteners (e.g., nuts, screws) are used to hold parts together [126], [128]–[133].

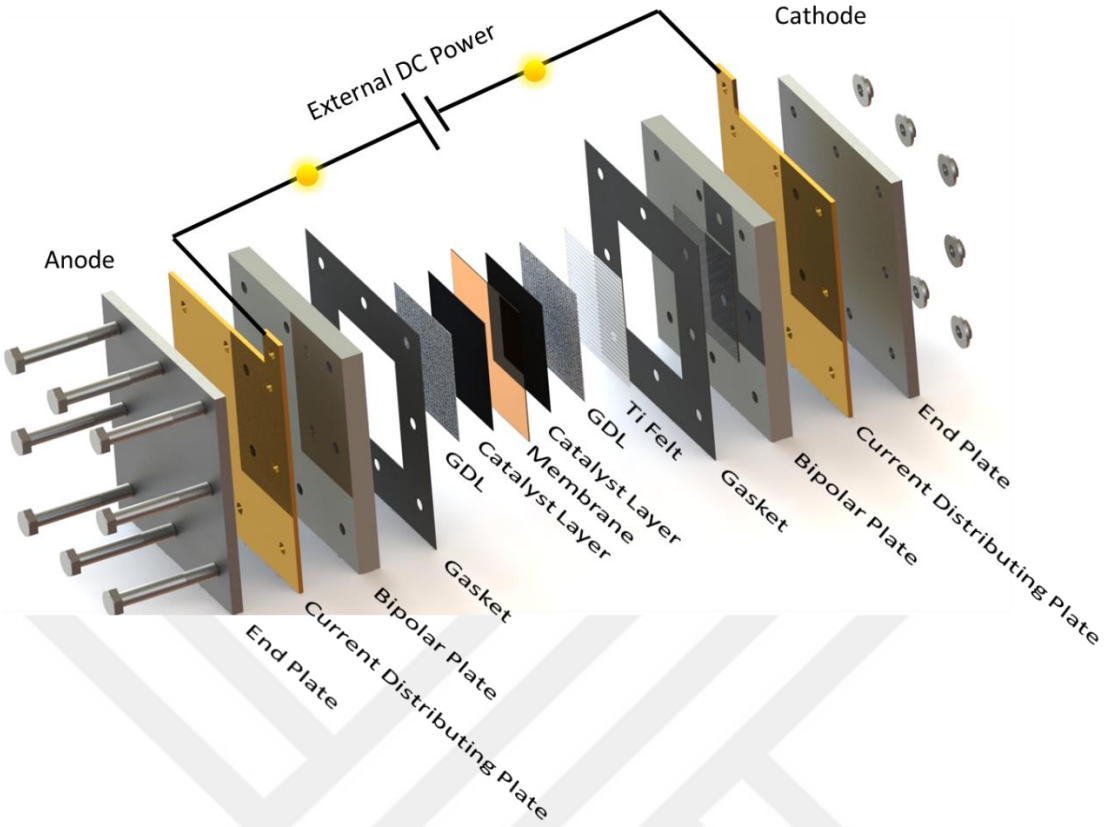

Figure 3.1 Components of the ECHC

The significant difference in these systems compared to the PEM fuel cell is that the ECHC is operated in an electrolytic mode rather than a galvanic mode. ECHC systems require power to complete electrochemical reactions. Since H_2 reactions are easy to oxidize and reduce and have an almost Nernstian electrochemical behavior, minimal power is needed to operate the cell [123]. The ECHC can be operated under atmospheric pressure to provide rapid H_2 purification, and the applied power controls the separation speed. High current densities cause poor performance due to the increasing resistance inside the cell. Therefore, ECHC systems should be operated at low power. Figure 3.2 illustrates the working principle of the ECHC.

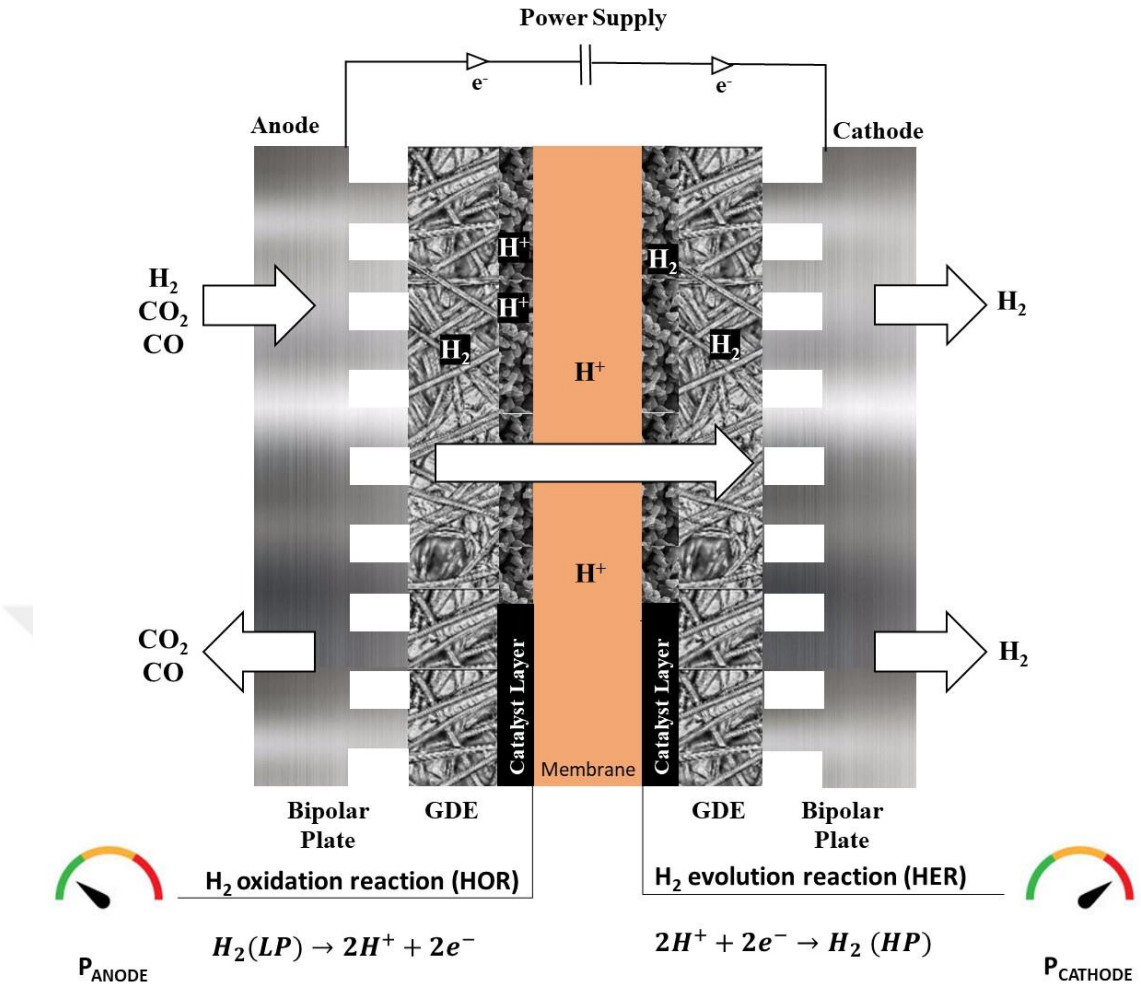

Figure 3.2 The working principle of the ECHC

DC power from an external source is used to run the ECHC. The theoretical minimum cell voltage (Nernst voltage) required for the ECHC only depends on the partial pressure of H_2 at the anode and the cathode, as well as the operating temperature (Eq. (8)) [134]. The supplied voltage must be greater than the Nernst Voltage due to the irreversibility associated with the activation overpotential, ohmic overpotential, and mass transfer limitations. Therefore, in practice, the necessary voltage is determined considering overpotentials and Nernst potential. This irreversibility needs to be reduced to improve the performance of the ECHC. In an ECHC, ohmic and activation overpotentials, caused by the activity of the catalyst and membrane ion conductivity, are often dominant [92].

$$E_{Nernst} = E° + \frac{RT}{nF} ln\left(\frac{P_{Cathode}^{H2}}{P_{Anode}^{H2}}\right) \quad (8)$$

For ECHC applications, the cell potential at standard conditions, E°, is 0 [92]. One mole of H_2 can be oxidized by passing n moles of electrons (n=2 from Eq. (5)). T stands for the temperature in K, R for the ideal gas constant (8.3144 J $mol^{-1} \cdot K^{-1}$), F is the Faraday's constant (96,485 C/mol), and $P_{Cathode}$ and P_{Anode} are the partial pressures of H_2 on the cathode and anode sides, respectively.

The DC power supplied to drive the ECHC can be obtained from Eq. (9) .

$$E_{cell} = E_{Nernst} + \Delta E_{Activation} + \Delta E_{Ohmic} + \Delta E_{Mass\ transfer} + E_{Back\ Diffusion} \quad (9)$$

Both the anode and the cathode of an ECHC exhibit activation polarization (Eq. (10)). The Volmer-Tafel mechanism dominates the HOR on the anode side, while the Volmer-Heyrovsky mechanism dominates the HER on the cathode side. The cathode shows a greater activation overpotential due to the Volmer-Heyrovsky mechanism's slow reaction rate [128]. The Tafel equation was used by Dale et al. [135] to demonstrate the activation overpotentials needed for the anode and cathode. These overpotentials can be determined using Equations (11) and (12) for the anode and cathode, respectively.

$$\Delta E_{Activation} = E_{Anode}^{Activation} + E_{Cathode}^{Activation} \quad (10)$$

$$E_{Anode}^{Activation} = \frac{RT}{2\alpha_{anode}F}\, ln\,(\frac{i}{i_{o,anode}}) \quad (11)$$

$$E_{Cathode}^{Activation} = \frac{RT}{2\alpha_{cathode}F}\, ln\,(\frac{i}{i_{o,cathode}}) \quad (12)$$

where, $i_{o,anode}$ and $i_{o,cathode}$ are the exchange current densities (A/cm^2) for anode and cathode, respectively, i is the current density (A/cm^2), and α indicates the transfer coefficient as 0.5 for anode and cathode [136]. Due to the rapid kinetics of H_2, $\Delta E_{Activation}$ is assumed to be very small [137].

The most prevalent overpotential is the ohmic overpotential caused by the membrane's ionic resistance [138]. Eq. (13) can be used to determine this ohmic overpotential.

$$\Delta E_{Ohmic} = iR_{ohmic} = i\frac{t_m}{\sigma} \quad (13)$$

In this equation, R_{ohmic} denotes the ohmic resistance of the cell, t_m denotes the thickness of the membrane (in cm), and σ denotes the ionic conductivity of the cell (S/cm). The significant elements influencing ohmic overpotential are the membrane's proton conductivity and electrical resistance. To minimize ohmic losses, a membrane with strong ionic conductivity is required. The membrane's operating temperature and water content (for low-temperature applications)/acid doping (for high-temperature applications) impact the conductivity. The membrane must have excellent mechanical, thermal, and chemical stability to resist working circumstances.

Mass transport overvoltage is estimated by considering mass flows inside the cell electrodes (Eq. (14) and (15)). The concentration of each species at the reaction sites can be estimated by applying Fick's Law of diffusion and then the Nernst equation is used to evaluate the diffusion overvoltage at each electrode [139]:

$$E_{Mass\ Transport,anode} = \frac{RT}{2F} ln \frac{C_{anode}}{C_{anode,0}} \quad (14)$$

$$E_{Mass\ Transport,cathode} = \frac{RT}{2F} ln \frac{C_{cathode}}{C_{cathode,0}} \quad (15)$$

where, C_{anode} and $C_{cathode}$ are H_2 concentration (mol/m^3), and $C_{anode,0}$ and $C_{cathode,0}$ are reference working condition (mol/m^3), "0" condition, for anode and cathode, respectively.

The anode and cathode sides are at atmospheric pressure at t=0. In this case, there is no back diffusion. However, as the pressure on the cathode side increases, and the pressure difference between the anode and cathode increases, back diffusion from the cathode to the anode side may occur [138]. This prevents the ECHC from reaching higher pressures.

3.2. Literature Survey on ECHC

One of the first studies in the literature was published by Rohland et al. [126], they used Nafion® 117 membrane with an active area of 100 cm^2 for compression, and they

reached a pressure of 43 bar in approximately 18 minutes. Ströbel et al. [128], used 100 cm^2 active area pressuring H_2 up to 54 bar at room temperature. Wong et al. [140] reported reaching about 830 bar pressure with multi-cell assembly in their patent studies. According to the Analytic Power Corp. report [141], published in 2006, a cathode pressure of 17.2 MPa was achieved using pure H_2 using Nafion® 117. Grigoriev et al. [73], used the modified Nafion® through a zirconyl phosphate membrane, and compressed H_2 up to 130 bar pressure and had to end the experiment due to a leakage problem. Bouwman et al. [142] compressed H_2 to 100 MPa using a series setup. Lee et al. [143], used H_2-N_2-CO_2 gas mixture and Nafion® 115 at 30 to 70 °C, which succeeded in purifying H_2 at a rate of 97.39%. Ibeh et al. [144] separated H_2 from a natural gas-H_2 gas mixture using platinum or platinum/ruthenium anode electrocatalysts in the temperature range of 293-343 K, with the cell they designed with 25 cm^2 active area. They also developed a mathematical model for this study and reported that the results were compatible with the experiment. Gardner et al. [145] used platinum and ruthenium electrocatalysts and Nafion® 115 membrane in their experiments with a single cell with a 25 cm^2 active area at room temperature. They separated H_2 from the gas mixture containing H_2-CO_2-CO and reported that the efficiency was poor when the gas mixture containing CO was used since the catalyst's poisoning. Perry et al. [123] reported the advantages of working at high temperatures in their experiments with PBI membrane in the temperature range of 120 to 160 °C. They have also proven the durability of ECHC with tests lasting approximately 4000 hours. Casati et al. [122], used N_2 and H_2 gas mixture, and claim that the specific energy consumption applied to the ECHC is only a function of the DC voltage. Onda et al. [146] declare that low-concentration H_2 can be separated and recovered almost 100% from the H_2-N_2-CO_2 gas mixture by ECHC. Nguyen et al. [147] discuss the characterization and optimization of ECHC using electrochemical impedance spectroscopy (EIS) with Nafion® 117 membrane. Their study focused on purification, used H_2 and N_2 gas mixture at a current density of 200 mA/cm^2, and showed that proton conductivity increases with increasing temperature. Yang et al. [148], in their study with a membrane based on poly-2-vinylpyridinium dihydrogenphosphate (P2VP-DHP) that can operate in the 105-180 °C range, demonstrated that ECHC technology could be used with a membrane that can work without water. Kim et al. [149] completed their experiments with H_2/CO_2 gas mixture at 160 °C using PBI/PA

membrane. Investigating the effects on ECHC performance by changing the Pt charge, researchers found that when the Pt charge was reduced from 1.1 mg/ cm^2 to 0.2 mg/cm^2, the voltage supplied to the ECHC increased by 72%. Wu et al. [150] evaluated the possibility of using a non-fluorinated proton exchange membrane to reduce cost when separating H_2/CO_2 in ECHC. In their experiments, keeping the limiting currents around 0.5−0.6 A, they obtained a minimal decrease in energy efficiency from Nafion®-based ECHC, and this was explained by the promising future applications. Hao et al. [151] ran the ECHC with an internal humidifier and reported that the PEM conductivity was higher than the conventional humidifier. In addition, it has been reported that the HER activation overpotential can be suppressed by increasing the cathode pressure. Rico-Zavala et al. [152] modified membranes based on Sulfonated Poly (Ether-Ether Ketone) (SPEEK) with Halloysite nanotubes (HNT) and Halloysite nanotubes impregnated with phosphotungstic acid (PWA/HNT30)15. Their results are introduced as when compared to the unmodified membrane, the proton conductivity of S70/HNT15 and S70/(PWA/HNT30)15 has increased by 42% and 88%, respectively. Sdanghi et al. [153] have worked experimentally and modeled with the Nafion® XL and Nafion® 117 membranes. Their modeling studies estimated that the ECHC could compress the H_2 up to 32 bar. For various input gas mixtures, Vermaak et al. [127] compared commercial H_2 separation technologies with an ECHC and concluded that the ECHC technology is tolerant of CO and CO_2 at high temperatures and sensitive to catalyst deactivation. A summary of different H_2 compression technologies was also provided by Zou et al. [92], with an emphasis on the ECHC performance in terms of thermal and water management, as well as the ECHC testing protocol. Table 3.1 and Table 3.2 summarize some of the patents and studies related to ECHC available in the literature, respectively.

Table 3.1 The patents for ECHC technology [48]

Patent Number	Tittle	Ref.
JP2018095953A	Electrochemical type hydrogen compression device	[154]
JP2019119654A	Electrochemical type hydrogen pump	[155]
US10202696B2	Electrochemical hydrogen pump	[156]
US7045233B2	Method and apparatus for electrochemical compression and expansion of hydrogen in a fuel cell system	[157]
US20210005899A1	Membrane electrode assembly of electrochemical device, membrane electrode assembly of fuel cell, fuel cell, membrane electrode assembly of electrochemical hydrogen pump, electrochemical hydrogen pump, membrane electrode assembly of hydrogen sensor, and hydrogen sensor	[158]
JP2019163521A	Electrochemical type hydrogen pump	[159]
CN111799483A	Composite bipolar plate and electrochemical hydrogen compression device	[160]
US2004/0211679A1	Electrochemical hydrogen compressor	[161]
EP3208880B1	Electrochemical hydrogen pump	[162]
US10480087B2	Membrane electrode assembly and electrochemical hydrogen pump	[163]
KR20200086530A	Electrochemical hydrogen compressor	[164]
US6994929B2	Electrochemical hydrogen compressor for electrochemical cell system and method for controlling	[165]

Table 3.2 Literature studies for ECHC studies

Process	Membrane	Temperature	Cathode Pressure	Purification (%)	Ref.
Compression	Nafion® 117	N/A	43 bar	N/A	[126]
Compression	N/A	N/A	54 bar	N/A	[128]
Compression	N/A	N/A	830 bar	N/A	[140]
Purification	Nafion® 115	30-70 °C	N/A	97.3	[143]
Compression	Nafion® 117	N/A	17.2 MPa	N/A	[141]
Compression	Nafion®	N/A	130 bar	N/A	[73]
Purification	PBI/PA	160 °C	N/A	N/A	[149]
Compression	N/A	N/A	12,800 psi	N/A	[166]
Compression	N/A	N/A	100 MPa	N/A	[142]
Compression	Nafion® XL/117	N/A	32 bar	N/A	[153]
Purification	TPS®-based	120-160 °C	N/A	99.63	[127]
Compression	Nafion® 115	22 °C	154 bar	N/A	[167]
Purification	PBI	160 °C	N/A	99.999	[168]
Purification	HT-PEM	200 °C	N/A	99.85	[169]
Compression	Nafion® 115	30-80 °C	50 bar	N/A	[170]

3.3. Components of ECHC

ECHC systems have similar components to fuel cells; however, the cathode polarization is very low since the ECHC has H_2 gas instead of O_2 at the cathode. Thus, ECHC can be operated with an efficiency of >80% [128]. A single-cell ECHC consists of a membrane electrode assembly, gas diffusion layers, bipolar plates, current distribution plates, and end plates.

3.3.1 Membrane Electrode Assembly

A typical membrane electrode assembly (MEA) consists of catalyst layers on both sides of a polymer electrolyte membrane and gas diffusion electrodes on the anode and cathode sides. MEA types can be categorized depending on the component arrangement. Catalyst-coated membrane (CCM) consists of the catalysts on both sides of the membrane and is called a 3-layer MEA. 5-layer MEA has two GDE, two catalysts and a membrane in the center. 7-layer MEA has a membrane, two catalyst layers, two GDE and two sealing layers. Figure 3.3 shows the 3-layer, 5-layer and 7-layer MEA structure. Because of its components, they are the most essential and costly parts of the ECHC cell. Especially at high-pressure differences, MEA can be considered the weakest part of the cell. The MEA chosen for this purpose should have an optimum thickness and a smooth surface area.

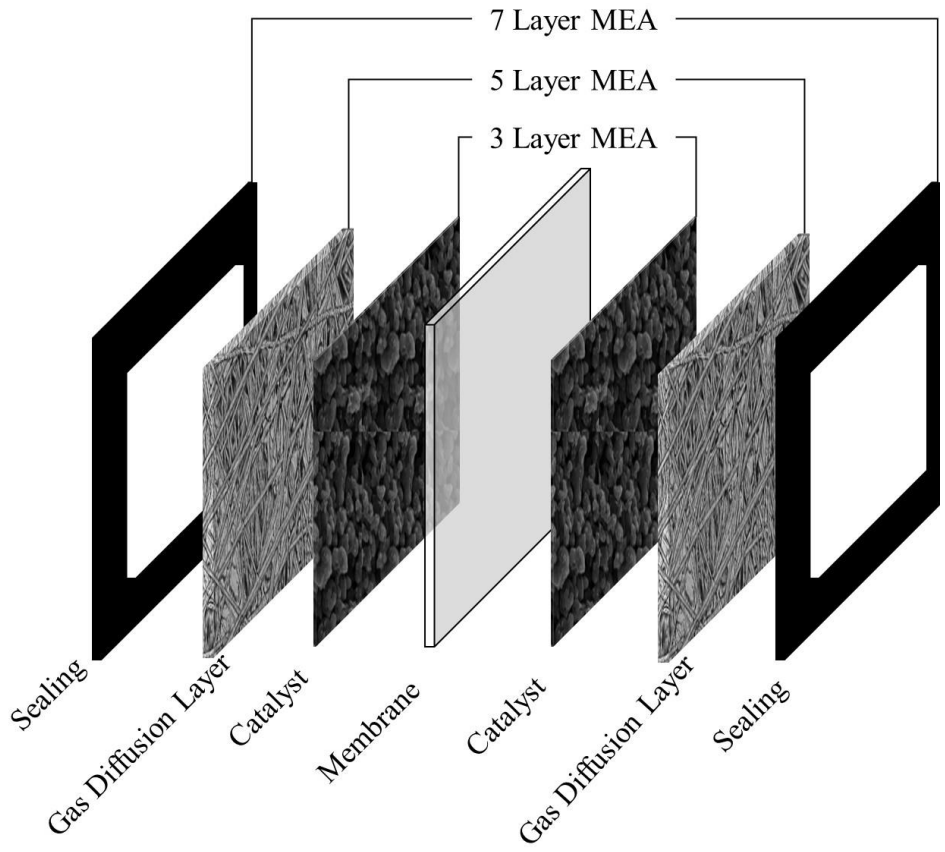

Figure 3.3 Components of 3-layer, 5-layer and 7-layer MEAs

3.3.1.1. ECHC Membranes

The membrane is the most fundamental component of the ECHC. Factors influencing cell performance, like proton conductivity and electrical resistance, should be considered when choosing the membrane. Similarly, the selected membrane must be impervious to high-pressure values.

3.3.1.1.1. Low-Temperature ECHC Membranes

The typical operating range for the low-temperature ECHC is 50 to 80 °C. Membranes based on perfluorosulfonic acid (PFSA) are frequently employed in LT-ECHC applications. High proton conductivities, strength, and stability are characteristics of PFSA membranes. Due to its high proton conductivity, thermal stability, and oxidative stability, the commercially available Nafion® membrane is the most frequently used PFSA membrane in LT-ECHC applications. The operating temperatures are low because proton conduction depends on the sulphonic acid groups in the membrane structure and, thus, moistening. Protons are transported through the membrane using structural diffusion when the relative humidity is high [171].

Casati et al. [122] found in their study that the MEA resistance is influenced by the membrane's surface area, crossover losses, and the purity of the H_2 produced. Nordio et al. [172] found that temperature increases the Nafion® 212 membrane's conductivity while decreasing its ohmic resistance. A feasibility study on the electrochemical H_2 recovery from natural gas and methanol using Nafion® 115 was carried out by Gardner et al. [145]. As a result, while the efficiency of separating H_2 from the CO_2 mixture is higher, and separating H_2 from a mixture with CO, the efficiency is only moderately high as poisoning occurred in the mixtures containing CO. Lee et al. [143] also found that temperature had a favorable impact on the Nafion® 115 membrane and overall efficiency.

Membranes based on sulfonated poly ether-ether ketone (SPEEK) is shown to be an alternative to Nafion® membrane. Depending on the sulfonation level, SPEEK, an aromatic polymer, offers high mechanical stability, proton conductivity, and thermal stability. Wu et al. [150] studied the SPEEK cross-linked CrPSSA (polystyrene

sulfonic acid) polymer membrane for LT-ECHC, and they discovered that it had an energy efficiency of 30%, which is a roughly less than Nafion®-based ECHC.

Although their common usage, proton exchange membranes have certain drawbacks, including low mechanical resistance, a requirement for humidification, and high H_2 gas permeability at low temperatures. To eliminate these drawbacks, research on composite membranes has been done. To enhance the functionality of membranes, inorganic proton-conducting substances can be added to their structures such as phosphotungstic acid, heteropoly acids, zirconyl phosphate salts, and hydrosulfates of metals [173]. Rico-Zavala et al. [152] created a modified SPEEK membrane containing halloysite nanotubes and halloysite nanotubes treated with phosphotungstic acid. By a membrane modified with phosphotungstic acid, they got improved proton conductivity and decreased crossover. Grigorev et al. [73] reduced the penetration of H_2 back to the anode with Nafion® zirconylphosphate composite membranes.

Water management is one of the most critical problems with LT-ECHC systems. For the Nafion® membrane inside the LT-ECHC to have excellent proton conductivity and longevity, it must be kept hydrated with appropriate humidification [174]. Due to inadequate humidification, water may build up in the electrode layers or along the gas flow channels [175]. Additionally, excessive moisture might limit access to active catalyst regions, which lowers cell performance. Low tolerance for contaminants is another drawback of low-temperature operation. CO poisoning is the primary issue that reduces cell performance [176].

3.3.1.1.2. High-Temperature ECHC Membranes

Operating at high temperatures (up to 200 °C) without humidification offers significant benefits to HT-ECHC. At high working temperatures, PBI membranes provide substantial advantages for HT-ECHC applications because of their improved thermal stability, excellent chemical resistance, and simple water management. PBIs are various amorphous thermoplastic polymers with excellent textile fiber characteristics, a high glass transition temperature, and excellent chemical resistance. Figure 3.4 shows the structure of the PBI membrane.

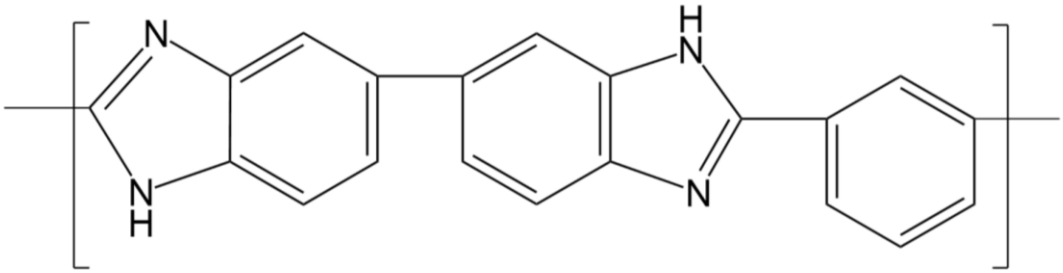

Figure 3.4 Chemical structure of PBI

However, the proton conductivity of the PBI membrane is inefficient. Strong acids, including sulfuric acid (H_2SO_4), phosphoric acid (PA), (H_3PO_4), nitric acid (HNO_3), and hydrochloric acid (HCl), should be added to PBI membranes to preserve proton conductivity. H_2SO_4 and H_3PO_4 have the highest conductivities among these acids, and PBI can readily react with each of them [177]. H_3PO_4 is typically used since H_2SO_4 can physically harm the membrane. Protons travel across the membrane using the proton hopping mechanism and diffuse between molecules by H_2-bonding. Here it attaches to the PA and causes another hydrogen ion to dissociate. Therefore, with the contribution of PA for proton transfer, a more dynamic H_2 bond network is formed [178]. Figure 3.5 shows the interaction between PBI and PA.

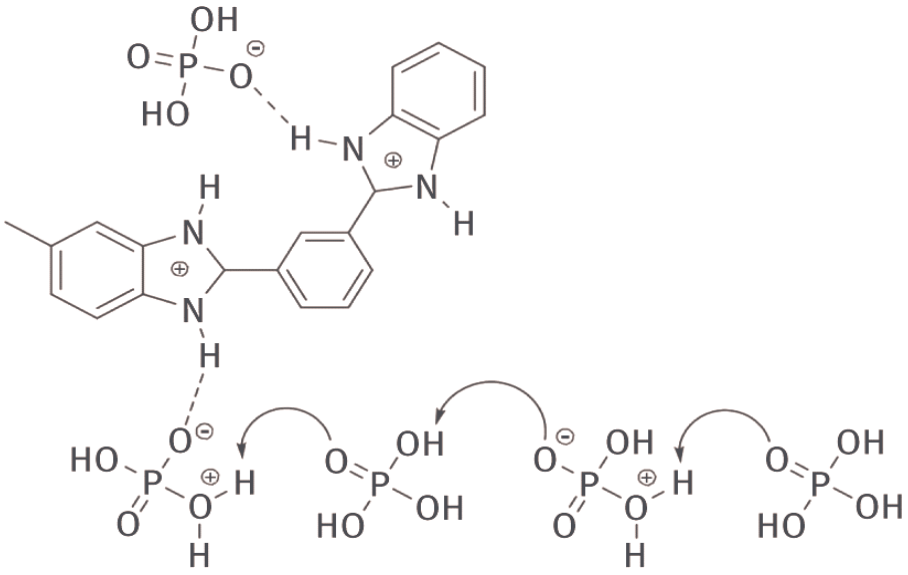

Figure 3.5 Proton conductivity mechanism of PA-doped PBI membrane

Huth et al. [138] searched the proton transport characteristics of the PBI membrane and discovered that its maximum proton transport capacity was comparable to the Nafion® membrane. Huang et al. [176] created three different PA-doped PBI membranes: para-PBI, m/p-PBI, and meta-PBI to test the effectiveness of the HT-ECHC with reformate gases at 160–200 °C. They obtained high H_2 purification levels (>99.6%) and high-power efficiency of up to 72%. Thomassen et al. [179] examine PBI membrane functioning by various gas mixes and purification levels. A gas mixture containing 50.5% H_2, 39% CO_2, 6.1% CH_4, and 4.4% CO was passed through a PBI membrane at 160 °C and achieved 99.9% purity of H_2 at the cathode side.

Proton conductivity of the PBI membranes depends on the acid in the membrane structure, and as the acid leaves the membrane over time, proton conductivity and performance are reduced. A practical method for increasing the protonic conductivity and enhancing acid retention capacity is the introduction of inorganic fillers in the membrane structure [180]. These materials must possess strong H-bonds and excellent acid retention. They should also be reasonably priced and chemically stable. The most popular inorganic fillers are zeolites, metal-organic frameworks (MOF), silicon dioxide (SiO_2), and titanium dioxide (TiO_2) [181].

MOFs are crucial in creating ECHC composite membranes. In contrast to porous materials like zeolite, MOF is a hybrid material made of covalent organic components and inorganic materials. MOFs are superior to conventional porous materials because they have a high surface area, adjustable pore size, and organic binders [182]. Chee et al. [183] claimed that MOFs gave membrane technology a fresh outlook. Due to their high chemical stability and promising technology, they are instrumental in gas and liquid separation due to their molecular sieving properties. They can be applied to almost all applications.

The solid oxide type HT-ECHC uses ceramic oxide electrolyte layers with conductive oxide ions or protons to operate between 500 and 900 °C. Electromotive force and electrochemical H_2 transfer are the two primary uses of proton conductive ceramics in the solid oxide type HT-ECHC. The ceramic membrane's impermeability makes it possible to utilize significantly less expensive non-Pt materials as catalysts. Iwahara et al. [184] investigated $SrCe_{0.95}Yb_{0.05}O_{3-\alpha}$, a ceramic-based material, for use as an

electrode and proton conductor in high-temperature solid oxide applications. Le et al. [185] employed $BaCe_{0.4}Zr_{0.4}Y_{0.1}Yb_{0.1}O_{3-d}$, a ceramic substance, as a proton-conducting electrolyte for a maximum temperature of 600 °C. They showed that at the same current density, higher temperature also leads to an increase in pressure. Kawamura et al. [186] produced a perovskite-type $SrCe_{0.95}Yb_{0.05}O_{3-\delta}$ ceramic proton conductor for solid oxide-type HT-ECHC application. The materials utilized as components in ceramic-based solid oxide type HT-ECHC are thermally strained because of the high operating temperatures. Additionally, significant issues must be resolved regarding the expensive and complicated production processes. Other drawbacks are a lengthy startup process and the requirement for extensive thermal insulation [187], which are similar to high-temperature solid oxide fuel cell (SOFC) applications. Creating appropriate sealing materials presents a significant obstacle for ceramic proton conductors. Seals that are highly stable at high working temperatures and allow compression under the given load are necessary to guarantee the required mechanical stability. Due to the fragility of ceramic materials, metallic, metallic-ceramic, and ceramic-ceramic composite gaskets have been examined [188].

Due to its high proton conductivity, and high thermal stability, PA-doped PBI is thought to be the most promising among the alternative membranes for high-temperature applications [189] because of its excellent proton conductivity, and remarkable thermal stability, phosphoric acid is the most promising of these acids.

3.3.1.2. Catalyst Layer

A catalyst layer is inserted at the anode and cathode sides of an ECHC. The polymer electrolyte membrane divides these catalyst layers, and GDLs are in touch with them on the other side of the catalyst layers. Each half-reaction (oxidation and evolution) occurs at these layers, and the layers can lower the activation energy of the reactions. Carbon-based support and electroactive metal are the catalyst layer's primary materials. Because of its strong electrocatalytic activity and excellent resistance to corrosion and oxidation, platinum (Pt) is employed frequently as a metal. Despite its successful performance, Pt is a costly precious metal. To decrease precious metal usage and support materials such as carbon black, carbon nanotubes (CNT), and graphene have been employed. Innovative and promising materials, like nanocarbon

supports like nanotubes, can be utilized to minimize Pt usage [152]. Important factors, including good metal-catalyst material interactions, high electrical conductivity, high surface area, and enhanced water management, should be considered when choosing the catalyst support materials utilized in ECHCs [92]. To enhance ECHC performance, Lubers et al. [190] examined the improved XC72R carbon support. Trimethyl(methylcyclopentadienyl) platinum (IV) (MeCpPtMe3) was chosen as the reagent for delivering platinum.

Reformate gas frequently contains CO, which significantly affects Pt's catalytic activity. CO aggressively adsorbs on Pt and obstructs the catalysts' active sites for further H_2 oxidation and reduction processes [72]. As a result, a significant decrease in performance with the poisoning of Pt-containing anode catalysts by contaminants like CO or H_2S is observed [72], [145]. The impact of CO and CO_2 on HT-ECHC with Pt catalyst and PBI membrane was studied by Perry et al. [123].

To lower the price and improve the catalyst's CO tolerance, Pt catalysts were alloyed with non-Pt group metals [92]. When Jackson et al. [191] examined the CO tolerance of PtRu/C, Pt/C, and PtNi/C catalysts, they found that the PtRu/C bimetallic catalyst performed the best. Kim et al. [192] developed an Ir/C-based catalyst and they saw improved performance. In comparison to Pt catalysts, Ir-based catalysts offer good performance with lower material costs. According to Wu et al.'s [193] comparison of the LT-ECHC performances of Pt/C and Pd/C catalysts with Nafion®115 membrane, the Pd/C catalyst had an energy efficiency for H_2 recovery from reformate mixtures that was 80% greater than that of the Pt/C catalysts.

3.3.2 Gas Diffusion Layer

For both the anode and cathode compartments, GDLs are porous layers that are in contact with the catalyst layers. An ideal GDL should have strong electrical and thermal conductivities and the ability to move reactants toward catalyst layers. While thermal conductivity is required for heat transfer from catalysts to other components, electrical conductivity is required for the movement of electrons. Because they offer strong gas permeability, which facilitates the movement of reactants, good electronic

conductivity, good compressibility, and stability in acid environments, carbon-based compounds are preferred [194] like carbon paper and carbon cloth.

Careful management of the liquid water inside the cells is required for the dependable and long-term operation of LT-ECHCs. As in the PEM fuel cell, overflooding can be avoided by covering the GDL with hydrophobic polytetrafluoroethylene (PTFE or Teflon) dispersion. However, LT-ECHCs are subject to some limitations when using coating methods based on PTFE to maintain water management. PTFE particles frequently block the holes in a low-porous GDL structure and may not stick to the porous surface very effectively. Additionally, the PTFE treatment procedure must be carried out at a high temperature in a protected environment, which raises the complexity and expense of the process.

As a result, various strategies can be used in GDL applications. Lee et al. [195] applied a hydrophobic coating made of a Nafion® and O-CNT mixture on porous copper metallic GDL. They noticed that the Nafion®/O-CNT coating eliminated anode flooding. Lee et al. [196] used silver particles in another research for a hydrophobic metallic GDL. Additionally, they discovered that the hydrophobic porous metallic GDL improved the water management capability. In contrast to fuel cell applications, high anode-cathode pressure differences should be considered in ECHC, and GDL should withstand the pressure difference. SUS316L was used by Hao et al. [151] as the mechanical support and backing layer to shield the MEA from the pressure differential during the ECHC operation.

3.3.3 Bipolar Plates

Graphite is used mostly as a bipolar plate material in fuel cells due to its excellent electrical conductivity and chemical stability [197]. However, there are drawbacks of graphite plates, such as high permeability, difficult machining, and expensive manufacturing. Thicker graphite plates should be used as bipolar plates due to their brittleness, which increased the volume and mass of stacks [198]. Metals and composites are alternative materials to graphite [199] (as shown in Figure 3.6). Bipolar plates can be made from a variety of non-coated and coated metals [200]. Metallic bipolar plates demonstrate strong mechanical strength, good machinability, low gas

permeability, reduced thickness and weight, good electrical and thermal conductivity, and ease of mass production [201]. In ECHC studies, there is a significant pressure difference between the anode and cathode compartments. Therefore, metal bipolar plates are used instead of graphite material.

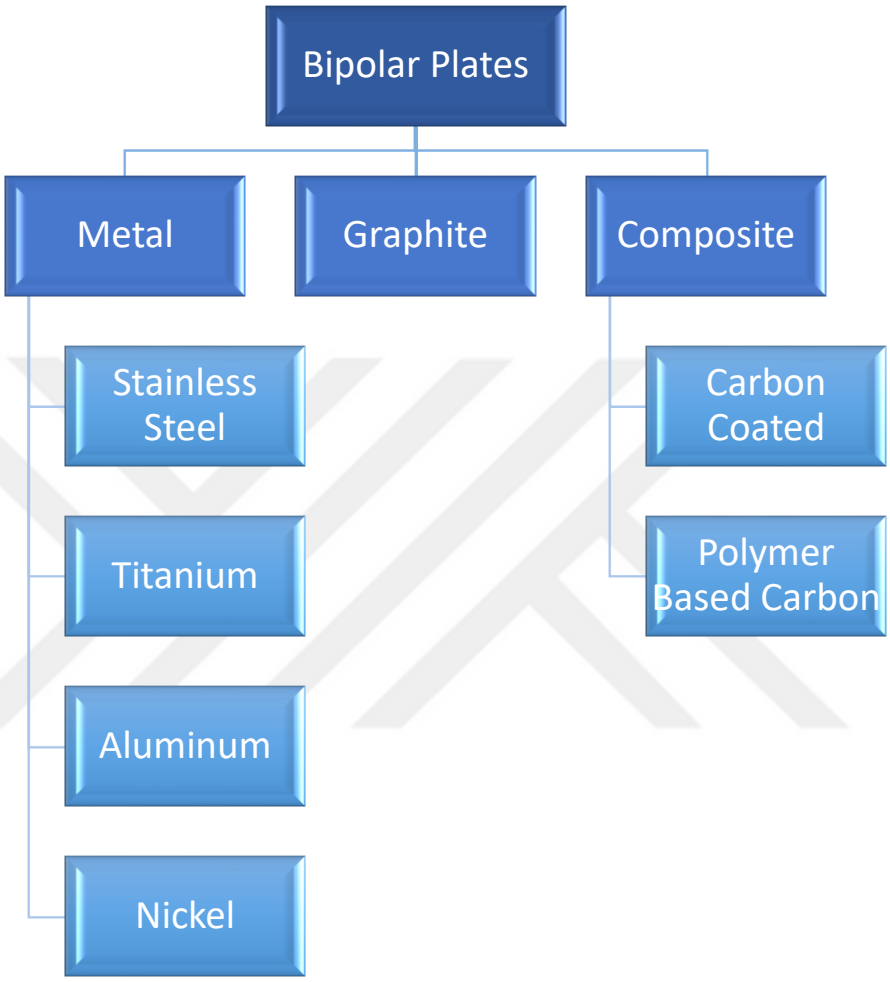

Figure 3.6 Bipolar plate materials (based on Ref. [202])

They supply the flow of reactants as well as collect and conduct electrons. Since ECHC applications are not commercialized as fuel cells or electrolyzers, there is not much research in the literature on flow channels. However, it is possible to find commonly used flow geometries in fuel cells and electrolyzers in the literature and based on these findings suitable flow geometry can be found for ECHC. Figure 3.7 shows bipolar plates with different flow geometries.

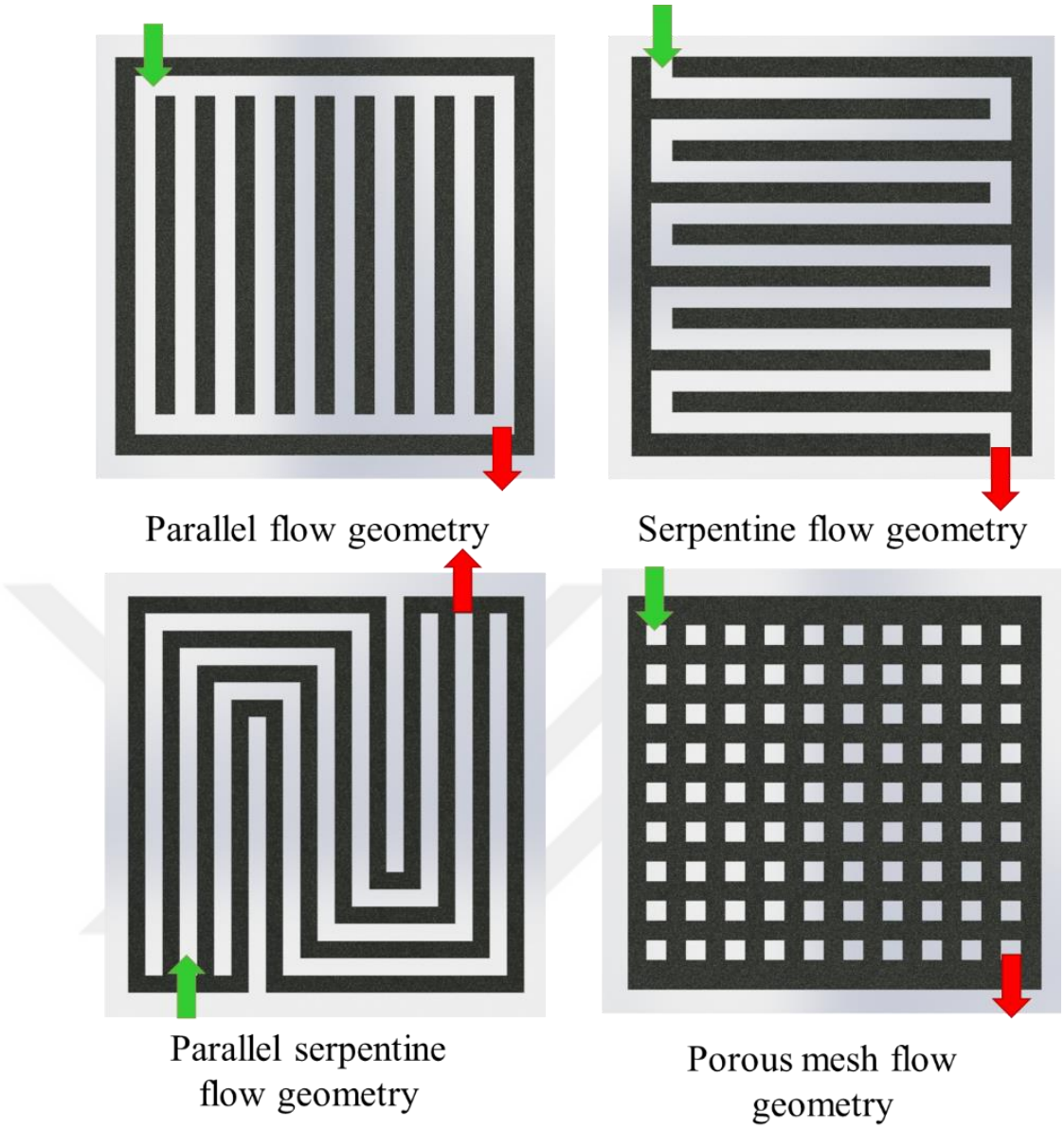

Figure 3.7 Bipolar plate flow geometries with inlet (green) and exit (red) directions of the reactant

3.3.4 Sealing and O-rings

Gaskets ensure that the gas stays in the MEA and moves only in the desired path. In addition, it is one of the most critical components in pressurization experiments. They must be able to keep the gas inside, being resistant to high temperatures and chemical corrosion. Polymeric materials are generally used as gaskets [203].

Kapton seals and o-rings are preferred for compression tests in the literature. O-rings are machine elements used for sealing purposes. It ensures that the overlapping

machine parts fit together perfectly. The most important features of Viton o-rings are that they can operate under high temperatures. These o-rings can work without any problems at temperatures of +240 °C [204]. In addition, it appears with its chemical-resistant structure. It can be used for many years with its flexible and durable structure. They can be installed quickly and easily [205].

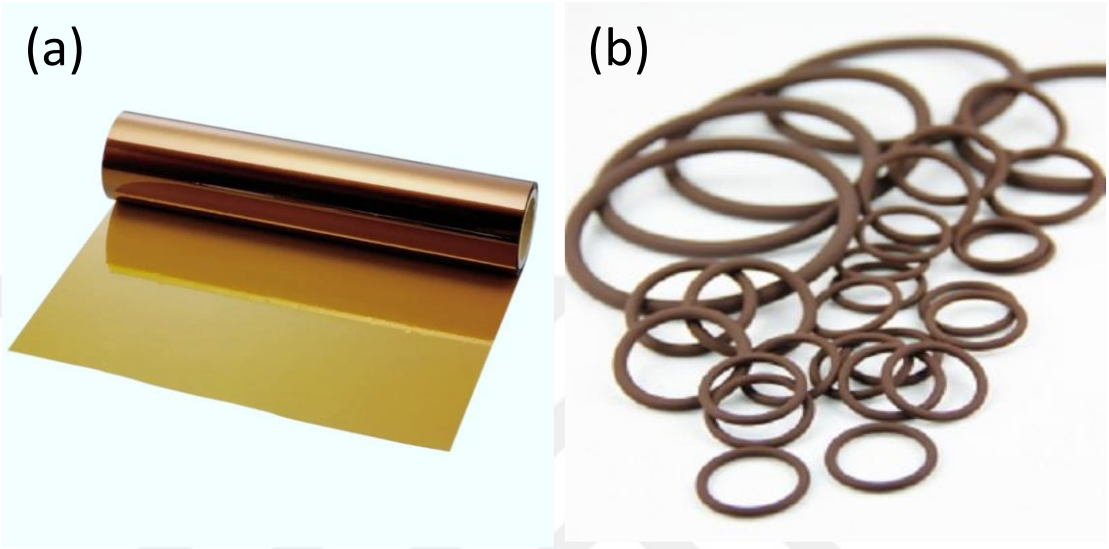

Figure 3.8 a) Kapton seal and b) Viton o-rings

3.3.5 End Plates

The end plates must be resistant to mechanical and chemical degradation because they serve as the ECHC's primary structural support. The materials should not deform under high pressure and temperature in an acidic environment. For better pressure distribution, the thickness of the end plates must be carefully determined, as the number of bolts. During ECHC operation, the anode and cathode end plates must be electrically isolated [206], [207]. The end-plate material should be inert to the gases utilized since the end plates also serve as gas connectors for supplied and exit gases. According to their operating temperatures, active areas, and current densities, the materials used for ECHC are listed in Table 3.3 briefly.

Table 3.3 Literature survey on ECHC components

Membrane	Anode Catalyst	Gas Diffusion Layer	Bipolar Plate	Operating Temperature (°C)	Ref.
Nafion® 117	Pt/Ru	Metal felt	N/A	24- 70	[126]
Nafion® 212	Pt	Carbon	Graphite	20	[172]
Nafion® 117	Pt	Carbon paper	N/A	35, 55, 75	[73]
Nafion® 115	Pt/Ru	N/A	Graphite	20- 70	[144]
Nafion® 115	Pt	N/A	Titanium	30- 70	[143]
Nafion® 105, Nafion® 115, Nafion® 117	Pt	N/A	N/A	25±2	[128]
Nafion® 117	Pt	N/A	Graphite	25- 60	[122]
PBI	Pt	N/A	Graphite	120- 160	[123]
Nafion® 1110	Pt/C	Stainless steel	N/A	60	[125]
SPEEK-CrPSSA	Pt/C	N/A	N/A	80	[150]
Nafion® 115	Pt/Ru	N/A	Graphite	25	[145]
PBI	Pt	N/A	Carbon flow field	160- 200	[179]
Nafion® 212	Pt	Carbon-based	N/A	60	[190]
Nafion® 212	Ir, Pt	Carbon-based	N/A	70	[192]
Nafion® and O-CNT	Pt	Hydrophobic coated metallic	N/A	65	[195]
Nafion®	Pt	Porous metal @anode/ pristine porous metal @cathode	N/A	65	[196]

Table 3.3 Literature survey on ECHC components (continued)

Nafion® 115	Pt	Carbon	Graphite	22	[140]
Nafion® 117	Pt/C	Carbon paper @cathode/ carbon cloth @anode	N/A	30, 60	[151]
Nafion® 115	Pt/C	N/A	N/A	25	[208]
$La_{0.9}Ba_{0.1}YbO_{3-a}$	Pt	N/A	N/A	600, 800	[209]
Nafion® 117/XL Nafion® XL	N/A	Carbon-based @cathode/a gold-coated Ti @anode	N/A	60	[153]
Nafion® 115	Pt	Carbon cloth	Aluminum	25	[137]

3.4. Effects of Operating Parameters on ECHC Performance

The performance of the ECHC is significantly influenced by various operating factors, including H_2 permeability and thickness of the membrane operating temperature, humidification level for low-temperature applications/ acid doping for high-temperature applications, and ECHC design. The literature contains numerous studies that evaluate how these factors affect performance.

Appropriate humidity/acid doping and temperature are factors that significantly impact proton transport in the ECHC. Nafion® membrane must be humidified for proton transport in ECHC systems because it is frequently used at low operating temperatures. The lack of water production on the cathode side means there is not enough water in the cathode to moisten the membrane through electro-osmotic drift, therefore, ECHC systems require external humidification. The ECHC was examined by Hao et al. [151] with an internal humidifier. Liquid water is present in the internal humidifier, which directly moistens a polymer electrolyte membrane. The internal humidifier led to improved proton conductivity. To determine the effects of various humidity levels, Zou et al. [210] conducted an experimental study at operating temperatures between 30 and 90 °C, and inlet pressures between 30 and 90 kPa. Their findings showed that the increase in current density resulted in H_2 dehydration and inadequate humidity

increased ohmic losses. The electro-osmotic drag from the anode to the cathode caused by the high current density is another factor that raises ohmic losses. These observations collectively demonstrated the need to maintain the equilibrium between proton transport and humidity levels carefully. Grigoriev et al. [73] compressed H_2 up to 130 bar. According to the findings, from the start of the experiment, the gas humidification level should be observed since the lack of moisture in the H_2 gas causes mass transportation restrictions, which raises energy consumption and reduces efficiency.

H_2 gas permeates from the cathode to the anode due to the pressure differential between the two electrodes. Ströbel et al. [128] examined the influence of membrane thickness on H_2 permeability. They discovered that as membrane thickness is reduced, H_2 permeability increases. Also, they indicate that although back diffusion cannot be entirely stopped, acceptable back diffusion rates can be established. Zou et al. [92] investigated the impact of membrane thickness on mechanical strength. According to their research, the mechanical strength of the membrane is crucial because of the high pressure present in ECHC operating conditions. Thin membranes with excellent mechanical strength should be created for ECHC applications, while H_2 permeability is also considered.

Chouhan et al. [137] tested a Nafion® 115 membrane at room temperature. An experimentally confirmed theoretical formulation for the ECHC was proposed to investigate back diffusion's impact. They used a single cell with a voltage of 0.1 V to achieve a pressure of 150 bar. Although high-performance ECHCs appear more attractive than conventional mechanical compressors, it was found that back diffusion is a significant issue limiting ECHC performance. Huang et al. [176] reported a fascinating investigation on 160, 180, and 200 °C and found that, when utilizing para-PBI, the CO tolerance for the Pt catalyst rose as the temperature climbed (from 38% to 72%). m-PBI looks to be the best high-temperature membrane that can be utilized for ECHC, despite para-PBI having the maximum proton permeability due to its good permeability and long-term durability.

Kim et al. [149] investigated the impact of various Pt loading on the ability of the ECHC to compress H_2 and separate H_2-CO_2 at a temperature of 160 °C. They obtained

80 mV voltage and 0.8 A/cm^2 current density for H_2 compression. Additionally, when the Pt loading on the anode side was reduced from 1.1 mg/cm^2 to 0.2 mg/cm^2, the cell voltage in the separation experiment increased by 72%.

The ECHC stack performance was compared by Chouhan et al. [130] between the electrically connected in series and the flows being parallel (ESFP), the electrically connected in series and the flows being in series (ESFS), and the hybrid of ESFP and ESFS. With the same number of cells and under the same operating conditions, it was found that the ESFP configuration had a higher power and work efficiency than the other two configurations. In the ESFP configuration, all membranes have a greater propensity to fail because they are exposed to high-pressure differentials. It implies that if even one membrane fails, the stack will lose pressure and become useless. The pressure difference will also be divided in series in the ESFS configuration, where electrical connection and flow are both in series, and membrane failure will be less likely. Therefore, it is advised to choose the configuration that is connected in series in both the electrical and flow directions for ECHC applications.

3.5. Importance of High-Temperature ECHC

Before ECHC can be fully commercialized, a few problems must be handled. CO poisoning is the primary issue that reduces cell performance [176]. CO molecules are strongly adsorbed on one Pt atom (terminal site), two adjacent Pt atoms (bridging site), or three adjacent Pt atoms (three-fold hollow site). In the first two cases, the reaction efficiency is reduced because the active area required for HOR is occupied by CO. In the case of CO, which is tightly bound to three adjacent Pt atoms, a blocking layer forms on the surface and Pt loses much of its active site for the reaction [211]. The poisoning of Pt by CO is shown in Figure 3.9.

Hydrocarbon-based H_2 production contains 20% CO_2 by volume in the fuel, and the CO_2 can be converted to CO by the RWGS reaction. According to Gu et al. [212], 1% by volume of CO released at low temperatures can cover more than half of the catalyst surface [213]. Therefore, besides CO, CO_2 can be considered one of the critical factors that reduce performance in low-temperature applications.

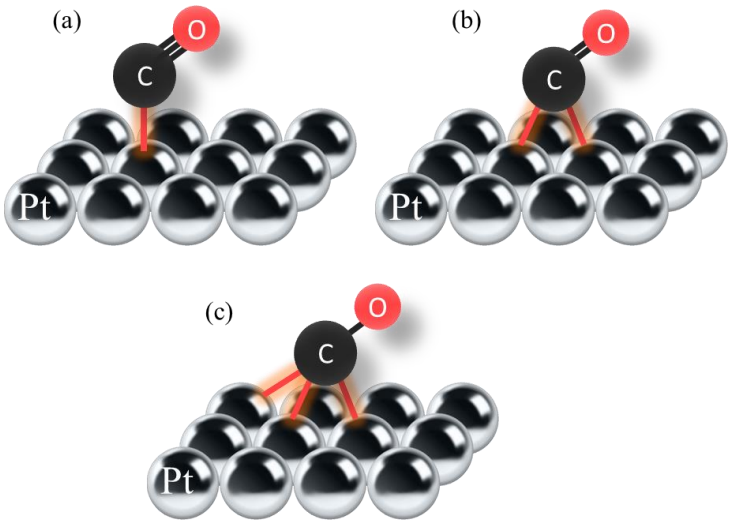

Figure 3.9 CO poisoning of the bare Pt surface a) terminal site, b) bridging site, c) three-fold hollow site (modified from Ref. [214])

The other important factor is maintaining proton conductivity and high durability. The Nafion® membrane inside the LT-ECHC must be properly humidified and kept hydrated [174]. Due to inadequate humidification, water may build up in the electrode layers or along the gas flow channels [175]. Excessive moisture can block access to catalyst active regions, lowering cell performance. The HT-ECHCs are unable to humidify the membrane with water because it was operating above the boiling point of water. As a result, HT-ECHC applications (up to 200 °C) without water management offer significant benefits and PBI membranes provide substantial advantages for HT-ECHC applications due to their superior thermal stability, high chemical resistance, and simple water management. The high operating temperatures provide higher impurity tolerance to Pt catalyst and faster electrode kinetics for anodic and cathodic reactions [175], [176].

The best option appears to be a membrane made of PBI, which operates at high temperatures while having excellent proton conductivity and high thermal stability [189]. However, the proton conductivity of the bare PBI membrane is low. H_2SO_4 and H_3PO_4 have the highest conductivities of these acids, and PBI can readily react with both [177].

CHAPTER 4

EXPERIMENTAL STUDIES

4.1. Materials

PBI polymer was synthesized according to the reported procedure [189]. Diaminobenzidine tetrachloride hydrate (DAB.4HCl.2H_2O, 98%), isophthalic acid (IPA, 99%), polyphosphoric acid (PPA, 115%), phosphoric acid (H_3PO_4, 85%), and N,N Dimethylacetamide (DMAc) isopropyl alcohol ($CH_3CH(OH)CH_3$), purchased from Sigma-Aldrich (USA) and used exactly as received. Polytetrafluoroethylene (60 wt. % dispersion in H_2O, Sigma-Aldrich), gas diffusion layer (GDL) (Freudenberg, Germany), and platinum-supported carbon catalyst (Pt/C 40 wt. %, Johnson Matthey, UK) were used for MEA preparation. High-purity H_2, CO_2, CO, and N_2 gases (>99.98%) were provided from Linde (Turkey).

4.2. MEA Preparation

4.1.1. Membrane Preparation

The solution casting method was used to preparation of the PBI membrane. First, PBI polymer (5 wt.%) (Figure 4.1 (a)) was dissolved in DMAc solution at atmospheric pressure (Figure 4.1 (b)), and the homogeneous solution was cast onto the glass surface (Figure 4.1 (c)). The surface of the cast glass was dried for 12 hours at 80 °C in a ventilated oven. shows the PBI membrane preparation steps.

PBI membrane must be doped with strong acid for proton conductivity. For acid doping, PBI membranes were kept in H_3PO_4 for a week (Figure 4.1 (d)). The membranes were taken out of the solution, the excess acid was wiped off with blotting paper, and they were stored in an airtight container until the tests.

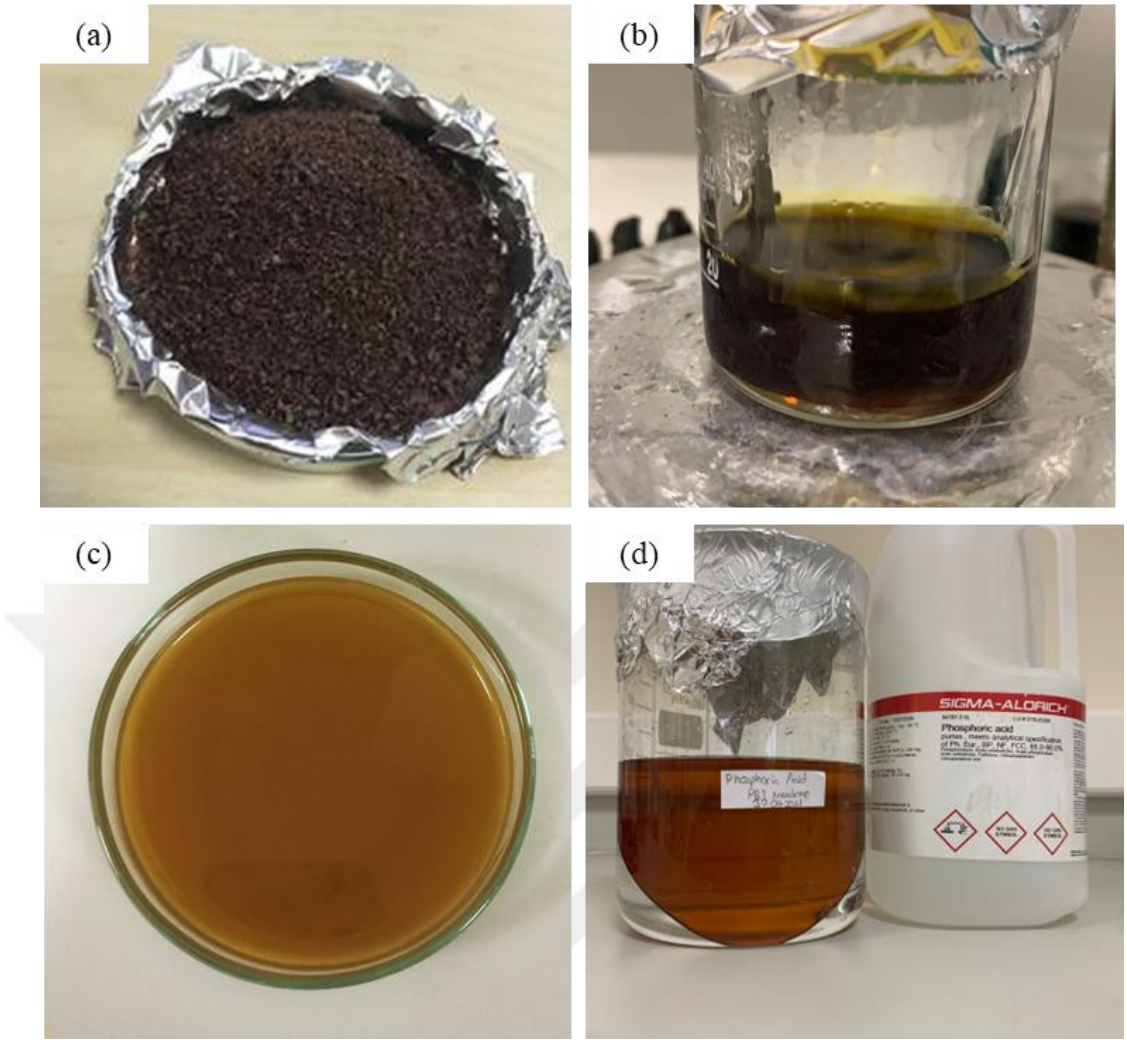

Figure 4.1 PBI membrane preparation steps

Membrane acid doping level can be determined from Equation (16):

$$Acid\ doping = \frac{W_{PA}}{W_{dry}} \times \frac{MW\ of\ PBI\ repeat\ unit}{MW\ of\ H_3PO_4} \quad (16)$$

where W_{PA} and W_{dry} are the weight of the H_3PO_4 doped membrane, and dry membrane (g), respectively, and MW indicates molecular weight (g/mol) [176]. The acid doping level of the PBI membrane was determined as 12.

The proton conductivity of the PA-doped PBI membrane was determined by a four-probe analysis with Electrochemical Workstation (WonATech, Korea). The conductivity tests were executed in the longitudinal direction under non-humidified conditions. Equation (17) was used to calculate the proton conductivity.

$$\sigma = \frac{L}{r \times w \times t} \tag{17}$$

where σ (S/cm) is the proton conductivity, r (Ω) is the membrane resistance, w (cm) is the membrane width, t (cm) is the membrane thickness, and L (cm) is the space between the conductivity cell's two probes. Table 4.1 shows the properties of undoped PBI and PA-doped PBI membrane.

Table 4. 1 Properties of the undoped and PA-doped PBI (modified from Ref. [215])

Properties	**Undoped PBI**	**PA-doped PBI**
Proton Conductivity (S/cm)	-	0.083
σ_{UT} (MPa)	140.9 ± 5.0	13.1 ± 1.2
E (GPa)	2.030 ± 0.12	0.080 ± 0.01
Elongation at break (%)	83 ± 10	151 ± 5
H_2 Permeability at 160 °C (Barrer)	12.7	836

4.1.2. Gas Diffusion Electrode Preparation

The process outlined by Devrim [216] was used to prepare the catalyst ink. Catalyst ink contains PVDF, DMAc, 5 wt. % PBI solution, and Pt/C catalyst (Figure 4.2 (a)). The ultrasonic coating process was used to manufacture the gas diffusion electrode (GDEs) (Figure 4.2 (b)) due to the high homogenous distribution of catalyst with the least amount of loss [217]. An ultrasonic spray coater (Sono-Tek/the model ExactaCoat) and 120 kHz Impact Nozzle were used on commercial carbon paper GDL at 80 °C. The coating procedure was fully computer-controlled and programmed concerning the coated area. Before atomization at the nozzle, the catalyst ink was loaded into a syringe pump, leveled to a flow rate of up to 0.5 mL/min, and sprayed over the GDLs to create 1 mg/cm^2 catalyst loading. Figure 4.2 (c) shows the prepared GDE.

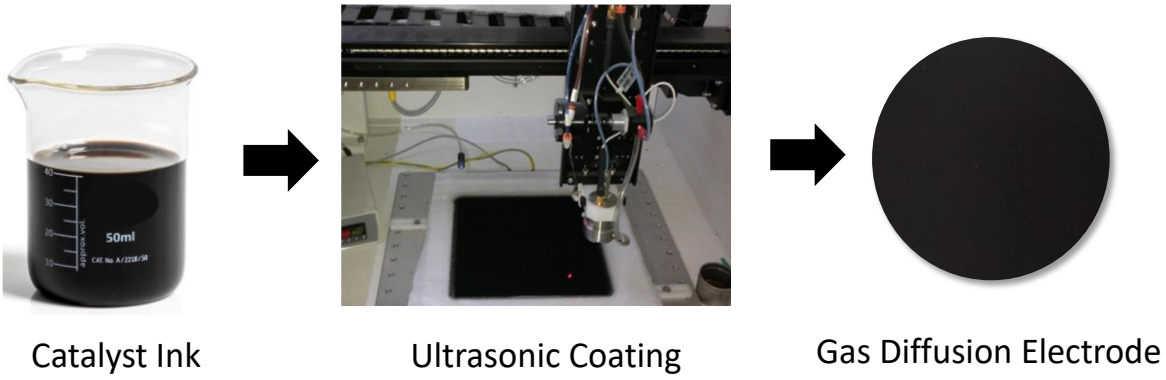

Figure 4.2 GDE preparation steps

Finally, GDEs were hot pressed onto the H_3PO_4 doped PBI membrane at 150 °C and 172 N/cm^2 for 15 minutes. Figure 4.3 shows the steps of the MEA preparation steps.

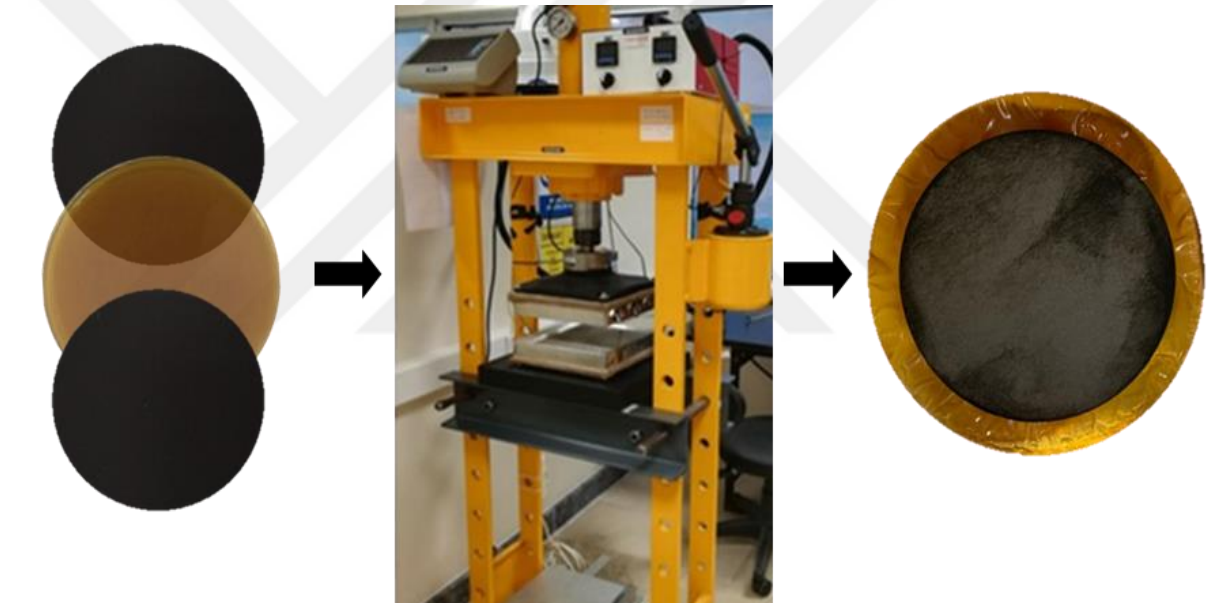

Figure 4.3 MEA preparation steps

4.3. HT-ECHC Single Cell and Stack

When the literature is examined, it is seen that the PEM fuel cell design and components are used in ECHC studies. Although ECHCs show similarities with PEM fuel cells, there are differences in cell design and components, especially considering high-pressure conditions. A single cell consists of two compression plates, two gas and current distribution plates, o-rings, Ti mesh and felt group, and an MEA.

HT-ECHC systems should have compression plates that provide the desired homogeneous force distribution. Compression plates are made of 316 quality stainless steel with a thickness of 40 mm. In addition to the holes for the gas supply and exit on the anode and cathode end plates, holes for the thermocouples are also created. To maintain a constant pressure distribution over the MEA and reduce the resistances of the GDEs, the HT-ECHC test cell was compressed using a torque wrench. Figure 4.4 shows the anode and cathode end plates with a technical drawing.

Within the scope of the thesis, considering the flow plate simulation results and the latest studies in the literature, a two-layer gas distribution plate was used to obtain low-pressure loss in the flow channels and homogeneous gas distribution in the gas diffusion layer. Although graphite plates can often be used in gas flow channels in PEM fuel cells, titanium materials are preferred in ECHC when high-pressure conditions and cell strength are considered [125], [126], [196]. However, it is a difficult method to process the gas flow channels used in PEM fuel cells bipolar plates on pure Ti plates with the CNC machining technique. Therefore, bipolar plates were manufactured with Ti-alloyed stainless steel.

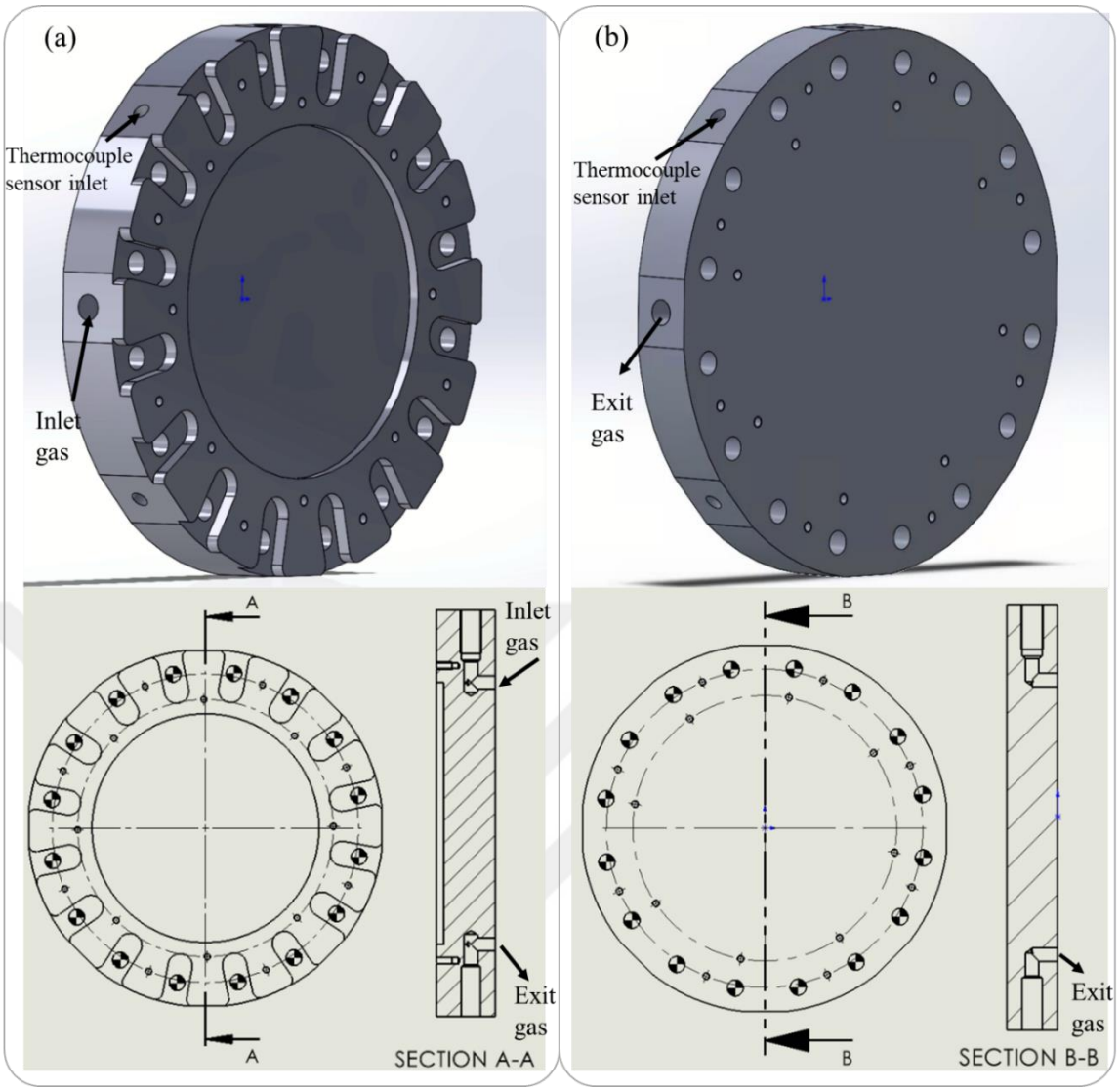

Figure 4.4 a) Anode end plate, b) cathode end plate

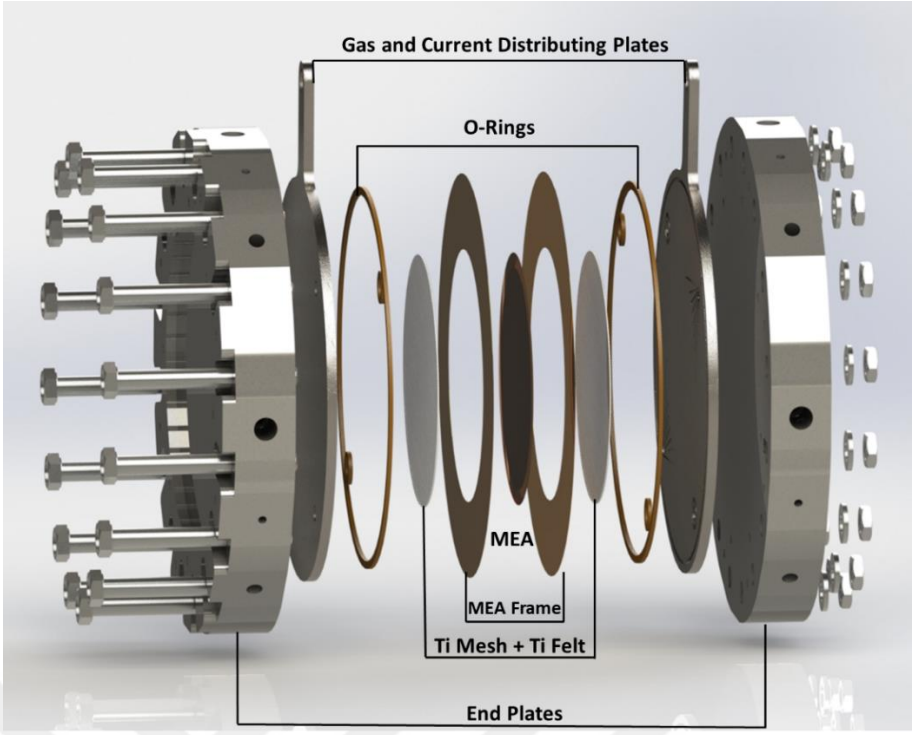

Figure 4.5 Single-cell HT-ECHC

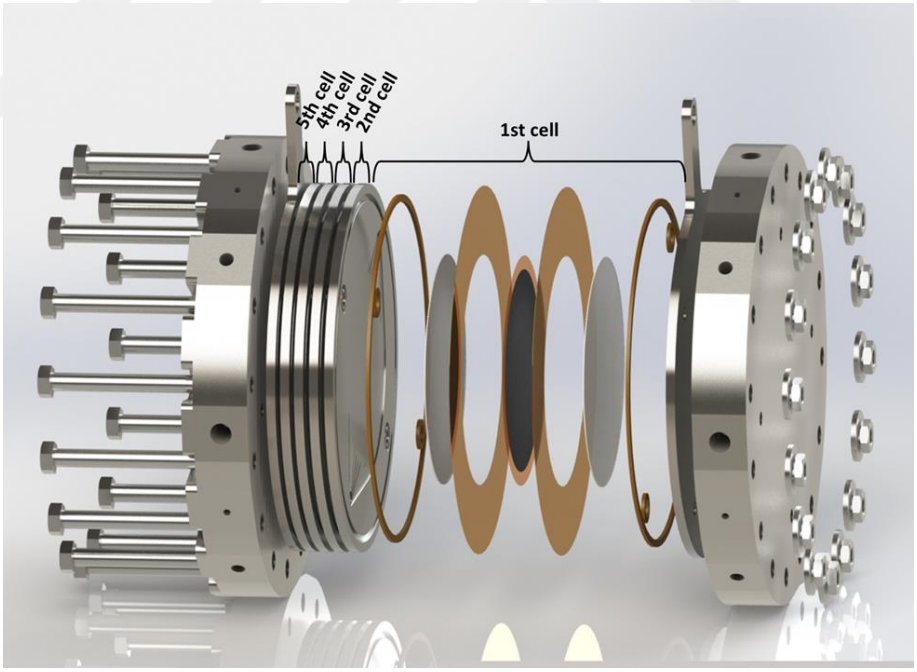

Figure 4.6 HT-ECHC stack with 5 cells

In the design, 5 mm 316-Ti doped steel gas distribution plates are placed in front of the Ti mesh gas distribution plate. Considering the acidic operating conditions in the cell, porous titanium sieve plates with a porosity of 56% and a thickness of 0.2-0.3

mm (uncompressed height) were used due to high corrosion resistance. The gas fed to the cell reaches the porous Ti sieve gas distribution plate and the gas mixture is homogeneously distributed in the HT-ECHC with the help of the mesh structure. In HT-ECHC systems, impermeability is important in terms of both purification and pressurization. The Viton o-rings were preferred with their resistance to high temperature and high mechanical stress. In Figure 4.5 and Figure 4.6, 3D designs of HT-ECHC single-cell and HT-ECHC stack with five cells are given, respectively. Within the scope of the thesis, a 5-cell HT-ECHC stack was designed with the same active area as a single HT-ECHC cell. The 5-cell HT-ECHC is electrically connected in series so that one side of the stack remains as the anode and the other as the cathode pole.

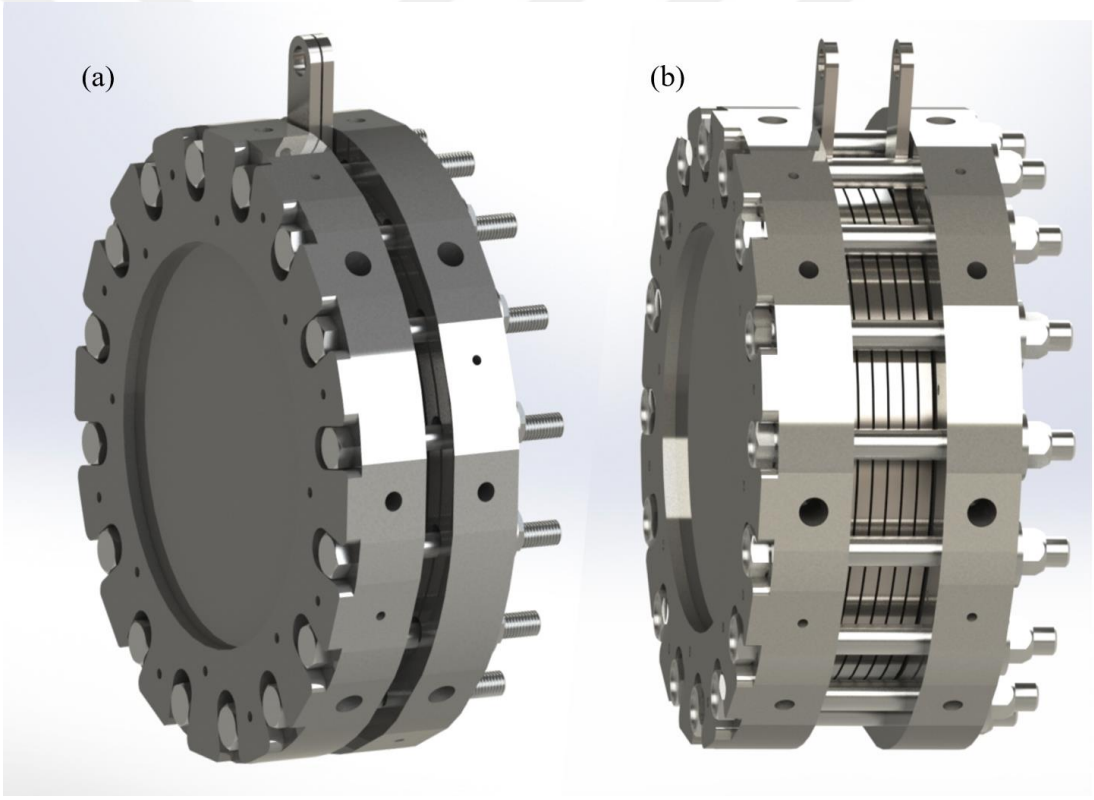

Figure 4.7 Assembled render view for (a) single cell and (b) stack

The anode bipolar plate was first placed on the end plate and o-rings were placed in the channels available on the bipolar plate. After, the MEA structure was placed on the bipolar plate. A single cell consists of this assembly closed with the cathode bipolar plate and the end plate. For the stack, bipolar plates and MEA structures were placed step-by-step and similar to the single cell, the stack closed with a cathode end plate.

Figure 4.8 shows the HT-ECHC cell preparation. Assembled single cell and the stack are shown in Figure 4.9.

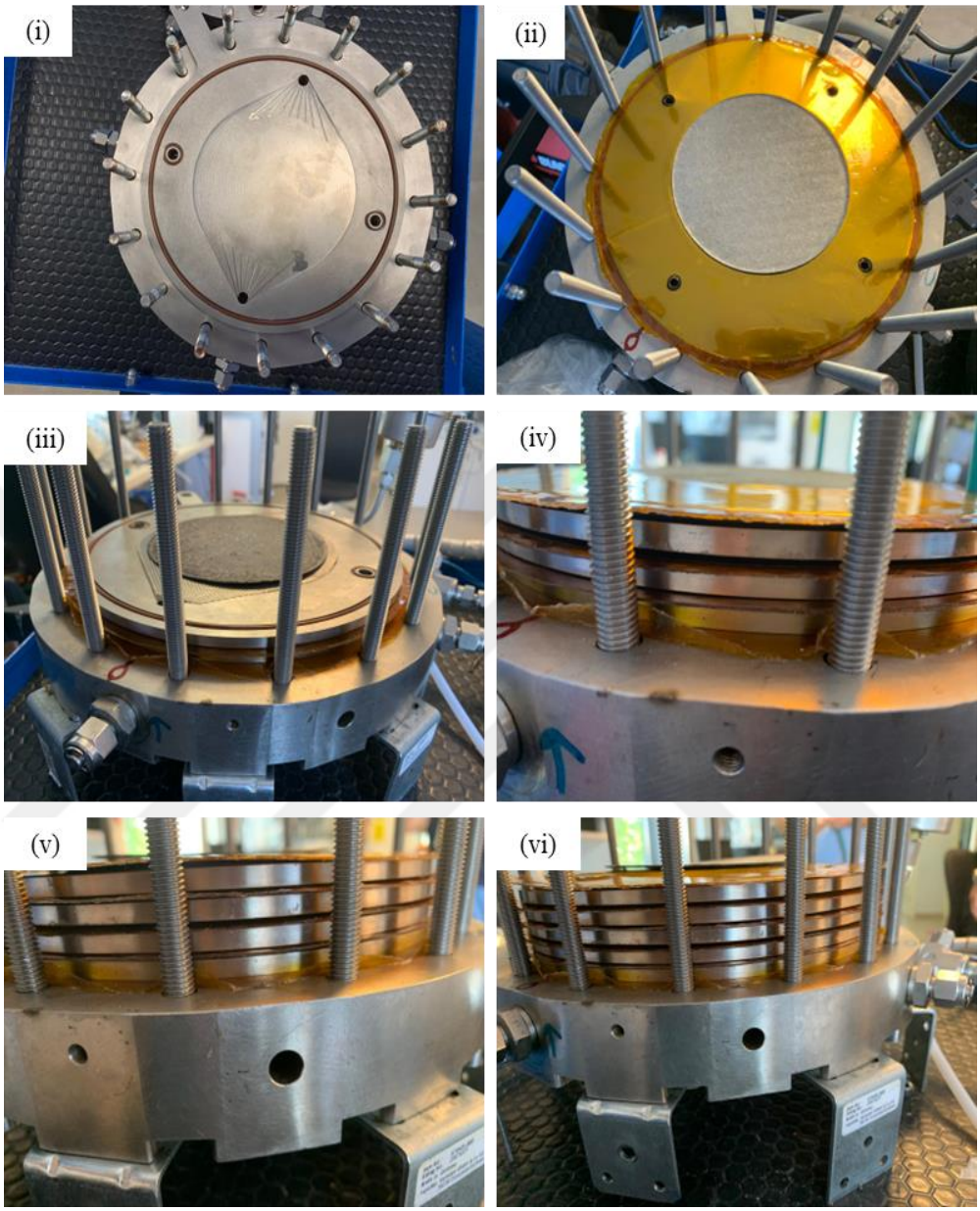

Figure 4.8 HT-ECHC cell preparation

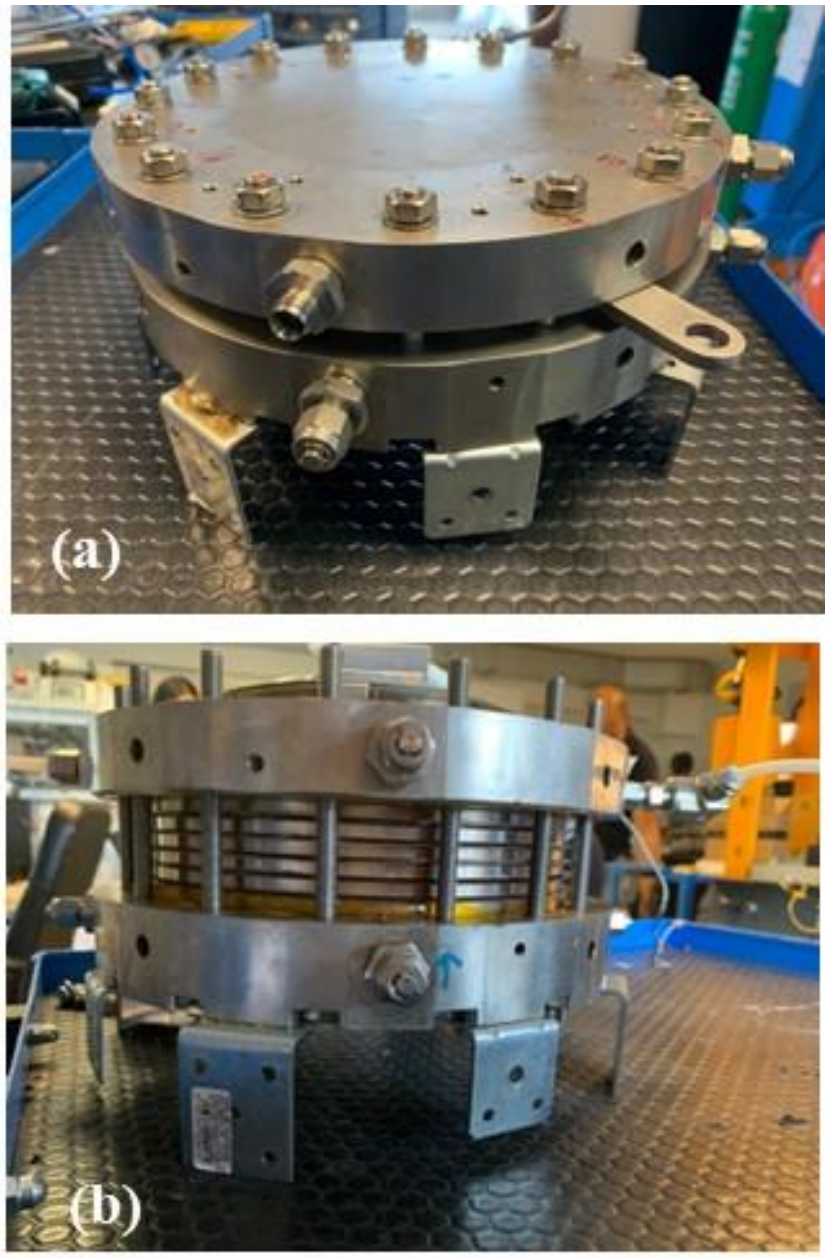

Figure 4.9 Assembled HT-ECHC single cell and stack

4.4. HT-ECHC Test System

Figure 4.10 shows the flow diagram of the HT-ECHC test station. After the gas mixtures are adjusted at the desired rates with mass flow controllers, enter the anode. N_2 acts as a purge gas. All gases were kept in high-pressure gas cylinders, and Teflon tubing was used to connect them to the HT-ECHC cell test station. The gas temperature was raised from room temperature to cell temperature during the performance tests using heated gas lines. The flow of the gas streams was regulated using mass flow

controllers (Alborg). The current collector plates of the HT-ECHC test cell were wired to an external DC power source.

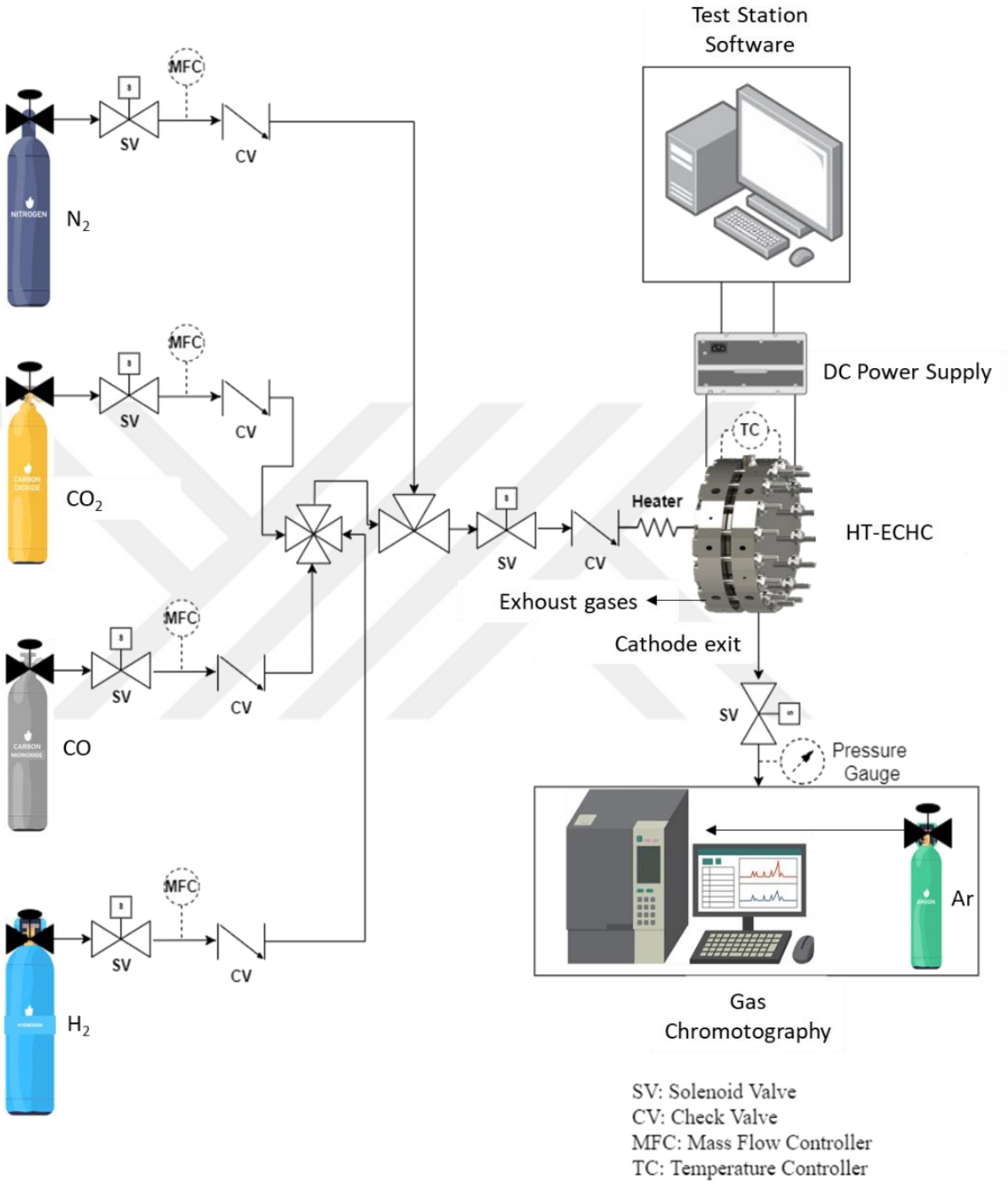

Figure 4.10 Diagram of HT-ECHC test station

Two heating rods, one on the cathode side and one on the anode side, were used to keep the cell temperature constant. The operating temperature of the HT-ECHC test

cell was determined by thermocouples connected to the cell, and the temperature was controlled by heaters. Swagelok supplied every fitting.

Figure 4.11 HT-ECHC test station

The HT-ECHC cell was stabilized at 0.2 V for 2 hours before the performance tests, then voltage and current data were collected. From the open-circuit voltage (OCV) to 1 V for pure H_2 and 1.4 V for reformate gas mixtures, the current values in steps of 0.05 V were recorded. At 140, 150, 160, 170, and 180 °C, HT-ECHC performance

curves were obtained using a variety of gas streams, including pure H_2 and the reformate gases RG-1 (H_2:CO_2:CO-75:25:0), RG-2 (H_2:CO_2:CO-72:26:2), RG-3 (H_2:CO_2:CO-75:22:3), RG-4 (H_2:CO_2:CO-75:20:5), RG-5 (H_2:CO_2:CO-97:0:3), RG-6 (H_2:CO_2:CO-95:0:5). Reformate gas compositions are shown in Table 4.2. The tests conducted under atmospheric pressure.

Table 4.2 Gas compositions for HT-ECHC purification experiments

Gases	**H_2 (Vol. %)**	**CO_2 (Vol. %)**	**CO (Vol. %)**
H_2	100	-	-
RG-1	75	25	-
RG-2	72	26	2
RG-3	75	22	3
RG-4	75	20	5
RG-5	97	0	3
RG-6	95	0	5

A gas chromatograph (GC) (Shimadzu Co., Nexis GC-203) was used to analyze the gas composition (H_2, CO_2, and CO) of the HT-ECHC cathode stream using an automated gas sample valve. The thermal conductivity detector (TCD) was installed in the GC, and Ar was chosen as the carrier gas. Before the experiments, the TCD detector was calibrated for the quantitative analysis using different gas mixtures (including CH_4, NH_3, CO, CO_2, N_2, and H_2) with known concentrations. Gas calibration curves based on peak area were used to determine the compositions of the cathode exits.

After the sample is injected into the system since the velocity of the components in the sample varies depending on the compound, they separate from each other in the column Curves are drawn with the electrical signals coming out of the detector. In a typical chromatogram, the horizontal axis shows the time until the component reaches the detector, if the component is defined, a peak is drawn according to its intensity (Figure 4.12). The vertical axis shows the intensity of this signal [218]. HT-ECHC

purification tests were repeated twice while the cell was operating at constant voltage and the margin of error of the GC analysis was determined as ±0.001.

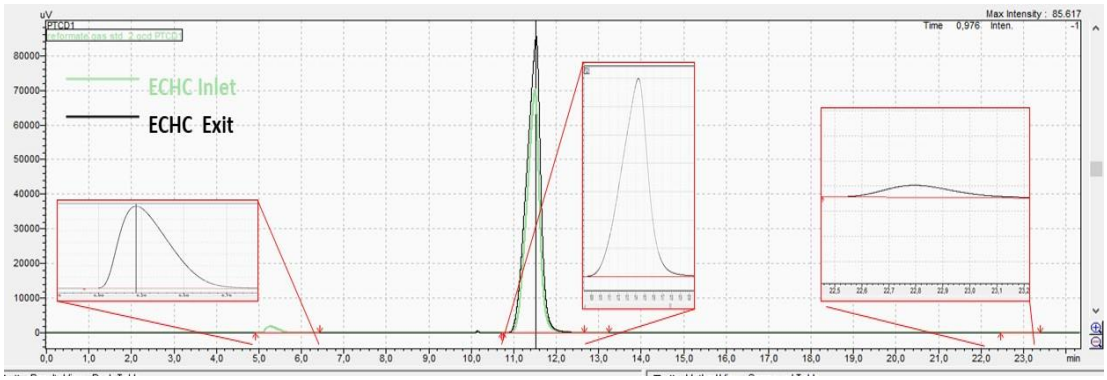

Figure 4.12 Typical GC chromatogram for RG-3

CHAPTER 5

RESULTS AND DISCUSSION

5.1. Bipolar Plate Design and Flow Analysis Results

The H_2 purification rate in ECHC systems depends on the gas composition supplied to the system, the components used in the cell and the cell design. One of the most important parameters affecting the performance of ECHC systems is the design of gas flow channels through which the H_2 and/or reformate gas mixture is distributed to the cells. Flow plates' crucial functions in the cell are controlling electrical conductivity, current density distribution, thermal conductivity, and mass transport. In addition, the design of flow plates directing the flow of gases entering the ECHC stack affects the pressure drop on both the anode and cathode sides, thus affecting the ECHC performance. Since both purification and pressurization will be done in ECHC, the flow geometry that will minimize the pressure drop is selected. Within the scope of the thesis, gas flow analyses were performed using SolidWorks Flow Simulation software to visualize gas flows, which are difficult to determine experimentally, and to examine the effect of different flow channel designs on pressure drop.

The designs of PEM fuel cell flow geometries have been used for bipolar plate geometries because there isn't enough information about HT-ECHC design in the literature. Firstly, flow plates were designed with square geometries based on the examples in the literature. Channel depth, width and height are taken as 1mm x1mm x1mm. Designed flow geometries with "Solidworks" shown in Figure 5.1 shows the wavy flow channel, parallel flow channel, serpentine flow channel, triple coil flow channel, parallel serpentine flow channel, pin flow channel, multiple serpentine flow channel, leaf flow channel, enmeshed flow channel-1, enmeshed flow channel-2, spiral flow channel, grid flow channel. As a result of the analysis, it has been determined that in square designs, pressure drops occur along the flow of gases in the flow channel. This situation causes problems in high pressurization conditions in ECHC systems.

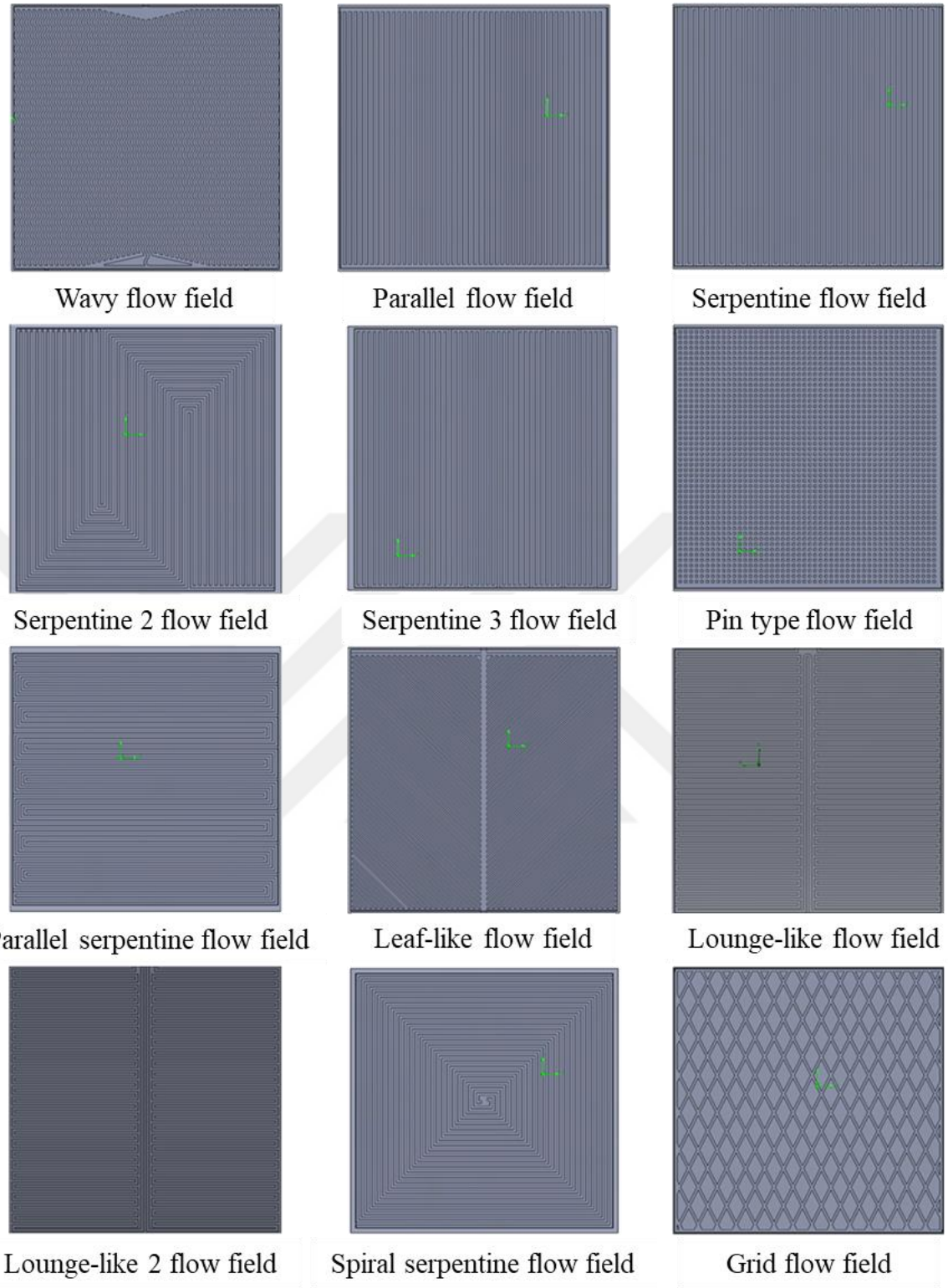

Figure 5.1 Bipolar plates of square flow geometries

In the literature, it has been observed that recent studies were also carried out with a circular design. The design is changed, and the circular designs were investigated to ensure homogeneous pressure distribution.

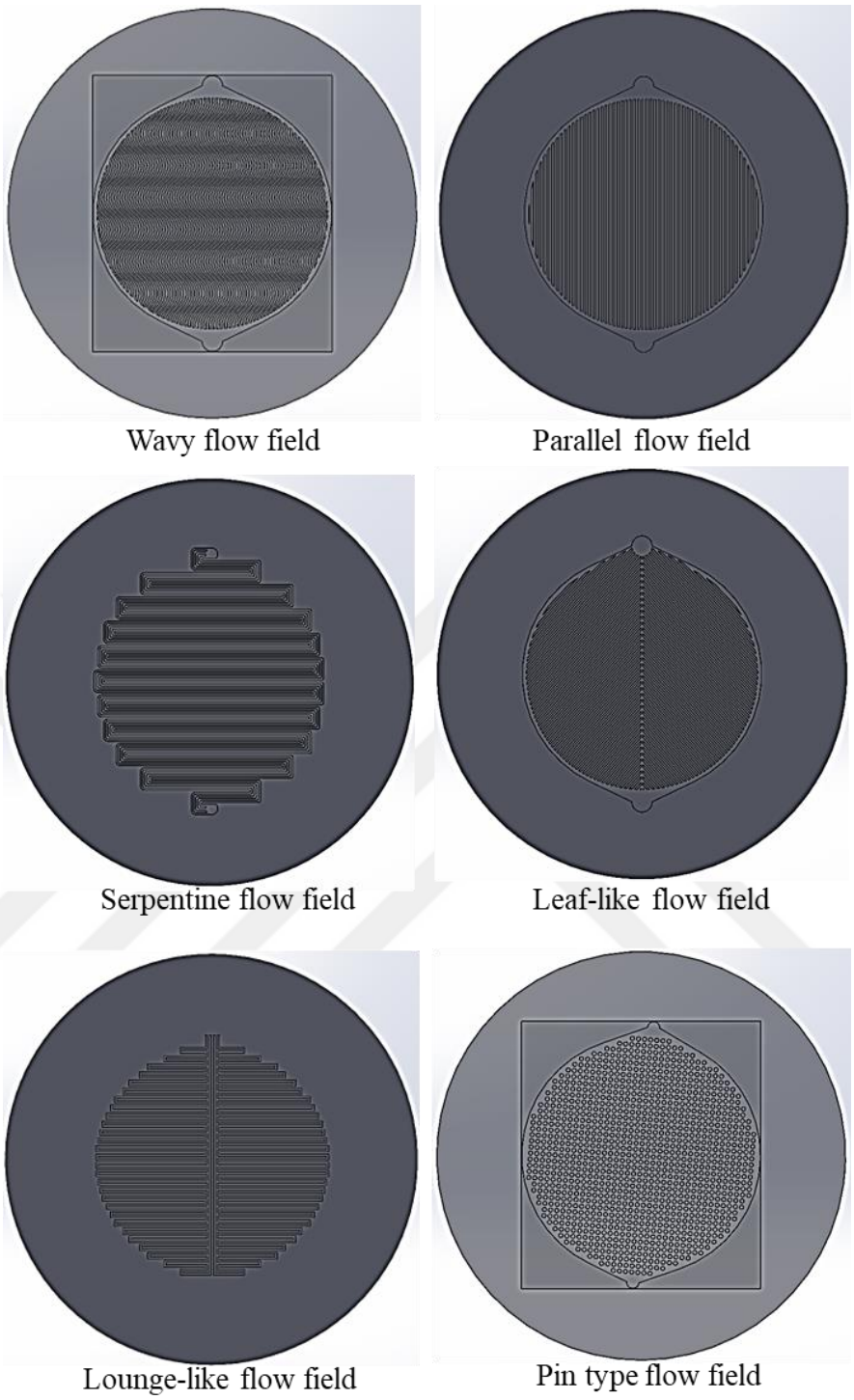

Figure 5.2 Bipolar plates of circular flow geometries

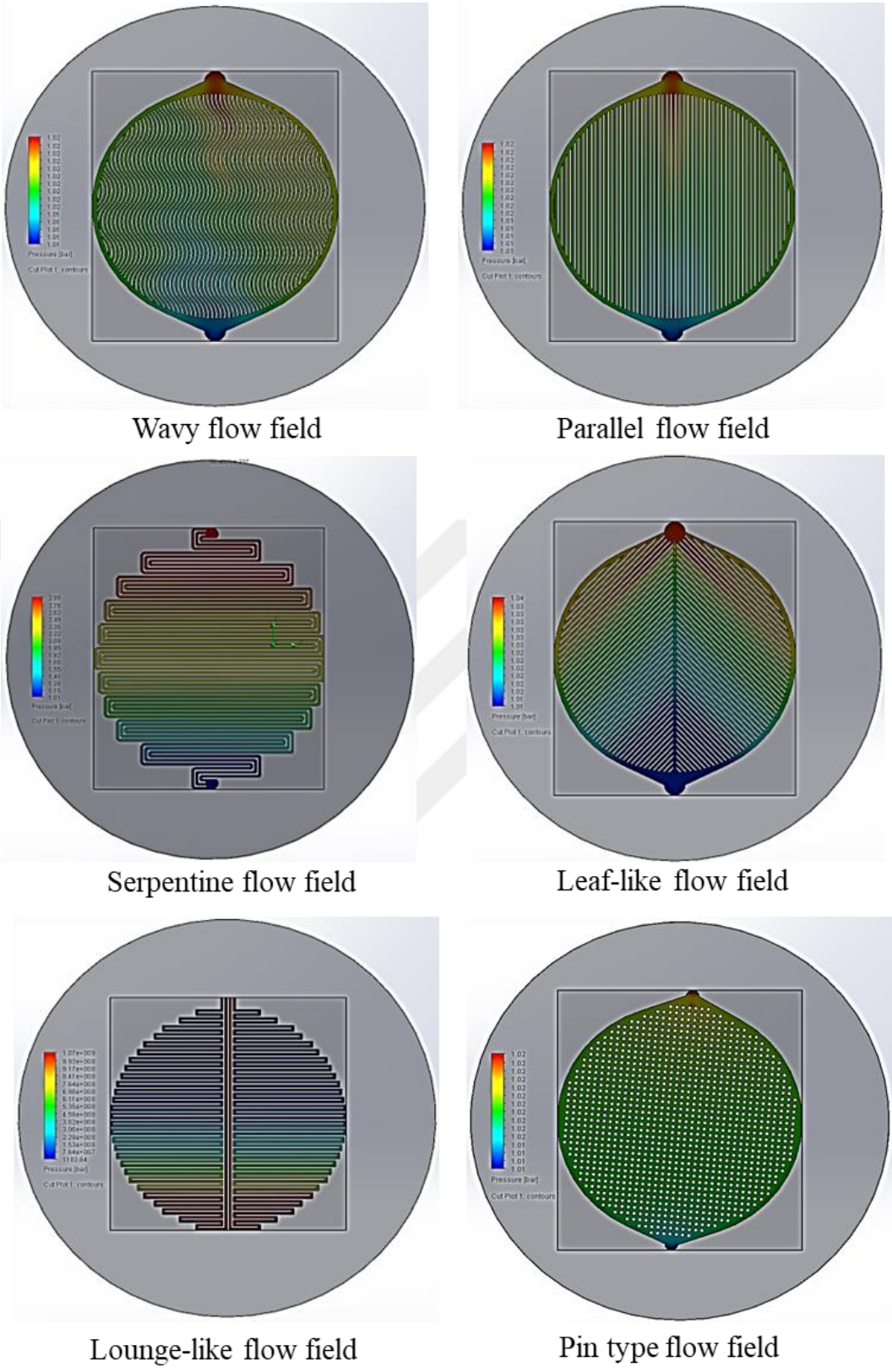

Figure 5.3 Pressure analysis of the bipolar plates

Flow simulation analyses were performed where channel depth, width, and height are taken as 1mm x1mm x1mm. 160 °C temperature and H_2 gas were used in all flow simulations. By the flow analysis results for each geometry, the pressure difference between the gas entering the flow channel and the gas leaving the channel was examined. Figure 5.3 shows the pressure contours of the wavy flow field, parallel flow field, serpentine 2 flow field, leaf-like flow field, lounge-like flow field, pin type flow field simulation where the “red” indicates higher pressures and “blue” indicates relatively low pressures.

According to the results of the analysis, it was determined that lower outlet pressure was obtained with the increase of the residence time of the gas in the cell. While the highest pressure was obtained in the different serpentine flow channels, it was observed that the pressure drop decreased in the flow channel with parallel flow geometry. The best results were obtained with grid and pin-type flow channels. However, the reduction of pressure drop across the flow channel is not sufficient for optimum flow channel design. Since the reaction time of the gas in the cell is reduced in the channels with low-pressure drops, the chance of the gas reacting also decreases. For this reason, a different flow channel design for the HT-ECHC application is investigated.

In the scope of the thesis, a two-layer gas distribution plate is used to obtain low-pressure loss in the flow channels and homogeneous gas distribution in the gas diffusion layer. In the two-layer gas distribution plate, a 5 mm 316-titanium doped steel gas distribution plate and integrated Ti mesh on the plate are used. The gases enter the cell with the channel on the flow plate and reach the MEA layer by dispersing homogeneously from the porous titanium mesh layer on the plate. With this design, since the first layer does not contain a flow channel as in classical designs, the gases are transmitted to the porous layer without pressure drop. Thanks to the Ti mesh integrated into the flow channel, the gases entering the cell are more homogeneously distributed over the MEA. Figure 5.4 shows the flow plate design of the HT-ECHC cell.

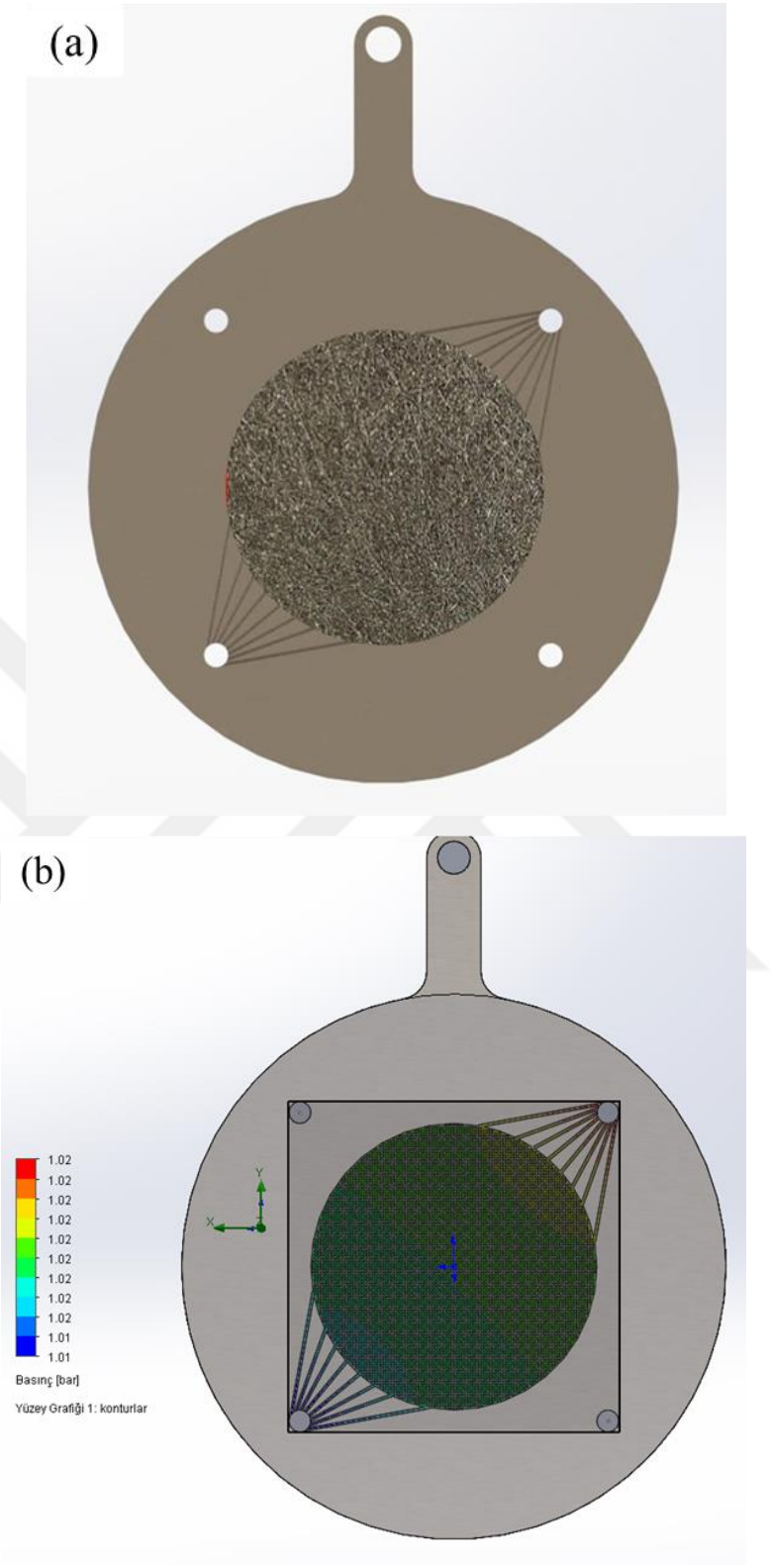

Figure 5.4 a) Flow plate of HT-ECHC cell, b) pressure analysis of flow plate

5.2. HT-ECHC Purification Test Results

5.2.1. Pure H_2 Experiments

First, pure H_2 was fed from the anode side. By adjusting the gas flow rate between 0.05 slpm and 1 slpm at 160 °C, it was possible to assess how the gas flow rate affected the performance of the HT-ECHC cell. The polarization curves for HT-ECHCs supplied by pure H_2 at various gas flow rates are shown in Figure 5.5.

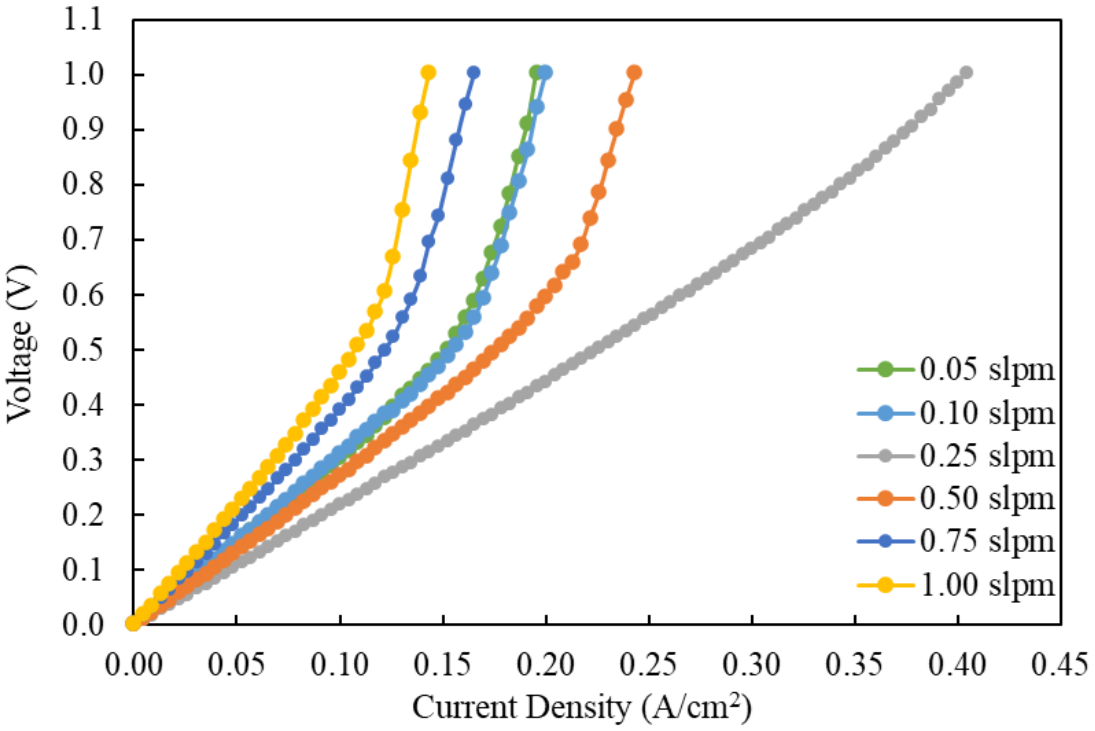

Figure 5.5 Polarization curves for pure H_2 at 160 °C with different H_2 inlet flow rates

The maximum current density recorded was 0.404 A/cm^2 with a flow rate of 0.25 slpm at 160 °C and 1 V. When the gas flow rate on the anode side is reduced, poor performance occurs as the reactants on the electrode surface are consumed [127]. As anticipated, performance degraded noticeably at flow rates lower than 0.25 slpm (0.1 slpm and 0.05 slpm). At 0.05 slpm and 1 slpm, the highest current densities were measured to be 0.195 A/cm^2 and 0.199 A/cm^2, respectively. It may be inferred that as the gas flow rate increases on the anode side, the gas exits the cell without undergoing an electrochemical reaction, which lowers performance. 1 slpm flow rate produced the lowest performance, which was followed by 0.75 slpm. In these circumstances, the gas

is fed quickly, sweeping the gas into the active area and lowering an electrochemical reaction. For 1 slpm and 0.75 slpm, respectively, the highest current densities were measured as 0.143 A/cm^2 and 0.165 A/cm^2.

The polarization curves of an HT-ECHC fed by pure H_2 at various operating temperatures are shown in Figure 5.6. At temperatures of 140, 150, 160, 170, and 180 °C, respectively, the voltage and current values were measured. All the experiments were conducted at atmospheric pressure (101.320 Pa) and a 0.25 slpm H_2 flow rate. The power supply's limiting voltage was maintained at 1 V, and data on current were recorded starting from 0 A and every 0.1 A. It has been noted that performance improves when the operating temperature rises from 140 °C to 160 °C.

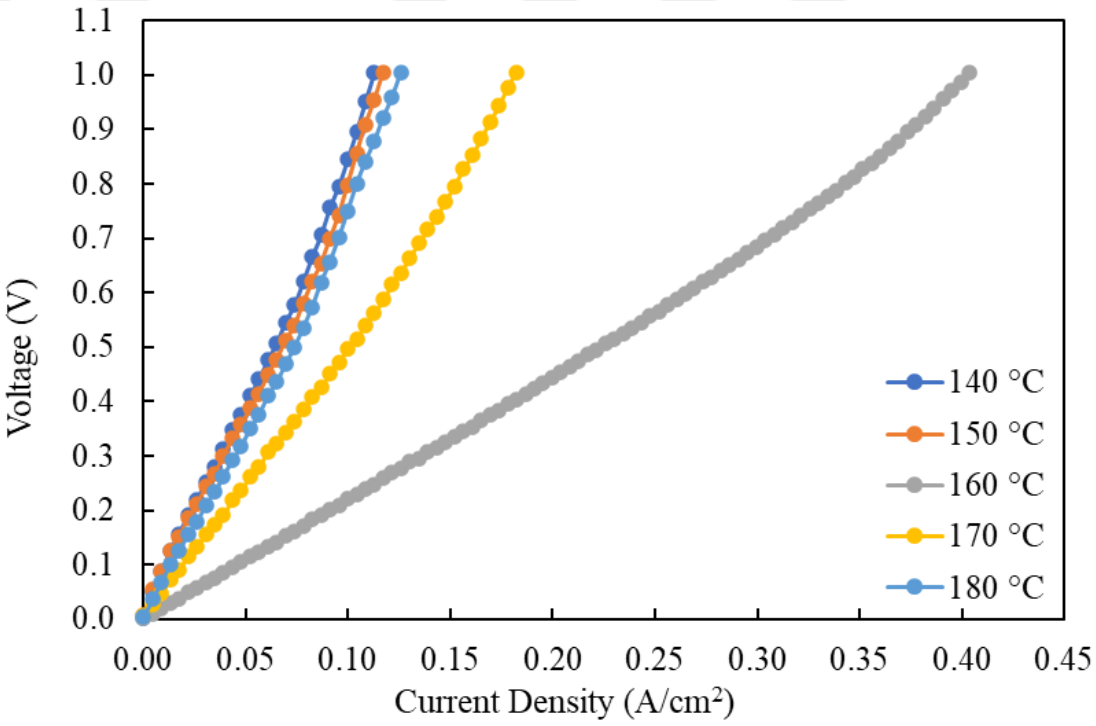

Figure 5.6 Polarization curves of HT-ECHC with pure H_2 at different operating temperatures

The relationship between temperature and membrane resistance can be used to explain how temperature has a favorable impact on cell performance [219]. The improved reaction kinetics of the electrodes at higher temperatures was observed. At 160 °C, the maximum achievable current density was measured as 0.404 A/cm^2. Consistent performance was not possible between 160 °C and 180 °C, the maximum current

densities at 170 °C and 180 °C were recorded as 0.126 A/cm^2 and 0.182 A/cm^2, respectively. Temperatures exceeding 160 °C, a drop in conductivity caused by the dehydration of orthophosphoric acid to pyrophosphoric acid [220], and potential stability problems occurred. Damage to other cell components due to increased HT-ECHC temperature may have resulted in lower performance [219], [221].

5.2.2. H_2 Separation from Reformate Gas Mixture

In this part, the effect of H_2, CO_2, and CO ratios in the reformate gas mixture on HT-ECHC performance was examined. In contrast to pure H_2 experiments, it was discovered that the OCV values of reformate gas mixtures were not zero because of variations in partial pressures [123]. Because reformate gas mixtures have contaminants, a higher voltage is needed for electrochemical purification than for pure H_2. Vermaak et al. [127] reported similar outcomes. Ohmic and mass transport resistance are the two main types of resistance in the HT-ECHC since the separation of H_2 is limited by contaminants in the supplied gas [221]. The performance of the RG-1 gas with 75% H_2 and 25% CO_2, is shown in Figure 5.7.

For the RG-1, the required voltages were measured as 0.396 V, 0.377 V, 0.360 V, 0.481 V and 0.545 V at a current density of 0.1 A/cm^2 and a temperature of 140, 150, 160, 170 and 180 °C. The minimum power consumption was found to be 0.036 W at 160 °C (Eq. (18)).

$$P = i \times A \times V \tag{18}$$

The performance of HT-ECHC cells improved with temperatures up to 160 °C. Due to the increasing reaction activity of electrodes with the increased temperature, it was found that overall performance had improved. The literature has noted comparable outcomes [127], [143].

However, a decline in HT-ECHC performance was observed as the operating temperature was raised higher. The performance loss may be connected to the reverse water-gas shift (RWGS) process at the high working temperature, where the CO_2 is converted to CO (Eq. (19) and (20)) [222].

$$2Pt + H_2 \rightarrow 2Pt - H \quad (19)$$

$$CO_2 + 2Pt - H \rightarrow Pt - CO + H_2O + Pt \quad (20)$$

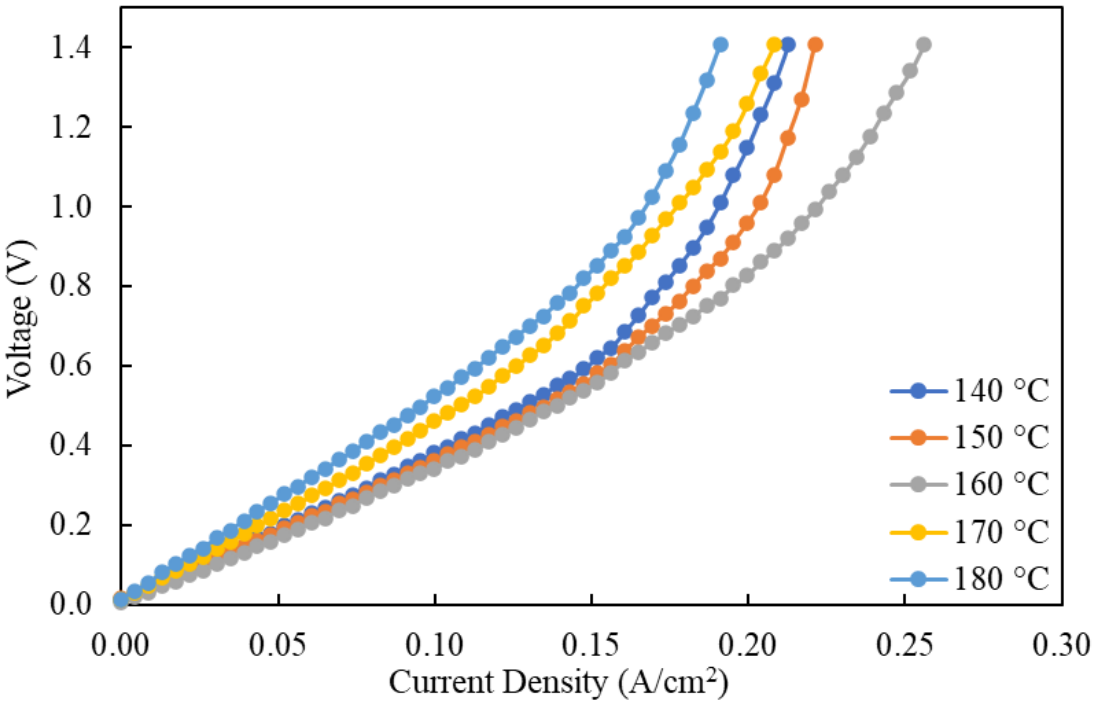

Figure 5.7 Polarization curves of HT-ECHC with RG-1 at different operating temperatures

In the RWGS reaction, CO_2 and H_2 on the catalyst combine to create CO, which subsequently adsorbs to the active areas of the catalyst and limits H_2 separation [223]. Even though CO_2 is considered inert, it has a harmful effect because of the creation of CO because of the RWGS [224]. The temperature is one of the critical factors impacting CO production because of the endothermic RWGS reaction. When the amount of CO_2 in the feed gas is high, even if the gas does not contain CO, the performance can degrade significantly because the RWGS reaction accelerates with increasing operating temperature. De Bruijn et al. [225] demonstrated similar results in their work. They discovered the production of CO increases as temperature rises. As a result of the RWGS reaction, CO would be formed up to 1% at the operating temperature range of 125-200 ℃ [226].

CO can be formed by the electrochemical reduction of CO_2 when voltage is applied, however, its contribution is negligible compared to the RWGS reaction [223]. Equation (21) shows that electrochemical CO_2 reduction reaction [227]:

$$CO_2 + 2H^+ + 2e^- + Pt \rightarrow Pt - CO + H_2O \quad (21)$$

In contrast to RG-1 gas, when RG-2, RG-3, RG-4, RG-5, and RG-6 reformate gases were fed, performance was better as the temperature increased from 140 °C to 180 °C. The increased operating temperature leads to improved catalytic activity, enhanced electrochemical reactions [228], and reduced ohmic overpotential caused by the conductivity of the membrane [223]. The CO adsorption on the Pt catalyst is also decreased by the high operating temperature, which lowers Pt poisoning [229], [230]. CO is adsorbed on Pt-H sites formed during HOR and on bare Pt surfaces [231] given in the following equations:

$$CO + Pt \rightarrow Pt - CO \quad (22)$$

$$H_2 + 2Pt \rightarrow 2Pt - H \quad (23)$$

$$2CO + 2Pt - H \rightarrow 2Pt - CO + H_2 \quad (24)$$

Since CO adsorption is an exothermic process, the active site of Pt is covered by CO faster at low operating temperatures, forming poorly at high temperatures [232].

The performances of RG-2, RG-3 and RG-4 gases are shown in Figure 5.10, Figure 5.9, and Figure 5.10, respectively. In RG-2, RG-3 and RG-4 gases, the CO concentrations are 2%, 3% and 5%, while the CO_2 concentrations are 26%, 22% and 20% by volume. In all three gases, besides the direct negative effect of the CO, the above-mentioned RWGS reaction also causes the conversion of CO_2 to CO and performance degradation is expected in HT-ECHC. Polarization curves for RG-2, RG-3 and RG-4 reveal that performance decreases when CO content rises. Therefore, it can be concluded that as the vol.% CO increases, it has a greater effect than the RWGS reaction. Depending on the operating environment, these processes compete with one another [233]. The performance of the HT-ECHC is decreased by adding more CO to the reformate gas mixture because the CO adsorption is significantly faster than the RWGS reaction [234].

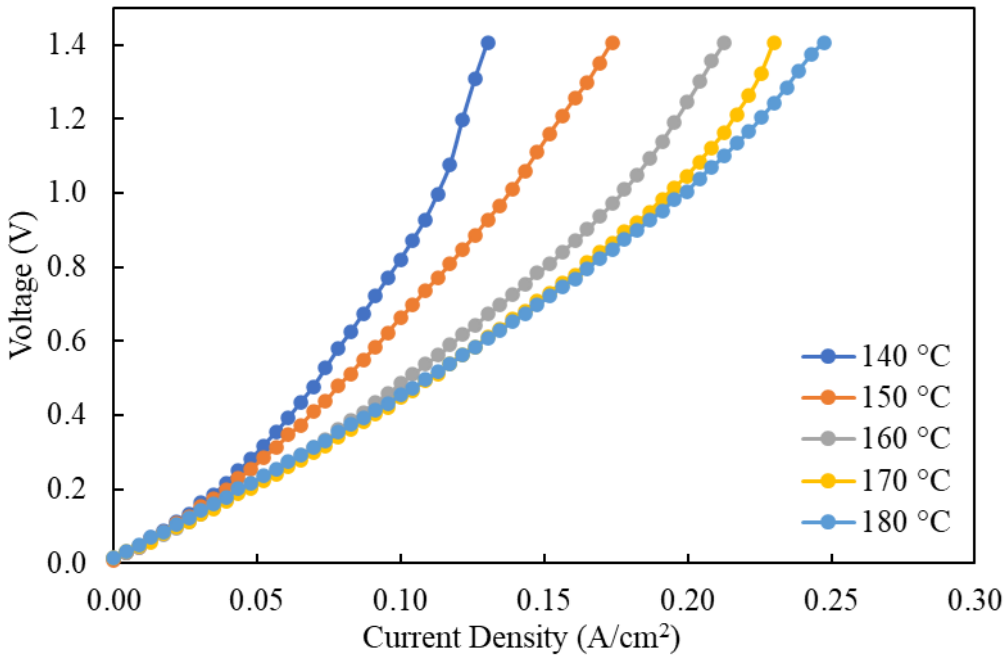

Figure 5.8 Polarization curves of HT-ECHC with RG-2 at different operating temperatures

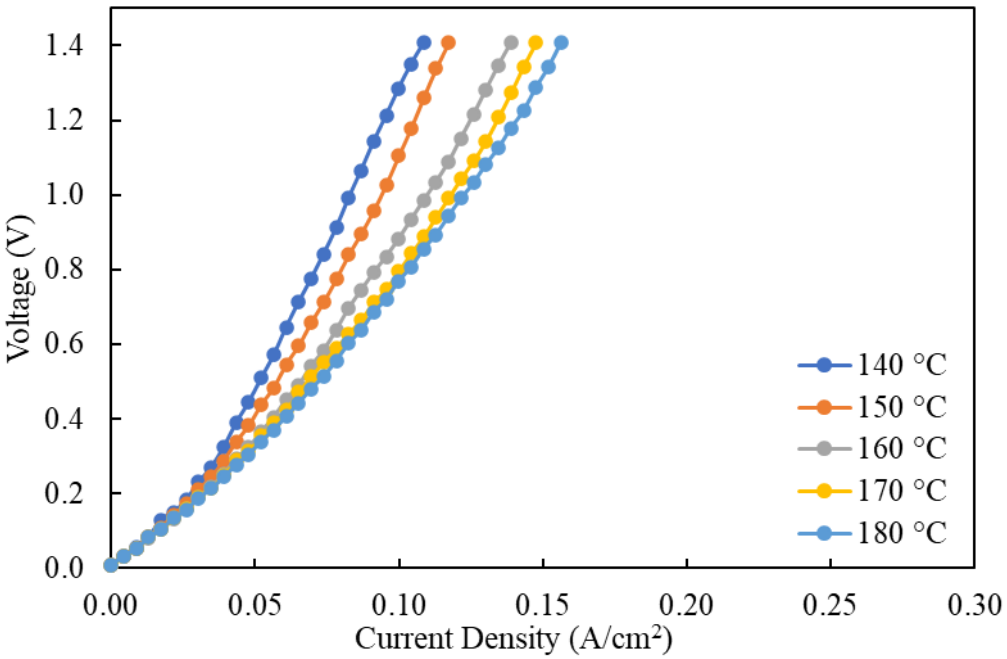

Figure 5.9 Polarization curves of HT-ECHC with RG-3 at different operating temperatures

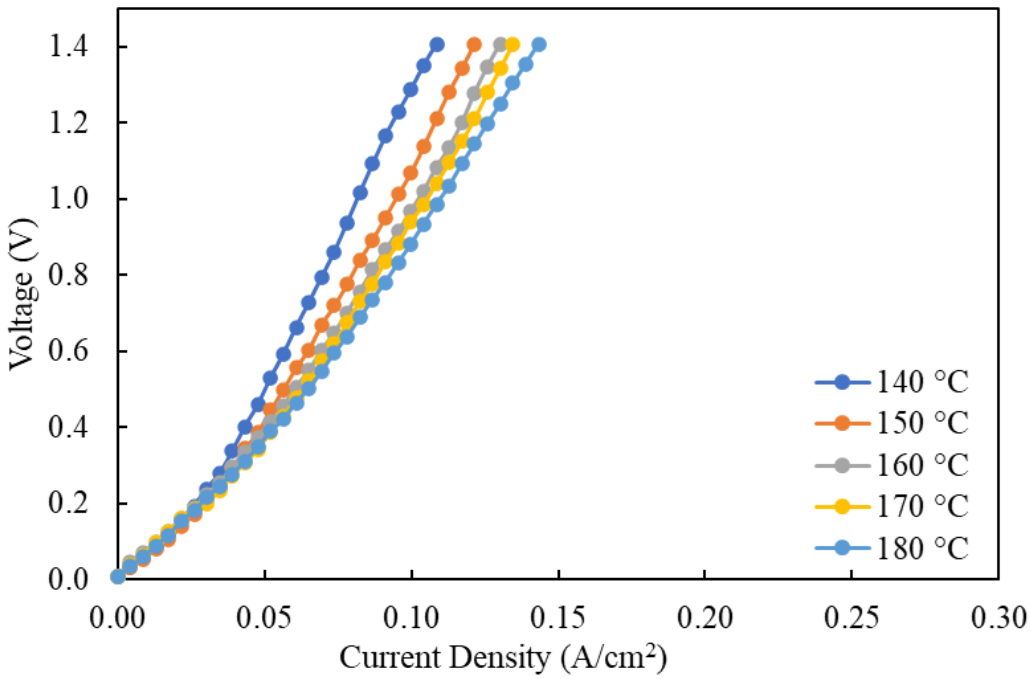

Figure 5.10 Polarization curves of HT-ECHC with RG-4 at different operating temperatures

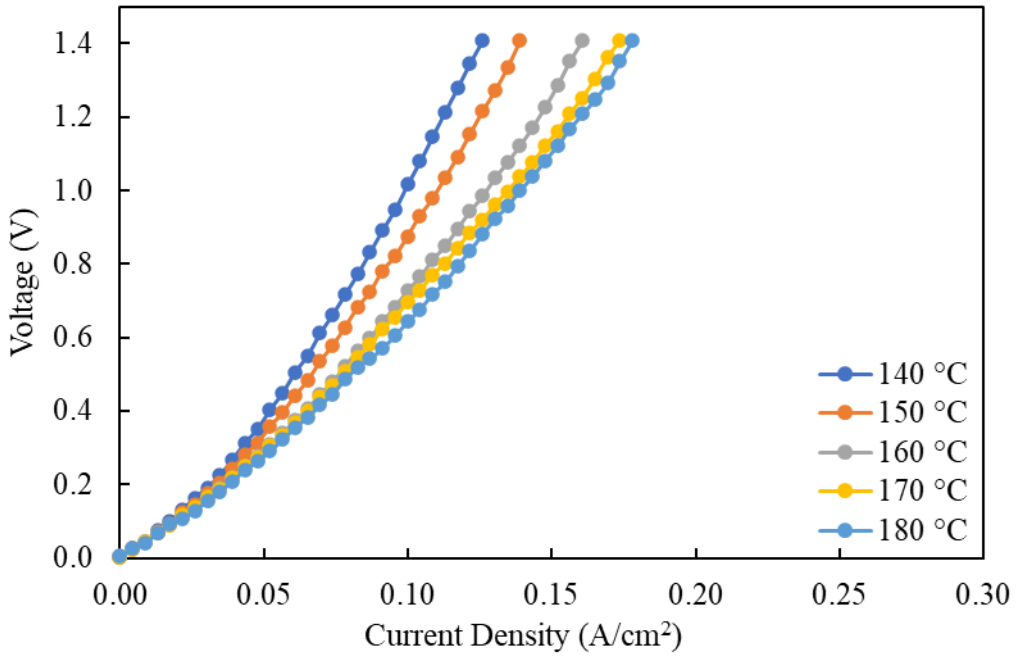

Figure 5.11 Polarization curves of HT-ECHC with RG-5 at different operating temperatures

Due to its low heat of adsorption, CO adheres to the Pt surface more easily than H_2. When more CO is adsorbed on the catalyst surface, less active areas for H_2 oxidation

are accessible. Therefore, there is a significant decrease in HT-ECHC cell performance in tests of RG-5 and RG-6 gases containing 3% and 5% CO by vol. as shown in Figure 5.11 and Figure 5.12, respectively. The cell performance also decreases with increased voltage [235].

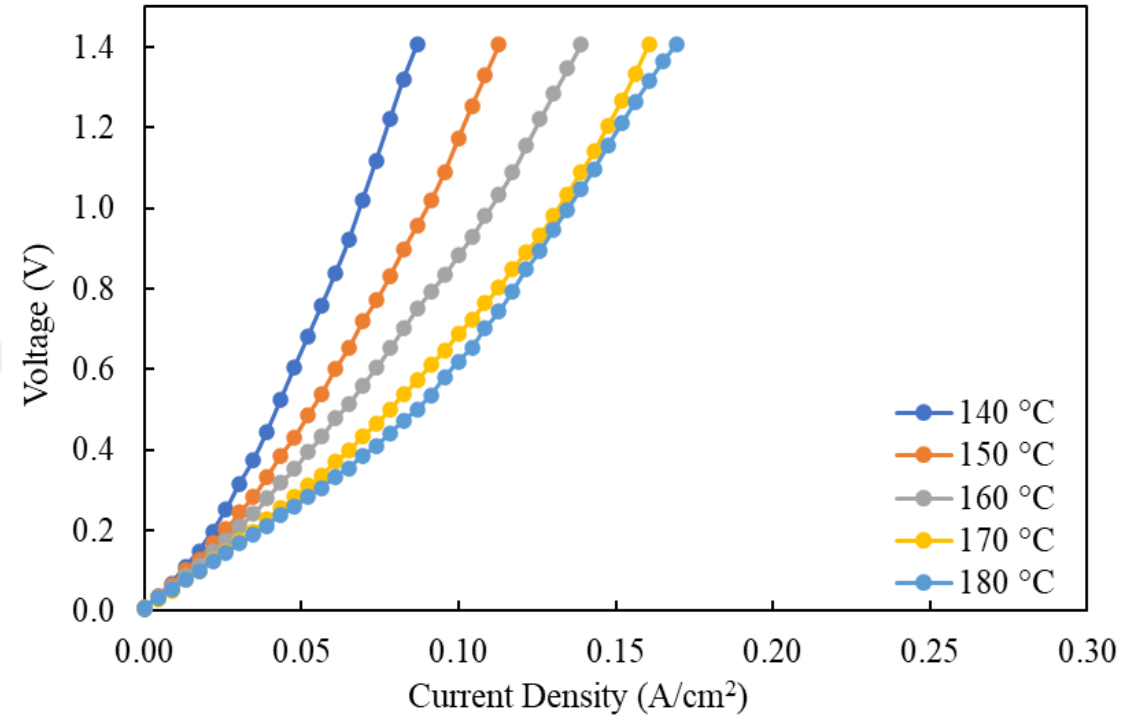

Figure 5.12 Polarization curves of HT-ECHC with RG-6 at different operating temperatures

To determine the electrochemical H_2 purification level, the GC analyzer was coupled to the HT-ECHC cell cathode output. Table 5.1 displays the analysis results. The two repetitions of GC analysis show the admirable reproducibility of the experiments (±0.001). When results were examined, it was determined that higher purification was obtained with RG-2 at 160 °C with 99.999%. The highest purification levels for RG-1, RG-3, RG-4, RG-5, and RG-6 gases were obtained as 99.66% (160 °C), 99.561% (180 °C), 99.890% (160 °C), 99.389% (160 °C), and 98.821% (180 °C), respectively.

When CO_2 and CO are present in the gas stream, the CO effect is more significant than the CO_2. The reason may occur the rapid and more considerable CO adsorption kinetics in the gas phase [227].

Table 5.1 Purification grades of H_2 purified from reformate gas mixture

Temperature (°C)	**RG-1 (%)**	**RG-2 (%)**	**RG-3 (%)**	**RG-4 (%)**	**RG-5 (%)**	**RG-6 (%)**
140	99.309	99.742	99.212	99.674	99.326	98.574
150	99.651	99.916	99.163	99.829	99.338	98.594
160	99.660	99.999	99.216	99.890	99.389	98.647
170	99.548	99.848	99.527	99.762	99.240	98.681
180	99.527	99.899	99.561	99.776	99.222	98.821

The separation efficiencies were determined according to Equation (25) [236]:

$$\varepsilon_{separation} = \frac{I}{2F(\dot{n}_{H_{2in}}^{anode})} \quad (25)$$

where I is the current (A), F is Faraday's constant as 96468 coulombs/mol, and $\dot{n}$ is the molar flow of H_2 at the inlet of the anode (mol/s). The separation efficiency is directly proportional to the applied current and it is expected that the separation efficiency will increase as the current increases.

The separation efficiency of the RG-1 at 160 °C temperature, corresponding to 0.1 V, was 4.4%, while the efficiency was calculated as 37.7% at 1.4 V voltage. As RG-1 does not contain CO, the catalyst active sites were not covered by CO, and the efficiency increased from 140 °C to 160 °C. The highest separation efficiency was found as 37.7% at 160 °C. However, as explained above, the efficiency decreased after 160 °C to 31.4% and 29.4% at 170° C and 180 °C, respectively. The separation efficiency of RG-1 at various temperatures is shown in Figure 5.13.

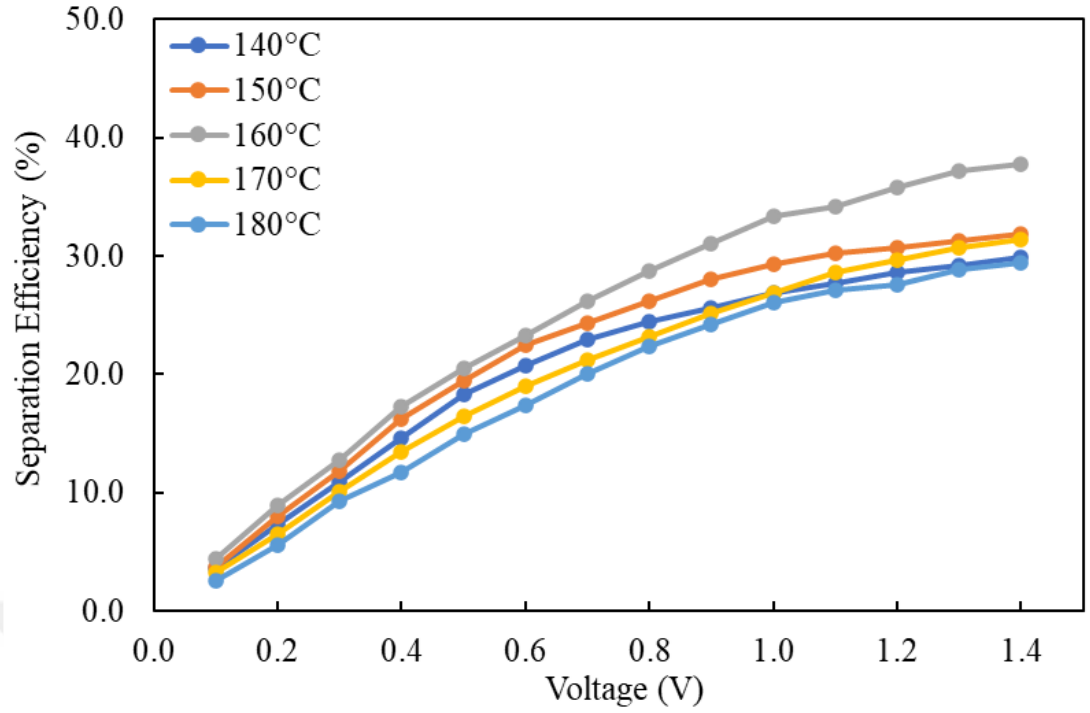

Figure 5.13 Separation efficiencies of HT-ECHC with RG-1 at different operating temperatures

RG-2, RG-3, RG-4 gases contain 2%, 3% and 5% CO, respectively. Since the effect of CO is more dominant than the presence of CO_2, the efficiency decreases as the amount of CO increases in these gases. The highest separation efficiencies for RG-2, RG-3, RG-4 were calculated as 40%, 24% and 22% at 180 °C, respectively. The separation efficiencies of RG-2, RG-3, RG-4 at various temperatures are shown in, Figure 5.14, Figure 5.15 and Figure 5.16, respectively.

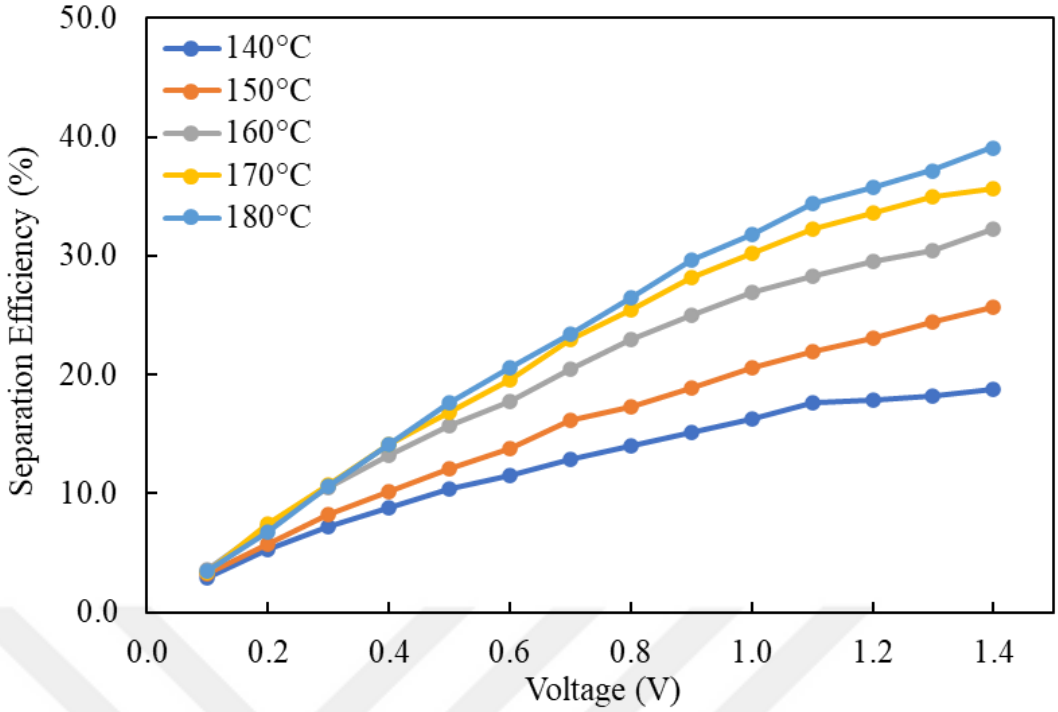

Figure 5.14 Separation efficiencies of HT-ECHC with RG-2 at different operating temperatures

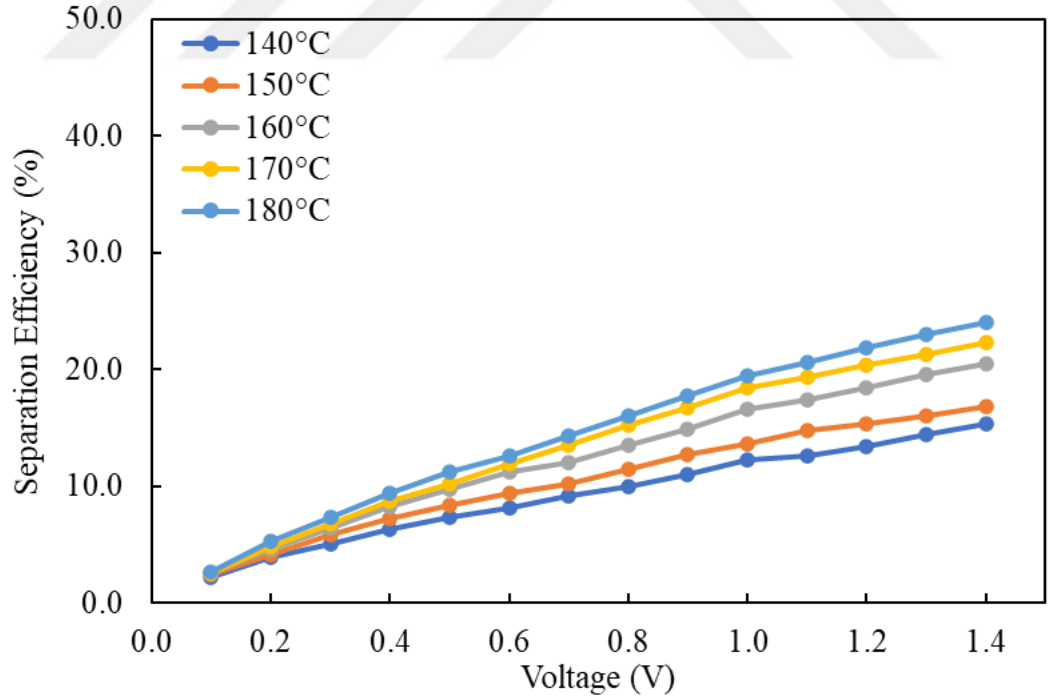

Figure 5.15 Separation efficiencies of HT-ECHC with RG-3 at different operating temperatures

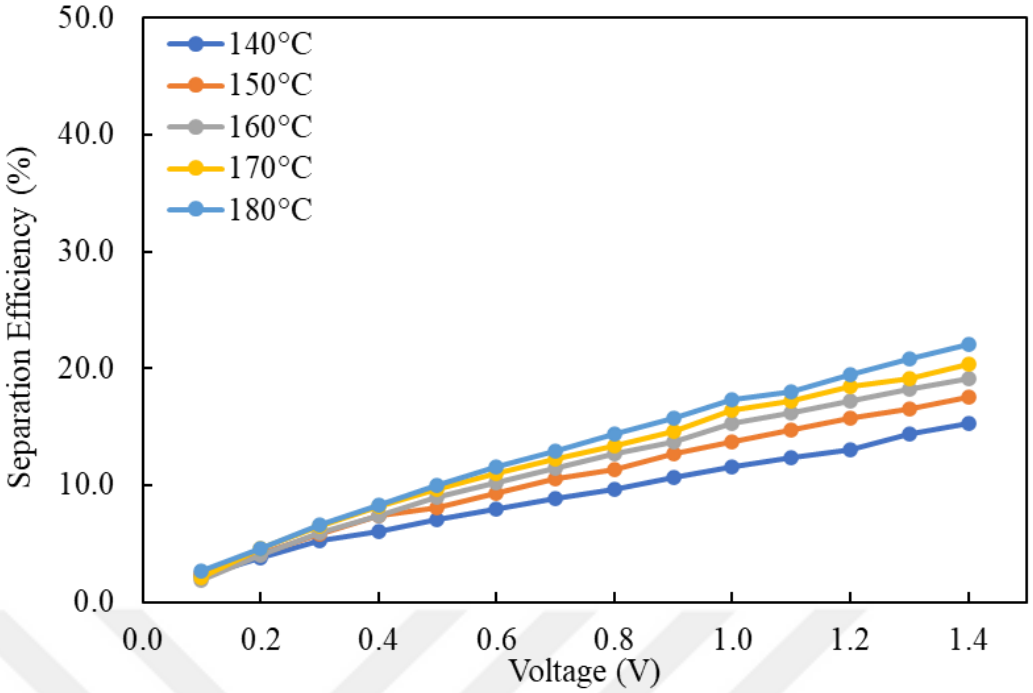

Figure 5.16 Separation efficiencies of HT-ECHC with RG-4 at different operating temperatures

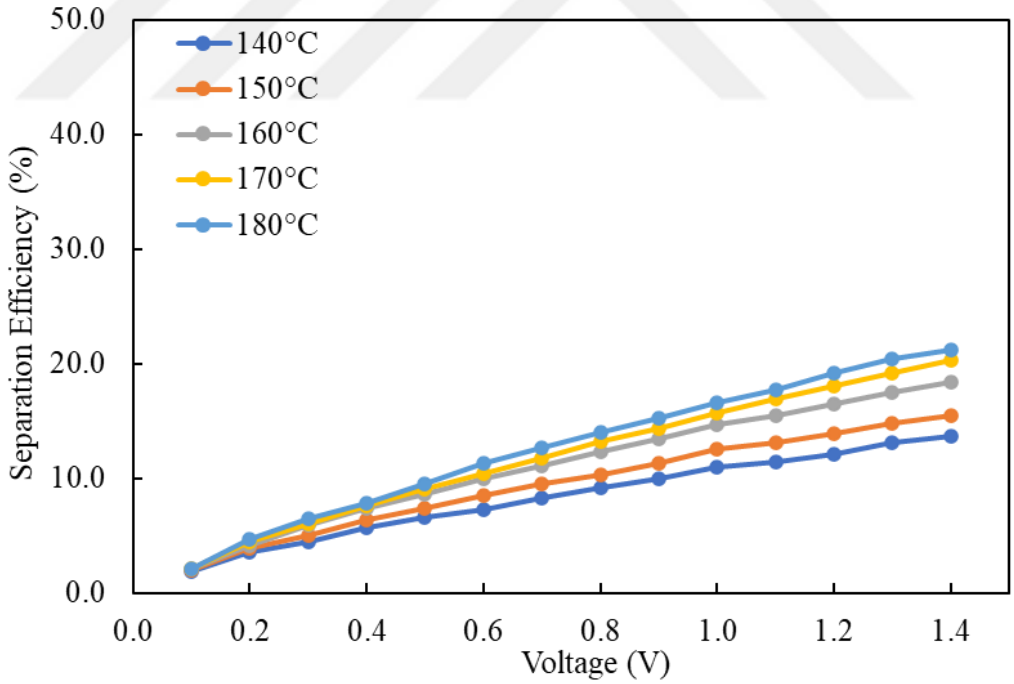

Figure 5.17 Separation efficiencies of HT-ECHC with RG-5 at different operating temperatures

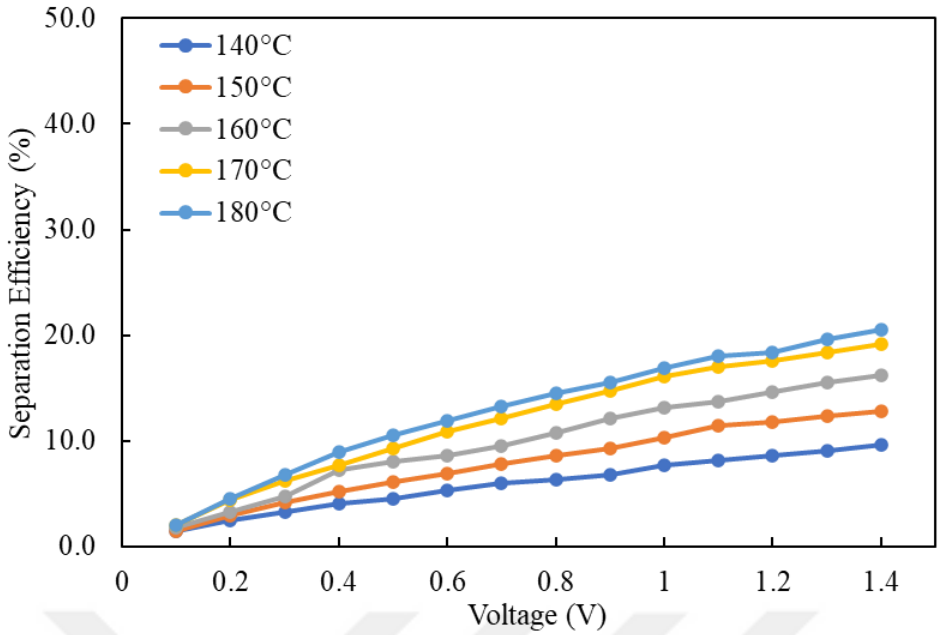

Figure 5.18 Separation efficiencies of HT-ECHC with RG-6 at different operating temperatures

Since RG-5 and RG-6 gases contain 3% and 5% CO, respectively, separation efficiencies are expected to be lower than other reformate gases. The highest separation efficiencies for RG-5 and RG-6 were 21% and 21% at 180 °C, respectively. The separation efficiencies of RG-5 and RG-6 at various temperatures are shown in Figure 5.17 and Figure 5.18.

As a result, it is possible to observe the positive effect of temperature on catalyst poisoning and its direct effect on cell performance. As the molar ratio of CO increased, the separation efficiencies decreased. For RG-1 gas, the highest separation efficiency of 38% was found at 160 °C, in contrast to other CO-containing reformate gases. As the RWGS reaction speeds up as the temperature rises, CO production from CO_2 and catalyst poisoning increase as well. Abdulla et al. [236] claimed that mass transfer through the GDE is one of the most important factors affecting efficiency.

5.3. Compression Results

Compression experiments were conducted with pure H_2. Low-pressure H_2 is fed into the anode flow field. The current-distributing plates receive voltage from the external DC power source. The H_2 molecule is split into two atoms; each oxidized into a proton

H^+ and an e^- at the anode catalyst layer. Only protons pass through the acid-doped PBI membrane before being reduced to H_2 at the cathode catalyst layer with the help of electrons. Under higher pressure, H_2 is collected on the cathode side.

The required power to obtain compressed H_2 at the HT-ECHC cathode is low when compared the conventional compressors. Since the Nernst equation provides the theoretical compression work for the HT-ECHC [126], [128], [134] and uses only a thermodynamic approach based on anodic and cathodic pressures, the theoretical approach is insufficient to account for a phenomenon like the ohmic resistance and some mass transport constraints. Ohmic and mass transport resistances increase with applied voltage, reducing the energy efficiency of an HT-ECHC [57].

The HT-ECHC cell experienced a gas leak test before the performance tests. The anode and cathode compartment exits were closed, and N_2 was gradually fed at 160 °C up to 60 bar. The manometers on the anode and cathode were used to determine whether the pressure in the cell had remained constant for an hour. The cell was considered gas-tight because the anode and cathode pressure gauges display the same bar pressure after 1 hour. The tests were then conducted using H_2 under the same circumstances. Since the best electrochemical H_2 separation performance was found at 160 °C in the previous experiments [168], all compression performance tests were carried out with pure H_2 at this temperature. The cell was first run through the tests in cathode open mode for an hour at a constant 0.4 V. After that, the cathode outlet was closed, and pressurization tests were conducted with a steady supply of H_2. A manometer at the cathode outlet was used to measure the pressure in the HT-ECHC cell, and data were gathered until a total pressure of 60 bar was reached. Then the H_2 valve was closed and the N_2 valves were opened for cleaning. Finally, the HT-ECHC cell temperature was lowered to room temperature.

The polarization curve of the HT-ECHC fed with H_2 in the open cathode condition at 160 °C is shown in Figure 5.19. When the obtained result was examined, 61.2 A was recorded as the highest current at 160 °C.

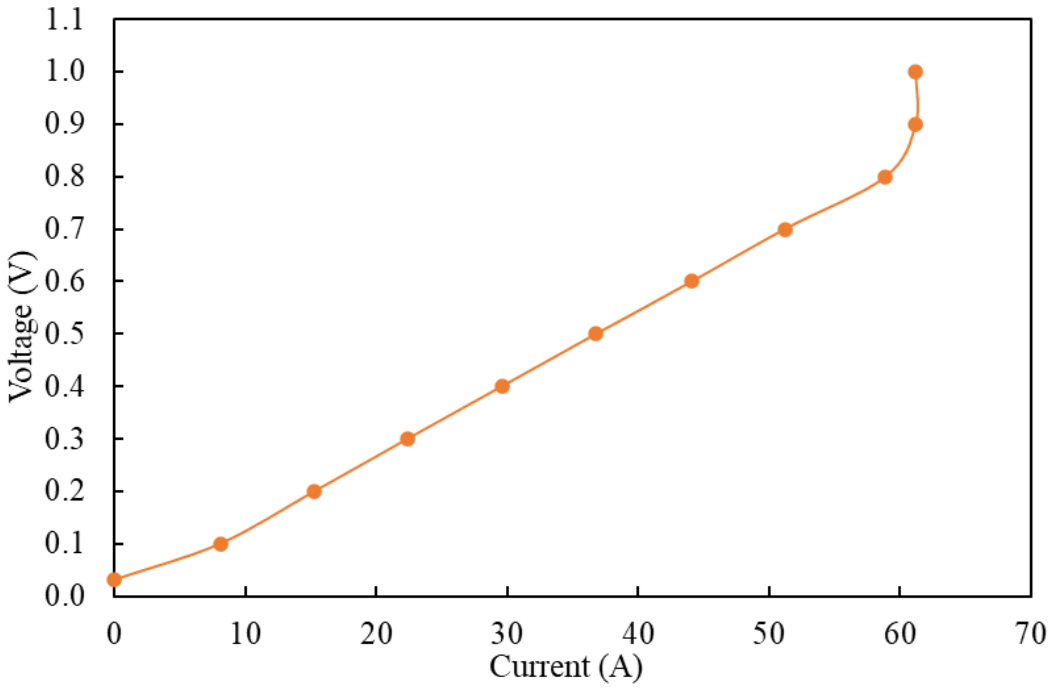

Figure 5.19 HT-ECHC polarization curves at 160 °C for open cathode

The time variation of the cathode pressure at different voltages is shown in Figure 5.20. The minimum voltage required for a $P_{cathode}$ compression of 10, 30, 40, and 50 bar can be calculated as 0.030, 0.051, 0.056, and 0.060 V, respectively, using the Nernst Equation at 160 °C. In experimental studies, this equation is insufficient. When the results were examined, it was discovered that operating voltages of 0.1, 0.2, 0.4, 0.6, 0.8, 1, 1.3, and 1.5 V, respectively, were used to achieve pressures of 10, 14, 22, 30, 36, and 38, 50, and 60 bar. The difference between the actual applied voltage and the theoretical applied voltage (E_{Nernst}) increases as the pressure increases. The increased applied voltage is related to the constraints experienced in real-world applications. For instance, in the HT-ECHC system, the pressure differential causes back diffusion of H_2. This overpotential is represented by $E_{Back\ Diffusion}$. The increased H_2 pressure at the cathode causes the H_2 molecules to traverse the membrane from the cathode to the anode [128]. Chouhan et al. [167] measured pressure as 6.84 bar, whereas the estimated pressure for 0.025 V is 7.24 bar. This is explained by the considerable increase in back diffusion in the cathode closed mode, which primarily affects the applied voltage.

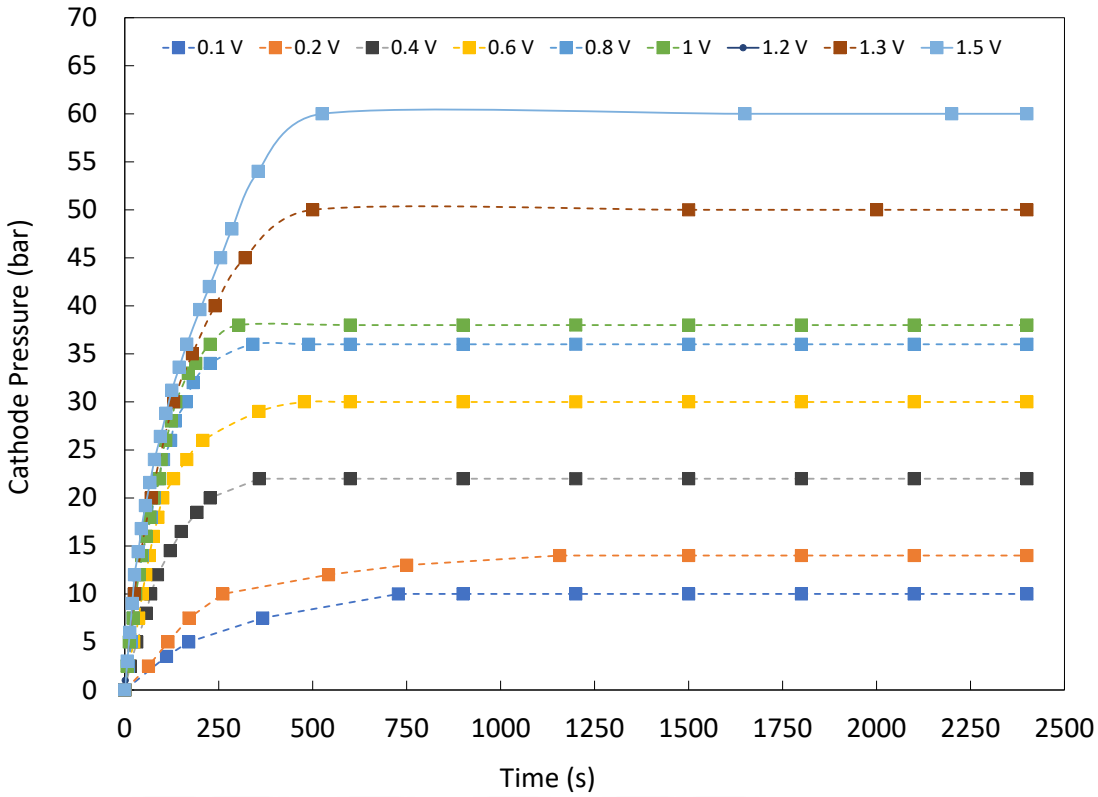

Figure 5.20 The change of cathode pressure of HT-ECHC at 160°C

Due to the equilibrium between H_2 passing from the anode side to the cathode side and H_2 back diffusion from the cathode side to the anode side, high compression pressure could not be achieved at low operating voltages. As demonstrated in Figure 5.20, the applied voltage affects the compression time since the HT-ECHC compression time depends on the cathodic region's compression volume, H_2 flow across the membrane, and the H_2 volume returned to the anode by back diffusion. Pineda-Delgado et al. [170] reported observing a comparable outcome. The HT-ECHC cell required a voltage of 0.1 V and 728 seconds of compression to reach 10 bar. A more significant proton flow to the cathodic side was observed when the voltage was raised to 1.5V. In 525 seconds, the HT-ECHC cell attained its maximum compression pressure of 60 bar.

CHAPTER 6

CONCLUSIONS

Considered a carbon-free energy source, H_2 plays an important role as an energy carrier to provide sustainable and reliable energy. Fossil fuels are currently the primary source to produce H_2. In comparison to some alternatives, fossil fuel-based H_2 production technologies are already sophisticated and mature industrial processes that can generate high-quality H_2 at relatively lower costs. However, the emission of CO and the resulting low-efficiency electrochemical device applications are one of the main problems. To make these applications more efficient, high-purity and compressed H_2 must be made portable and easily accessible. H_2 supply costs have increased significantly due to the challenges associated with H_2 pressurization, such as storage and delivery. Because of the above factors, H_2 pressurization issues get more challenging.

Within the scope of this thesis, H_2 purification and compression studies with HT-ECHC single cell and batch prepared with PA-doped PBI membrane were successfully carried out. Electrochemical H_2 purification performances of acid doped PBI membranes prepared within the scope of the thesis were determined with reformed gas mixtures with different $H_2/CO_2/CO$ compositions. H_2 purification experiments were carried out at operating temperatures of 140-180^oC. Within the scope of the study, besides H_2 purification, H_2 pressurization was also examined. The results obtained in the thesis study are given below:

- Within the scope of the thesis, the first single HT-ECHC cell design was made and H_2 purification tests were performed. As a result of the performance tests, it was determined that 99.99% H_2 purity was reached with the RG-3 reformate gas containing 72% H_2, 26% CO_2 and 2% CO at 160 °C.
- The obtained results show that HT-ECHC operating temperatures and cell voltage directly affect the H_2 purification performance.

- Based on the data obtained as a result of the HT-ECHC single performance tests, the 5-cell HT-ECHC stack was designed and manufactured.
- H_2 has been successfully compressed from atmospheric pressure to 60 bar with the developed HT-ECHC stack without any gas leakage.

Today, H_2 is compressed using stepper mechanical compressors. However, lack of reliability and high maintenance costs are the main problems of traditional H_2 compressors that can compromise an efficient H_2 infrastructure. In mechanical compressor systems, when one of the compressor stages fails or needs maintenance, the entire system is out of use. Despite this, ECHC systems offer a single-stage, quiet and compact compaction system with low maintenance and downtime. In addition, ECHC systems, where H_2 purification can be performed in reformate gas mixtures, will have an important place in the spread of the H_2 economy in the future. The findings indicate that the HT-ECHC system has the potential for use in the future for purifying H_2 produced by fossil fuels. However, they are relatively new technologies, HT-ECHC systems still require much research to be more competitive with traditional technologies. A deeper understanding of electrochemical H_2 compression is needed, particularly regarding H_2 recovery and performance factors like different impurities, temperature, flow rate, etc. Despite all the encouraging advancements, the literature lacks sufficient data and modeling research. Increased research is needed in coated or supported CL materials, composite membranes, flow field geometries, composite GDL materials, and alternative materials that can be employed for more excellent insulation, particularly on the cathode side. The thesis study will also be basic research for the fuel cell integration of ECHC in future research of fuels such as natural gas, biogas, etc. Additionally, cells capable of simultaneously purifying and compressing H_2 can be developed. New design approaches can be explored to enable the performance of both tasks within the same cell. Today, as they are fairly new technologies, a lot of research still needs to be done before ECHC systems can be more competitive with today's traditional technologies.

REFERENCES

[1] P. Fragiacomo and M. Genovese, "Developing a mathematical tool for hydrogen production, compression and storage," *Int J Hydrogen Energy*, vol. 45, no. 35, pp. 17685–17701, Jul. 2020.

[2] "World Energy Outlook 2019 – Analysis - IEA." https://www.iea.org/reports/world-energy-outlook-2019# (accessed Sep. 17, 2020).

[3] J. O. Abe, A. P. I. Popoola, E. Ajenifuja, and O. M. Popoola, "Hydrogen energy, economy and storage: Review and recommendation," *Int J Hydrogen Energy*, vol. 44, no. 29, pp. 15072–15086, Jun. 2019.

[4] H. Nazir *et al.*, "Is the H2 economy realizable in the foreseeable future? Part III: H2 usage technologies, applications, and challenges and opportunities," *Int J Hydrogen Energy*, vol. 45, no. 53, pp. 28217–28239, Oct. 2020.

[5] N. Sazali, "Emerging technologies by hydrogen: A review," *Int J Hydrogen Energy*, vol. 45, no. 38, pp. 18753–18771, Jul. 2020.

[6] M. Ball and M. Wietschel, "The future of hydrogen - opportunities and challenges," *Int J Hydrogen Energy*, vol. 34, no. 2, pp. 615–627, 2009.

[7] A. Ajanovic and R. Haas, "Economic prospects and policy framework for hydrogen as fuel in the transport sector," *Energy Policy*, vol. 123, pp. 280–288, 2018.

[8] D. Gielen, F. Boshell, D. Saygin, M. D. Bazilian, N. Wagner, and R. Gorini, "The role of renewable energy in the global energy transformation," *Energy Strategy Reviews*, vol. 24, pp. 38–50, Apr. 2019.

[9] E. Kötter, L. Schneider, F. Sehnke, K. Ohnmeiss, and R. Schröer, "The future electric power system: Impact of Power-to-Gas by interacting with other renewable energy components," *J Energy Storage*, vol. 5, pp. 113–119, Feb. 2016.

[10] F. Dawood, M. Anda, and G. M. Shafiullah, "Hydrogen production for energy: An overview," *Int J Hydrogen Energy*, vol. 45, no. 7, pp. 3847–3869, Feb. 2020.

[11] J. Liu, X. Duan, Z. Yuan, Q. Liu, and Q. Tang, "Experimental study on the performance, combustion and emission characteristics of a high compression ratio heavy-duty spark-ignition engine fuelled with liquefied methane gas and hydrogen blend," *Appl Therm Eng*, vol. 124, pp. 585–594, Sep. 2017.

[12] N. P. Brandon and Z. Kurban, "Clean energy and the hydrogen economy," *Philosophical Transactions of the Royal Society A: Mathematical, Physical and Engineering Sciences*, vol. 375, no. 2098, Jul. 2017.

[13] C. He, R. Yu, H. Sun, and Z. Chen, “Lightweight multilayer composite structure for hydrogen storage tank,” *Int J Hydrogen Energy*, vol. 41, no. 35, pp. 15812–15816, Sep. 2016.

[14] D. Halm, F. Fouillen, E. Lainé, M. Gueguen, D. Bertheau, and T. van Eekelen, “Composite pressure vessels for hydrogen storage in fire conditions: Fire tests and burst simulation,” *Int J Hydrogen Energy*, vol. 42, no. 31, pp. 20056–20070, Aug. 2017.

[15] K. Mazloomi and C. Gomes, “Hydrogen as an energy carrier: Prospects and challenges,” *Renewable and Sustainable Energy Reviews*, vol. 16, no. 5, pp. 3024–3033, 2012.

[16] F. S. Mirhashemi and H. Sadrnia, “NOX emissions of compression ignition engines fueled with various biodiesel blends: A review,” *Journal of the Energy Institute*, vol. 93, no. 1. Elsevier B.V., pp. 129–151, Feb. 01, 2020.

[17] S. K. Hoekman and C. Robbins, “Review of the effects of biodiesel on NOx emissions,” *Fuel Processing Technology*, vol. 96. Elsevier, pp. 237–249, Apr. 01, 2012.

[18] I. - International Energy Agency, “Global Hydrogen Review 2022,” 2022, Accessed: May 04, 2023. [Online]. Available: www.iea.org/t&c/

[19] R. Kothari, D. Buddhi, and R. L. Sawhney, “Comparison of environmental and economic aspects of various hydrogen production methods,” *Renewable and Sustainable Energy Reviews*, vol. 12, no. 2. Pergamon, pp. 553–563, Feb. 01, 2008.

[20] C. Park, M. Koo, J. R. Woo, B. il Hong, and J. Shin, “Economic valuation of green hydrogen charging compared to gray hydrogen charging: The case of South Korea,” *Int J Hydrogen Energy*, vol. 47, no. 32, pp. 14393–14403, Apr. 2022.

[21] J. Szoplik and P. Muchel, “Using an artificial neural network model for natural gas compositions forecasting,” *Energy*, vol. 263, p. 126001, Jan. 2023.

[22] M. Steinberg and H. C. Cheng, “Modern and prospective technologies for hydrogen production from fossil fuels,” *Int J Hydrogen Energy*, vol. 14, no. 11, pp. 797–820, Jan. 1989.

[23] A. Ersöz, “Investigation of hydrocarbon reforming processes for micro-cogeneration systems,” *Int J Hydrogen Energy*, vol. 33, no. 23, pp. 7084–7094, Dec. 2008.

[24] V. S. Ke Liu, Chunshan Song, *Hydrogen and Syngas Production and Purification Technologies*. 2006. [Online]. Available: http://scholar.google.com/scholar?hl=en&btnG=Search&q=intitle:Kinetics,+catalysis+and+mechanism+of+methane+steam+reforming#0

[25] S. A. Bhat and J. Sadhukhan, “Process Intensification Aspects for Steam Methane Reforming: An Overview,” *AlChe Journal*, vol. 55, no. 2, pp. 408–422, 2009.

[26] J. Yoo, Y. Bang, S. J. Han, S. Park, J. H. Song, and I. K. Song, “Hydrogen production by tri-reforming of methane over nickel-alumina aerogel catalyst,” *J Mol Catal A Chem*, vol. 410, pp. 74–80, Dec. 2015.

[27] A. Ajanovic, M. Sayer, and R. Haas, “The economics and the environmental benignity of different colors of hydrogen,” *Int J Hydrogen Energy*, vol. 47, no. 57, pp. 24136–24154, Jul. 2022.

[28] M. Ji and J. Wang, “Review and comparison of various hydrogen production methods based on costs and life cycle impact assessment indicators,” *Int J Hydrogen Energy*, vol. 46, no. 78, pp. 38612–38635, Nov. 2021.

[29] L. Jiang *et al.*, “Coal decarbonization: A state-of-the-art review of enhanced hydrogen production in underground coal gasification,” *Energy Reviews*, vol. 1, no. 1, p. 100004, Sep. 2022.

[30] A. Midilli, H. Kucuk, M. E. Topal, U. Akbulut, and I. Dincer, “A comprehensive review on hydrogen production from coal gasification: Challenges and Opportunities,” *Int J Hydrogen Energy*, vol. 46, no. 50, pp. 25385–25412, Jul. 2021.

[31] P. Basu, “Design of Biomass Gasifiers,” *Biomass Gasification Design Handbook*, pp. 167–228, Jan. 2010.

[32] D. J. Jovan and G. Dolanc, “Can Green Hydrogen Production Be Economically Viable under Current Market Conditions,” *Energies (Basel)*, vol. 13, no. 6599, pp. 1–16, 2020.

[33] J. P. Viteri, S. Viteri, C. Alvarez-Vasco, and F. Henao, “A systematic review on green hydrogen for off-grid communities –technologies, advantages, and limitations,” *Int J Hydrogen Energy*, Mar. 2023.

[34] S. K. Dash, S. Chakraborty, and D. Elangovan, “A Brief Review of Hydrogen Production Methods and Their Challenges,” *Energies (Basel)*, vol. 16, no. 3, p. 1141, 2023.

[35] “Hydrogen: Clearing Up the Colours - Enapter.” https://www.enapter.com/newsroom/hydrogen-clearing-up-the-colours (accessed Mar. 06, 2023).

[36] A. M. Amin, E. Croiset, and W. Epling, “Review of methane catalytic cracking for hydrogen production,” *Int J Hydrogen Energy*, vol. 36, no. 4, pp. 2904–2935, 2011.

[37] M. Gautier, V. Rohani, and L. Fulcheri, “Direct decarbonization of methane by thermal plasma for the production of hydrogen and high value-added carbon black,” *Int J Hydrogen Energy*, vol. 42, no. 47, pp. 28140–28156, Nov. 2017.

[38] B. Lumbers, J. Barley, and F. Platte, “Low-emission hydrogen production via the thermo-catalytic decomposition of methane for the decarbonisation of iron ore mines in Western Australia,” *Int J Hydrogen Energy*, vol. 47, no. 37, pp. 16347–16361, Apr. 2022.

[39] P. Zhang, W. Laijun, C. Songzhe, and X. Jingming, “Progress of nuclear hydrogen production through the iodine-sulfur process in China,” *Renewable and Sustainable Energy Reviews*, vol. 81, pp. 1802–1812, 2018.

[40] S. Z. Zhiznin, V. M. Timokhov, and A. L. Gusev, “Economic aspects of nuclear and hydrogen energy in the world and Russia *,” *Int J Hydrogen Energy*, vol. 45, pp. 31353–31366, 2020.

[41] M. Yu, K. Wang, and H. Vredenburg, “Insights into low-carbon hydrogen production methods: Green, blue and aqua hydrogen,” *Int J Hydrogen Energy*, vol. 46, no. 41, pp. 21261–21273, Jun. 2021.

[42] A. Boretti, “White is the color of hydrogen from concentrated solar energy and thermochemical water splitting cycles,” *Int J Hydrogen Energy*, vol. 46, no. 39, pp. 20790–20791, Jun. 2021.

[43] A. Boretti, “There are hydrogen production pathways with better than green hydrogen economic and environmental costs,” *Int J Hydrogen Energy*, vol. 46, no. 46, pp. 23988–23995, Jul. 2021.

[44] Q. Yao, M. Dou, Y. Liu, and F. Wu, “High-efficient hydrogen purification through two-dimensional CrI3 membrane via a first-principles calculation,” *Appl Surf Sci*, vol. 529, p. 147024, Nov. 2020.

[45] R. Xu *et al.*, “Ultraselective carbon molecular sieve membrane for hydrogen purification,” *Journal of Energy Chemistry*, vol. 50, pp. 16–24, Nov. 2020.

[46] X. Wu and S. Wu, “Production of high-purity hydrogen by sorption-enhanced steam reforming process of methanol,” *Journal of Energy Chemistry*, vol. 24, no. 3, pp. 315–321, May 2015.

[47] L. Shao, B. T. Low, T. S. Chung, and A. R. Greenberg, “Polymeric membranes for the hydrogen economy: Contemporary approaches and prospects for the future,” *Journal of Membrane Science*, vol. 327, no. 1–2. Elsevier, pp. 18–31, Feb. 05, 2009.

[48] G. N. B. Durmus, C. O. Colpan, and Y. Devrim, “A review on the development of the electrochemical hydrogen compressors,” *J Power Sources*, vol. 494, p. 229743, May 2021.

[49] V. Kalman, J. Voigt, C. Jordan, and M. Harasek, “Hydrogen Purification by Pressure Swing Adsorption : High-Pressure PSA Performance in Recovery from Seasonal Storage,” *Sustainability*, vol. 14, no. 14037, pp. 1–16, 2022.

[50] N. A. Al-Mufachi, N. v. Rees, and R. Steinberger-Wilkens, “Hydrogen selective membranes: A review of palladium-based dense metal membranes,” *Renewable and Sustainable Energy Reviews*, vol. 47, pp. 540–551, 2015.

[51] M. Yáñez, F. Relvas, A. Ortiz, D. Gorri, A. Mendes, and I. Ortiz, “PSA purification of waste hydrogen from ammonia plants to fuel cell grade,” *Sep Purif Technol*, vol. 240, p. 116334, 2020.

[52] J. Xiao, L. Fang, P. Bénard, and R. Chahine, “Parametric study of pressure swing adsorption cycle for hydrogen purification using Cu-BTC,” *Int J Hydrogen Energy*, vol. 43, no. 30, pp. 13962–13974, 2018.

[53] F. Ye, S. Ma, L. Tong, J. Xiao, P. Bénard, and R. Chahine, “Artificial neural network based optimization for hydrogen purification performance of pressure swing adsorption,” *Int J Hydrogen Energy*, vol. 44, no. 11, pp. 5334–5344, Feb. 2019.

[54] W. Tao, S. Ma, J. Xiao, P. Bénard, and R. Chahine, “Simulation and optimization for hydrogen purification performance of vacuum pressure swing adsorption,” *Energy Procedia*, vol. 158, pp. 1917–1923, 2019.

[55] “Hydrogen Gas Purifier | Hydrogen Gas Cryogenic Purifiers.” https://www.abilityengineering.com/project/hydrogen-gas-cryogenic-purifiers/?gclid=EAIaIQobChMIpZ2VlsGk7AIVleF3Ch3ztQRwEAAYASAAEgIAR_D_BwE (accessed Oct. 08, 2020).

[56] G. J. Grashoff, C. E. Pilkington, and C. W. Corti, “Purification of Hydrogen.,” *Platin Met Rev*, vol. 27, no. 4, pp. 157–169, 1983.

[57] M. Rhandi, M. Trégaro, F. Druart, J. Deseure, and M. Chatenet, “Electrochemical hydrogen compression and purification versus competing technologies: Part I. Pros and cons,” *Chinese Journal of Catalysis*, vol. 41, no. 5, pp. 756–769, May 2020.

[58] X. He, “Techno-economic feasibility analysis on carbon membranes for hydrogen purification,” *Sep Purif Technol*, vol. 186, pp. 117–124, Oct. 2017.

[59] C. Zhao, B. Sun, J. Jiang, and W. Xu, “H2 purification process with double layer bcc-PdCu alloy membrane at ambient temperature,” *Int J Hydrogen Energy*, vol. 45, no. 35, pp. 17540–17547, Jul. 2020.

[60] A. D. Kiadehi and M. Taghizadeh, “Fabrication, characterization, and application of palladium composite membrane on porous stainless steel substrate with NaY zeolite as an intermediate layer for hydrogen purification,” *Int J Hydrogen Energy*, vol. 44, no. 5, pp. 2889–2904, 2019.

[61] L. Xiong, S. Liu, and L. Rong, “Fabrication and characterization of Pd/Nb40Ti30Ni30/Pd/porous nickel support composite membrane for hydrogen separation and purification,” *Int J Hydrogen Energy*, vol. 35, no. 4, pp. 1643–1649, Feb. 2010.

[62] D. A. Cooney, J. D. Way, and C. A. Wolden, “A comparison of the performance and stability of Pd/BCC metal composite membranes for hydrogen purification,” *Int J Hydrogen Energy*, vol. 39, no. 33, pp. 19009–19017, Nov. 2014.

[63] P. Rezaee and H. R. Naeij, “Graphenylene–1 membrane: An excellent candidate for hydrogen purification and helium separation,” *Carbon N Y*, vol. 157, pp. 779–787, 2020.

[64] W. Salim and W. S. W. Ho, “Hydrogen purification with CO2-selective facilitated transport membranes,” *Current Opinion in Chemical Engineering*, vol. 21. Elsevier Ltd, pp. 96–102, Sep. 01, 2018.

[65] D. Freund, A. Güngör, and B. Atakan, “Hydrogen production and separation in fuel-rich operated HCCI engine polygeneration systems: Exergoeconomic analysis and comparison between pressure swing adsorption and palladium membrane separation,” *Applications in Energy and Combustion Science*, vol. 13, p. 100108, Mar. 2023.

[66] I. Uehara, “Separation and Purification of Hydrogen,” *Encyclopedia of Life Support Systems*, vol. I, pp. 268–282, 2009.

[67] G. Bernardo, T. Araújo, T. da Silva Lopes, J. Sousa, and A. Mendes, “Recent advances in membrane technologies for hydrogen purification,” *Int J Hydrogen Energy*, vol. 45, no. 12, pp. 7313–7338, Mar. 2020.

[68] John Wiley & Sons, Ed., *Hydrogen and Syngas Production and Purification Technologies - Ke Liu, Chunshan Song, Velu Subramani - Google Kitaplar*. John Wiley & Sons, 2009. Accessed: Mar. 16, 2023. [Online]. Available: https://books.google.com.tr/books?hl=tr&lr=&id=HU2WDwAAQBAJ&oi=fnd&pg=PA357&ots=cpKkVrI7qM&sig=J56ZoQyLHpRXLze2PyeLXaA63Xg&redir_esc=y#v=onepage&q&f=false

[69] L. Schorer, S. Schmitz, and A. Weber, “Membrane based purification of hydrogen system (MEMPHYS),” *Int J Hydrogen Energy*, vol. 44, no. 25, pp. 12708–12714, May 2019.

[70] S. Peramanu, B. G. Cox, and B. B. Pruden, “Economics of hydrogen recovery processes for the purification of hydroprocessor purge and off-gases,” *Int J Hydrogen Energy*, vol. 24, no. 5, pp. 405–424, May 1999.

[71] D. Bastani, N. Esmaeili, and M. Asadollahi, “Polymeric mixed matrix membranes containing zeolites as a filler for gas separation applications: A review,” *Journal of Industrial and Engineering Chemistry*, vol. 19, no. 2, pp. 375–393, 2013.

[72] M. Trégaro, M. Rhandi, F. Druart, J. Deseure, and M. Chatenet, “Electrochemical hydrogen compression and purification versus competing technologies: Part II. Challenges in electrocatalysis,” *Chinese Journal of Catalysis*, vol. 41, no. 5, pp. 770–782, May 2020.

[73] S. A. Grigoriev, I. G. Shtatniy, P. Millet, V. I. Porembsky, and V. N. Fateev, “Description and characterization of an electrochemical hydrogen compressor/concentrator based on solid polymer electrolyte technology,” *Int J Hydrogen Energy*, vol. 36, no. 6, pp. 4148–4155, Mar. 2011.

[74] M. D. Nashchekin, K. B. Minko, and V. I. Artemov, “Numerical analysis of constructive and regime parameter effects on the efficiency of metal hydride systems for hydrogen purification,” *Case Studies in Thermal Engineering*, vol. 14, p. 100485, 2019..

[75] B. A. Talagañis, G. O. Meyer, D. G. Oliva, M. Fuentes, and P. A. Aguirre, “Modeling and optimal design of cyclic processes for hydrogen purification using hydride-forming metals,” *Int J Hydrogen Energy*, vol. 39, no. 33, pp. 18997–19008, Nov. 2014.

[76] G. D. Sandrock and P. D. Goodell, “Cyclic life of metal hydrides with impure hydrogen: Overview and engineering considerations,” *Journal of the Less Common Metals*, vol. 104, no. 1, pp. 159–173, Dec. 1984.

[77] V. I. Artemov, D. O. Lazarev, G. G. Yan’kov, V. I. Borzenko, D. O. Dunikov, and S. P. Malyshenko, “The effect of non-absorbable gas impurities on heat and mass transfer in metal-hydride devices for storage and purification of hydrogen,” *High Temperature 2004 42:6*, vol. 42, no. 6, pp. 987–995, Nov. 2004.

[78] K. D. Modibane, M. Williams, M. Lototskyy, M. W. Davids, Y. Klochko, and B. G. Pollet, “Poisoning-tolerant metal hydride materials and their application for hydrogen separation from CO2/CO containing gas mixtures,” *Int J Hydrogen Energy*, vol. 38, no. 23, pp. 9800–9810, 2013.

[79] G. Sdanghi, G. Maranzana, A. Celzard, and V. Fierro, “Review of the current technologies and performances of hydrogen compression for stationary and automotive applications,” *Renewable and Sustainable Energy Reviews*, vol. 102, pp. 150–170, Mar. 2019.

[80] J. W. Sheffield, K. B. Martin, and R. Folkson, “Electricity and hydrogen as energy vectors for transportation vehicles,” in *Alternative Fuels and Advanced Vehicle Technologies for Improved Environmental Performance: Towards Zero Carbon Transportation*, Elsevier Inc., 2014, pp. 117–137.

[81] H. Liu *et al.*, “Development of a gaseous and solid-state hybrid system for stationary hydrogen energy storage,” *Green Energy & Environment*, vol. 6, no. 4, pp. 528–537, Jun. 2020.

[82] “Hydro-Pac: high pressure gas compressors, pumps and related products.” http://www.hydropac.com/hydrogen-compression.html (accessed Jun. 25, 2020).

[83] S. Arai, H. Miura, F. Application, and P. Data, “E-202404,” 2012

[84] “Examples - Andreas Hofer Hochdrucktechnik.” https://www.hofer-hochdrucktechnik.de/en/products/diaphragm-compressors/examples/ (accessed Jun. 25, 2020).

[85] S. M. Leonard, “Increase reliability of reciprocating hydrogen compressors,” *Hydrocarbon Processing*, vol. 75, no. 1, pp. 67–74, 1996.

[86] N. Shade *et al.*, “Hydrogen Compression Application of the Linear Motor Reciprocating Compressor (LMRC); DOE Hydrogen and Fuel Cells Program FY 2016 Annual Progress Report,” 2016.

[87] D. Markus Mayer, “From prototype to serial production manufacturing hydrogen fuelling stations Cryogenic piston pump Content,” 2014.

[88] G. Petitpas, P. Bénard, L. E. Klebanoff, J. Xiao, and S. Aceves, “A comparative analysis of the cryo-compression and cryo-adsorption hydrogen storage methods,” *Int J Hydrogen Energy*, vol. 39, no. 20, pp. 10564–10584, Jul. 2014.

[89] Y. F. Shmal’ko, A. I. Ivanovsky, M. V. Lototsky, V. I. Kolosov, and D. V. Volosnikov, “Sample pilot plant of industrial metal-hydride compressor,” *Int J Hydrogen Energy*, vol. 24, no. 7, pp. 645–648, Jul. 1999.

[90] G. Sdanghi *et al.*, “A 70 MPa hydrogen thermally driven compressor based on cyclic adsorption-desorption on activated carbon,” *Carbon N Y*, vol. 161, pp. 466–478, May 2020.

[91] G. Hermosilla-Lara, G. Momen, P. H. Marty, B. Le Neindre, and K. Hassouni, “Hydrogen storage by adsorption on activated carbon: Investigation of the thermal effects during the charging process,” *Int J Hydrogen Energy*, vol. 32, no. 10–11, pp. 1542–1553, 2007.

[92] J. Zou *et al.*, “Electrochemical Compression Technologies for High-Pressure Hydrogen: Current Status, Challenges and Perspective,” *Electrochemical Energy Reviews*. 2020.

[93] M. Suermann, T. Kiupel, T. J. Schmidt, and F. N. Büchi, “Electrochemical Hydrogen Compression: Efficient Pressurization Concept Derived from an Energetic Evaluation,” *J Electrochem Soc*, vol. 164, no. 12, pp. F1187–F1195, Aug. 2017.

[94] H. P. B. and J. J. Hoefner, *Reciprocating Compressors:: Operation and Maintenance - Heinz P. Bloch, John J. Hoefner - Google Kitaplar*. 1996. Accessed: Mar. 20, 2023. [Online]. Available: https://books.google.com.tr/books?hl=tr&lr=&id=YMIZus6uRKAC&oi=fnd&pg=PP2&ots=4MofMdeG-T&sig=BI_GoYNbW6v_DRY1up_UPVnyrqw&redir_esc=y#v=onepage&q&f=false

[95] P. K. (Pawan K. Pahwa and G. K. (Gulshan K. Pahwa, *Hydrogen economy*. 2014. Accessed: Mar. 20, 2023. [Online]. Available:

https://books.google.com/books/about/Hydrogen_Economy.html?hl=tr&id=KnizBAAAQBAJ

[96] A. Peschel, "Industrial Perspective on Hydrogen Purification, Compression, Storage, and Distribution," *Fuel Cells*, vol. 20, no. 4, pp. 385–393, Aug. 2020.

[97] S. M. Altukhov, "Diaphragm compressors," *Chemical and Petroleum Engineering*, vol. 3, no. 8, pp. 619–623, 1967.

[98] D. Stolten, *Hydrogen and Fuel Cells: Fundamentals, Technologies and Applications - Google Kitaplar*. John Wiley & Sons, 2010. Accessed: Mar. 20, 2023. [Online]. Available: https://books.google.com.tr/books?hl=tr&lr=&id=-G5vyQqEGQoC&oi=fnd&pg=PR19&ots=sOS0_jN5Jn&sig=3JGc4Jb98aSbDmIpAF67aQtuPbs&redir_esc=y#v=onepage&q&f=false

[99] T. Predel, E. Schlücker, P. Wasserscheid, D. Gerhard, and W. Arlt, "Ionic Liquids as Operating Fluids in High Pressure Applications," *Chem Eng Technol*, vol. 30, no. 11, pp. 1475–1480, Nov. 2007.

[100] M. Armand, F. Endres, D. R. MacFarlane, H. Ohno, and B. Scrosati, "Ionic-liquid materials for the electrochemical challenges of the future," *Nature Materials 2009 8:8*, vol. 8, no. 8, pp. 621–629, Jul. 2009.

[101] C. M. N. R. B. Scott, W. H. Denton, *Technology and Uses of Liquid Hydrogen - Google Kitaplar*. Elsevier, 2013. Accessed: Mar. 20, 2023. [Online]. Available: https://books.google.com.tr/books?hl=tr&lr=&id=y7r9BAAAQBAJ&oi=fnd&pg=PP1&ots=WlR_z-rZ40&sig=CtUiZWC0_NHcK5eafc0WNWjGqhA&redir_esc=y#v=onepage&q&f=false

[102] S. Toghyani, E. Baniasadi, and E. Afshari, "Performance analysis and comparative study of an anodic recirculation system based on electrochemical pump in proton exchange membrane fuel cell," *Int J Hydrogen Energy*, vol. 43, no. 42, pp. 19691–19703, Oct. 2018.

[103] W. Chen, B. Cameron, and S. Narayanan, "A Cryocooler Driven by Electrochemical Compressors with No Moving Parts," in *International Cryocooler Conference*, 2014, pp. 487–496.

[104] G. Sdanghi, G. Maranzana, A. Celzard, and V. Fierro, "Towards non-mechanical hybrid hydrogen compression for decentralized hydrogen facilities," *Energies (Basel)*, vol. 13, no. 12, 2020.

[105] R. K. Ahluwalia *et al.*, "Technical assessment of cryo-compressed hydrogen storage tank systems for automotive applications," *Int J Hydrogen Energy*, vol. 35, no. 9, pp. 4171–4184, May 2010.

[106] Aline Léon, *Hydrogen Technology: Mobile and Portable Applications*. Springer Science & Business Media, 2008. Accessed: Mar. 20, 2023. [Online]. Available:

https://books.google.com.tr/books?id=JuGJHXj_jcwC&lr=&hl=tr&source=gbs_navlinks_s

[107] S. M. Aceves, G. Petitpas, F. Espinosa-Loza, M. J. Matthews, and E. Ledesma-Orozco, “Safe, long range, inexpensive and rapidly refuelable hydrogen vehicles with cryogenic pressure vessels,” *Int J Hydrogen Energy*, vol. 38, no. 5, pp. 2480–2489, Feb. 2013.

[108] “Hydrogen Technology: Mobile and Portable Applications - Google Kitaplar.” https://books.google.com.tr/books?hl=tr&lr=&id=JuGJHXj_jcwC&oi=fnd&pg=PA1&ots=OKCZTvJUoB&sig=qaQLKgopcQ4zoYLK40snHjc1iuE&redir_esc=y#v=onepage&q&f=false (accessed Mar. 20, 2023).

[109] J. Zhang, T. S. Fisher, P. V. Ramachandran, J. P. Gore, and I. Mudawar, “A Review of Heat Transfer Issues in Hydrogen Storage Technologies,” *J Heat Transfer*, vol. 127, no. 12, pp. 1391–1399, Dec. 2005.

[110] M. v. Lototskyy, V. A. Yartys, B. G. Pollet, and R. C. Bowman, “Metal hydride hydrogen compressors: A review,” *Int J Hydrogen Energy*, vol. 39, no. 11, pp. 5818–5851, Apr. 2014.

[111] K. D. Sattler, *Carbon Nanomaterials Sourcebook: Nanoparticles, Nanocapsules, Nanofibers, Nanoporous*. CRC Press, 2016. Accessed: Mar. 20, 2023. [Online]. Available: https://books.google.com.tr/books?hl=tr&lr=&id=wgnYCwAAQBAJ&oi=fnd&pg=PP1&ots=91SGQvpICw&sig=ljgH9Y1pjplZ_SCqMdSDOvz1RxQ&redir_esc=y#v=onepage&q&f=false

[112] F. Zhang, P. Zhao, M. Niu, and J. Maddy, “The survey of key technologies in hydrogen energy storage,” *International Journal of Hydrogen Energy*, vol. 41, no. 33. Elsevier Ltd, pp. 14535–14552, Sep. 07, 2016.

[113] T. Y. Wei, K. L. Lim, Y. S. Tseng, and S. L. I. Chan, “A review on the characterization of hydrogen in hydrogen storage materials,” *Renewable and Sustainable Energy Reviews*, vol. 79. Elsevier Ltd, pp. 1122–1133, Nov. 01, 2017.

[114] R. Moradi and K. M. Groth, “Hydrogen storage and delivery: Review of the state of the art technologies and risk and reliability analysis,” *International Journal of Hydrogen Energy*, vol. 44, no. 23. Elsevier Ltd, pp. 12254–12269, May 03, 2019.

[115] J. Andersson and S. Grönkvist, “Large-scale storage of hydrogen,” *International Journal of Hydrogen Energy*, vol. 44, no. 23. Elsevier Ltd, pp. 11901–11919, May 03, 2019.

[116] N. Bader, R. Zacharia, O. Abdelmottaleb, and D. Cossement, “How the activation process modifies the hydrogen storage behavior of biomass-derived activated carbons,” *Journal of Porous Materials*, vol. 25, no. 1, pp. 221–234, 2018.

[117] J. Purewal *et al.*, “Estimation of system-level hydrogen storage for metal-organic frameworks with high volumetric storage density,” *Int J Hydrogen Energy*, vol. 44, no. 29, pp. 15135–15145, Jun. 2019.

[118] Y. W. Liu, R. J. Wu, P. Yang, T. G. Wang, H. H. Liu, and L. H. Wang, “Parameter study of the injection configuration in a zero boil-off hydrogen storage tank using orthogonal test design,” *Appl Therm Eng*, vol. 109, pp. 283–294, Oct. 2016.

[119] M. Hirscher *et al.*, “Materials for hydrogen-based energy storage – past, recent progress and future outlook,” *J Alloys Compd*, vol. 827, p. 153548, Jun. 2020.

[120] G. A. Eisman, “The application of dow chemical’s perfluorinated membranes in proton-exchange membrane fuel cells,” *NASA, Lewis Research Center, Space Electrochemical Research and Technology (SERT), 1989*, 1989.

[121] P. Bouwman, “Fundamentals of Electrochemical Hydrogen Compression,” in *PEM Electrolysis for Hydrogen Production*, 2015, pp. 269–302.

[122] C. Casati, P. Longhi, L. Zanderighi, and F. Bianchi, “Some fundamental aspects in electrochemical hydrogen purification/compression,” *J Power Sources*, vol. 180, no. 1, pp. 103–113, May 2008.

[123] K. A. Perry, G. A. Eisman, and B. C. Benicewicz, “Electrochemical hydrogen pumping using a high-temperature polybenzimidazole (PBI) membrane,” *J Power Sources*, vol. 177, pp. 478–484, 2008.

[124] S. Toghyani, E. Afshari, and E. Baniasadi, “Parametric study of a proton exchange membrane compressor for electrochemical hydrogen storage using numerical assessment,” *J Energy Storage*, vol. 30, p. 101469, 2020.

[125] Y. M. Hao, H. Nakajima, A. Inada, K. Sasaki, and K. Ito, “Overpotentials and reaction mechanism in electrochemical hydrogen pumps,” *Electrochim Acta*, vol. 301, pp. 274–283, Apr. 2019.

[126] B. Rohland, K. Eberle, R. Ströbel, J. Scholta, and J. Garche, “Electrochemical hydrogen compressor,” *Electrochim Acta*, vol. 43, no. 24, pp. 3841–3846, Aug. 1998.

[127] L. Vermaak, H. W. J. P. Neomagus, and D. G. Bessarabov, “Hydrogen Separation and Purification from Various Gas Mixtures by Means of Electrochemical Membrane Technology in the Temperature Range 100 – 160 ◦ C,” *Membranes (Basel)*, vol. 11, no. 4, p. 282, 2021.

[128] R. Ströbel, M. Oszcipok, M. Fasil, B. Rohland, L. Jörissen, and J. Garche, “The compression of hydrogen in an electrochemical cell based on a PE fuel cell design,” *J Power Sources*, vol. 105, no. 2, pp. 208–215, Mar. 2002.

[129] Venugopalan G et . al, “Electrochemical Pumping for Challenging Hydrogen Separations,” *ACS Energy Lett*, vol. 7, pp. 1322–1329, 2022.

[130] A. Chouhan, U. R. Aryal, B. Bahar, and A. K. Prasad, “Analysis of an electrochemical compressor stack,” *Int J Hydrogen Energy*, vol. 45, no. 56, pp. 31452–31465, Nov. 2020.

[131] P. J. Bouwman, “Advances in Electrochemical Hydrogen Compression and Purification,” *ECS Trans*, vol. 47, no. 57, pp. 24179-24193, Aug. 2016.

[132] D. Marciu, A. Kova, and M. Firak, “Electrochemical hydrogen compressor : Recent progress and challenges,” *Int J Hydrogen Energy*, vol. 45, no. 56, pp. 31452–31465, Nov. 2020.

[133] P. Bouwman, “Electrochemical Hydrogen Compression (EHC) solutions for hydrogen infrastructure,” *Fuel Cells Bulletin*, vol. 2014, no. 5, pp. 12–16, May 2014.

[134] M. Bampaou, K. D. Panopoulos, A. I. Papadopoulos, P. Seferlis, and S. Voutetakis, “An electrochemical hydrogen compression model,” *Chem Eng Trans*, vol. 70, no. 1, pp. 1213–1218, 2018.

[135] N. V Dale, M. D. Mann, H. Salehfar, A. M. Dhirde, and T. Han, “Modeling and analysis of electrochemical hydrogen compression,” in *The NHA Annual Hydrogen Conference 2008*, 2008.

[136] K. C. Neyerlin, W. Gu, J. Jorne, and H. A. Gasteiger, “Study of the Exchange Current Density for the Hydrogen Oxidation and Evolution Reactions,” *J Electrochem Soc*, vol. 154, no. 7, p. B631, 2007.

[137] A. Chouhan, B. Bahar, and A. K. Prasad, “Effect of back-diffusion on the performance of an electrochemical hydrogen compressor,” *Int J Hydrogen Energy*, vol. 45, no. 19, pp. 10991–10999, Apr. 2020.

[138] A. Huth, B. Schaar, and T. Oekermann, “A ‘proton pump’ concept for the investigation of proton transport and anode kinetics in proton exchange membrane fuel cells,” *Electrochim Acta*, vol. 54, no. 10, pp. 2774–2780, Apr. 2009.

[139] “Direct High Pressure Hydrogen Production: a Laboratory Scale PEM Electrolyser Prototype. ECS Transactions | 10.1149/1.3142786.” https://sci-hub.se/10.1149/1.3142786 (accessed Oct. 21, 2022).

[140] Wong, “United States US,” Patent Application Publication, 2004.

[141] D. G. DE-FG02-05ER84220 and A. P. C. C104, “Electrochemical Hydrogen Compressor,” 2006. https://www.osti.gov/servlets/purl/883089-bUAbLO/ (accessed Jan. 24, 2021).

[142] Peter Jaime Bouwman, “Advances in Electrochemical Hydrogen Compression and Purification,” *ECS Trans*, vol. 75, no. 14, pp. 503–510, 2016.

[143] H. K. Lee, H. Y. Choi, K. H. Choi, J. H. Park, and T. H. Lee, “Hydrogen separation using electrochemical method,” *J Power Sources*, vol. 132, no. 1–2, pp. 92–98, 2004.

[144] B. Ibeh, C. Gardner, and M. Ternan, “Separation of hydrogen from a hydrogen/methane mixture using a PEM fuel cell,” *Int J Hydrogen Energy*, vol. 32, no. 7, pp. 908–914, May 2007.

[145] C. L. Gardner and M. Ternan, “Electrochemical separation of hydrogen from reformate using PEM fuel cell technology,” *J Power Sources*, vol. 171, no. 2, pp. 835–841, 2007.

[146] K. Onda, T. Araki, K. Ichihara, and M. Nagahama, “Treatment of low concentration hydrogen by electrochemical pump or proton exchange membrane fuel cell,” *J Power Sources*, vol. 188, no. 1, pp. 1–7, Mar. 2009.

[147] M.-T. Nguyen, S. A. Grigoriev, A. A. Kalinnikov, A. A. Filippov, • P Millet, and • V N Fateev, “Characterisation of a electrochemical hydrogen pump using electrochemical impedance spectroscopy,” *J Appl Electrochem*, vol. 41, pp. 1033–1042, 2011.

[148] B. Yang, A. Manohar, G. K. S. Prakash, W. Chen, and S. R. Narayanan, “Anhydrous proton-conducting membrane based on poly-2-vinylpyridinium dihydrogenphosphate for electrochemical applications,” *Journal of Physical Chemistry B*, vol. 115, no. 49, pp. 14462–14468, Dec. 2011.

[149] S. J. Kim *et al.*, “Characterizations of polybenzimidazole based electrochemical hydrogen pumps with various Pt loadings for H2/CO2 gas separation,” *Int J Hydrogen Energy*, vol. 38, no. 34, pp. 14816–14823, Nov. 2013.

[150] X. Wu, G. He, L. Yu, and X. Li, “Electrochemical hydrogen pump with speek/CrPSSA semi-interpenetrating polymer network proton exchange membrane for H2/CO2 separation,” *ACS Sustain Chem Eng*, vol. 2, no. 1, pp. 75–79, Jan. 2014.

[151] Y. M. Hao, H. Nakajima, H. Yoshizumi, A. Inada, K. Sasaki, and K. Ito, “Characterization of an electrochemical hydrogen pump with internal humidifier and dead-end anode channel,” *Int J Hydrogen Energy*, 2016.

[152] A. Rico-Zavala *et al.*, “Synthesis and characterization of composite membranes modified with Halloysite nanotubes and phosphotungstic acid for electrochemical hydrogen pumps,” *Renew Energy*, vol. 122, pp. 163–172, Jul. 2018.

[153] G. Sdanghi, J. Dillet, S. Didierjean, V. Fierro, and G. Maranzana, “Feasibility of Hydrogen Compression in an Electrochemical System: Focus on Water Transport Mechanisms,” *Fuel Cells*, vol. 20, no. 3, pp. 370–380, Jun. 2020.

[154] 悠介 藤田 脇田 英延, Hidenobu Wakita, 英延 脇田, 伊藤 靖彦, Yasuhiko Ito, 靖彦 伊藤, 悠介 藤田, Yusuke Fujita, “Electrochemical type hydrogen compression device - JP2018095953A.pdf,” 2018

[155] 貴司 大戸 脇田 英延, Hidenobu Wakita, 英延 脇田, 山本 恵一, Keiichi Yamamoto, 恵一 山本貴司 大戸, Takashi Oto, “Electrochemical type hydrogen pump - JP2019119654A.”

[156] H. W. Norihiko Kawabata, Kazuya Usirokawa, Shinji Yoshino, “Electrochemical hydrogen pump - US10202696B2,” vol. 2, 2019.

[157] R. L. C. James F. McElroy, Arne W. Ballantine, “Method and apparatus for electrochemical compression and expansion of hydrogen in a fuel cell system - US7045233B2,” vol. 2, no. 12, 2006.

[158] Y. O. Kosuke Yamauchi, Takehito Goto, Tomoya Kamata, Yuichi MIKAMI, Tomohiro Kuroha, Atsuo Okaichi, Yoichiro Tsuji, “Membrane electrode assembly of electrochemical device , membrane electrode assembly of fuel cell - US20210005899A1,” vol. 2021, 2021.

[159] 英延 脇田 酒井 修, Osamu Sakai, 修 酒井, 鵜飼 邦弘, Kunihiro Ukai, 邦弘 鵜飼, 脇田 英延, Hidenobu Wakita, “Electrochemical type hydrogen pump - JP2019163521A”

[160] 邹杰鑫, 金依琦, 文曾锟, 邢爽, 王亚军, 李辉王海江, “Composite bipolar plate and electrochemical hydrogen compression device - CN111799483A,” 2020

[161] T. V. Terrance Wong, Francois Girard, “Electrochemical hydrogen compressor - US 2004/0211679 A1,” vol. 1, no. 19, 2004.

[162] A. O. Yuuichi Yakumaru, “Electrochemical hydrogen pump - EP3208880B1,” *J Appl Electrochem*, vol. 41, no. 9, pp. 1033–1042, 2011.

[163] Y. Y. Kunihiro Ukai, “Membrane electrode assembly and electrochemical hydrogen pump -US10480087B2,” vol. 2, 2019.

[164] 김선일, 권혁률장세권, “Electrochemical hydrogen compressor - KR20200086530A,” 2020

[165] M. S. Frano Barbir, Bhaskar Balasubramanian, “Electrochemical hydrogen compressor for electrochemical cell system and method for controlling - US6994929B2,” vol. 2, no. 12, 2006.

[166] L. Lipp, “Electrochemical Hydrogen Compressor - Final scientific/technical report,” pp. 1–41, 2016, [Online]. Available: https://www.osti.gov/biblio/1235441

[167] Ashish Chouhan, “Electrochemical Compression: Performance Evaluation and The Role Of Back-Diffusion,” University of Delaware, 2021.

[168] G. N. B. ¸ Durmus, | C Ozgur Colpan, and | Yılser Devrim, "Investigation of the performance of high-temperature electrochemical hydrogen purification from reformate gases," *Int J Energy Res*, pp. 1–13, Apr. 2022.

[169] G. Venugopalan *et al.*, "Electrochemical Pumping for Challenging Hydrogen Separations," *ACS Energy Lett*, vol. 7, no. 4, pp. 1322–1329, 2022.

[170] J. L. Pineda-Delgado *et al.*, "Effect of relative humidity and temperature on the performance of an electrochemical hydrogen compressor," *Appl Energy*, vol. 311, p. 118617, Apr. 2022.

[171] T. Maiyalagan and S. Pasupathi, "Components for PEM fuel cells: An overview," *Materials Science Forum*, vol. 657, pp. 143–189, 2010.

[172] M. Nordio *et al.*, "Experimental and modelling study of an electrochemical hydrogen compressor," *Chemical Engineering Journal*, vol. 369, pp. 432–442, Aug. 2019.

[173] G. Alberti and M. Casciola, "Solid state protonic conductors, present main applications and future prospects," in *Solid State Ionics*, 2001.

[174] G. A. Eisman, "Proceedings of the Symposium on Diaphragms, Separators, and Ion-Exchange Membranes," in *The physical and mechanical properties of a new perfluorosulfonic acid ionomer for use as a separator/membrane in proton exchange processes*, 1986, p. 297. Accessed: Jul. 09, 2020. [Online]. Available: https://books.google.com.tr/books?hl=tr&lr=&id=CcjrAAAAMAAJ&oi=fnd&pg=PA156&dq=eisman+G+1986+the+physical+and+mechanical&ots=zsk7jSXw13&sig=56BYLOBO1d43j9xap7N8z8kPsLc&redir_esc=y#v=onepage&q=eisman G 1986 the physical and mechanical&f=false

[175] G. E. Kayley Fishel, Guoqing Qian and and B. C. Benicewicz, "Electrochemical Hydrogen Pumping," *High Temperature Polymer Electrolyte Membrane Fuel Cells: Approaches, Status, and Perspectives*, pp. 1–545, 2016.

[176] F. Huang, A. T. Pingitore, and B. C. Benicewicz, "Electrochemical Hydrogen Separation from Reformate Using High-Temperature Polybenzimidazole (PBI) Membranes: The Role of Chemistry," *ACS Sustain Chem Eng*, vol. 8, no. 16, pp. 6234–6242, 2020.

[177] Y. D. Premchand, M. L. Vona, and P. Knauth, "Proton-Conducting Nanocomposites and Hybrid Polymers," in *Nanocomposites*, Boston, MA: Springer US, 2007, pp. 71–117.

[178] C. Gao, M. Hu, L. Wang, and L. Wang, "Synthesis and Properties of Phosphoric-Acid-Doped Polybenzimidazole with Hyperbranched Cross-Linkers Decorated with Imidazolium Groups as High-Temperature Proton Exchange Membranes," *Polymers (Basel)*, vol. 12, no. 515, pp. 1–11, 2020.

[179] M. Thomassen, E. Sheridan, and J. Kvello, "Electrochemical hydrogen separation and compression using polybenzimidazole (PBI) fuel cell technology," *J Nat Gas Sci Eng*, vol. 2, no. 5, pp. 229–234, 2010.

[180] D. Aili *et al.*, "Polybenzimidazole-Based High-Temperature Polymer Electrolyte Membrane Fuel Cells: New Insights and Recent Progress," *Electrochemical Energy Reviews*, 2020.

[181] B. Sezgin, "Modeling Of a High Temperature PEM Fuel Cell," MIDDLE EAST TECHNICAL UNIVERSITY, 2016.

[182] T. Wu, N. Prasetya, and K. Li, "Recent advances in aluminium-based metal-organic frameworks (MOF) and its membrane applications," *Journal of Membrane Science*, vol. 615. Elsevier B.V., p. 118493, Dec. 01, 2020.

[183] D. N. A. Chee, M. A. M. Amin, F. Aziz, J. Jaafar, and A. F. Ismail, "Development of advanced nanocomposite membranes by molecular sieving nanomaterials (zeolite and MOF)," in *Nanocomposite Membranes for Water and Gas Separation*, Elsevier, 2020, pp. 163–198.

[184] H. Iwahara, H. Matsumoto, and K. Takeuchi, "Electrochemical dehumidification using proton conducting ceramics," *Solid State Ion*, vol. 136–137, pp. 133–138, 2000.

[185] L. Q. Le *et al.*, "Proton-conducting ceramic fuel cells: Scale up and stack integration," *J Power Sources*, vol. 482, p. 228868, Jan. 2021.

[186] Y. Kawamura, T. Arita, K. Isobe, W. Shu, and T. Yamanishi, "Enhancement of pumping performance of electrochemical hydrogen pump by modified electrode," *Fusion Engineering and Design*, vol. 83, pp. 625–633, 2008.

[187] W. A. Meulenberg, M. E. Ivanova, J. M. Serra, and S. Roitsch, "Proton-conducting ceramic membranes for solid oxide fuel cells and hydrogen (H2) processing," in *Advanced Membrane Science and Technology for Sustainable Energy and Environmental Applications*, 2011.

[188] J. W. Fergus, "Sealants for solid oxide fuel cells," *Journal of Power Sources*. 2005.

[189] D. Ergun, Y. Devrim, N. Bac, and I. Eroglu, "Phosphoric acid doped polybenzimidazole membrane for high temperature PEM fuel cell," *J Appl Polym Sci*, vol. 124, no. S1, pp. E267–E277, Jun. 2012.

[190] A. M. Lubers, A. W. Drake, D. J. Ludlow, and A. W. Weimer, "Electrochemical hydrogen pumping using a platinum catalyst made in a fluidized bed via atomic layer deposition," *Powder Technol*, vol. 296, pp. 72–78, Aug. 2016.

[191] C. Jackson, L. F. J. M. Raymakers, M. J. J. Mulder, and A. R. J. Kucernak, "Assessing electrocatalyst hydrogen activity and CO tolerance: Comparison of performance obtained using the high mass transport 'floating electrode' technique and in electrochemical hydrogen pumps," *Appl Catal B*, vol. 268, p. 118734, Jul. 2020.

[192] S. J. Kim *et al.*, "Highly active and CO2 tolerant Ir nanocatalysts for H2/CO2 separation in electrochemical hydrogen pumps," *Appl Catal B*, 2014.

[193] X. Wu, J. Benziger, and G. He, “Comparison of Pt and Pd catalysts for hydrogen pump separation from reformate,” *J Power Sources*, 2012.

[194] S. Park, J. W. Lee, and B. N. Popov, “A review of gas diffusion layer in PEM fuel cells: Materials and designs,” *Int J Hydrogen Energy*, vol. 37, no. 7, pp. 5850–5865, Apr. 2012.

[195] M. Lee and X. Huang, “Development of a hydrophobic coating for the porous gas diffusion layer in a PEM-based electrochemical hydrogen pump to mitigate anode flooding,” *Electrochem commun*, vol. 100, pp. 39–42, Mar. 2019.

[196] M. Lee and X. Huang, “An improved hydrophobic coating for the porous gas diffusion layer in a PEM-based electrochemical hydrogen pump to mitigate anode flooding,” *Electrochem commun*, vol. 117, p. 106777, Aug. 2020.

[197] A. Hermann, T. Chaudhuri, and P. Spagnol, “Bipolar plates for PEM fuel cells: A review,” *Int J Hydrogen Energy*, vol. 30, no. 12, pp. 1297–1302, 2005.

[198] R. A. Antunes, M. C. L. De Oliveira, G. Ett, and V. Ett, “Carbon materials in composite bipolar plates for polymer electrolyte membrane fuel cells: A review of the main challenges to improve electrical performance,” *J Power Sources*, vol. 196, no. 6, pp. 2945–2961, 2011.

[199] C. N. Li, F. Q. Ji, G. Yuan, J. G. Wang, D. S. Ren, and G. D. Wang, “Microstructure and mechanical properties of economical dual phase wheel steels based on CSP line with later ultra fast cooling,” *Materials Research Innovations*, vol. 19, pp. S85–S91, 2015.

[200] H. Tawfik, Y. Hung, and D. Mahajan, “Metal bipolar plates for PEM fuel cell-A review,” *J Power Sources*, vol. 163, no. 2, pp. 755–767, 2007.

[201] N. Saadat, H. N. Dhakal, J. Tjong, S. Jaffer, W. Yang, and M. Sain, “Recent advances and future perspectives of carbon materials for fuel cell,” *Renewable and Sustainable Energy Reviews*, vol. 138, no. October 2019, p. 110535, 2021.

[202] R. K. Gautam and A. Kumar, “A review of bipolar plate materials and flow field designs in the all-vanadium redox flow battery,” *J Energy Storage*, vol. 48, no. November 2021, p. 104003, 2022.

[203] S. Pehlivan-Davis, “POLYMER ELECTROLYTE MEMBRANE (PEM) FUEL CELL SEALS DURABILITY,” Loughborough University, 2015.

[204] “VİTON ORING-Properties.” http://www.atilimkaucuk.com/Urunler/VITON-ORING-1323 (accessed Mar. 23, 2023).

[205] “Viton Oring - Egekaucuk.” https://www.egekaucuk.com.tr/viton-oring (accessed Mar. 23, 2023).

[206] “Fuel cell end plate assembly,” US 2005/0095485 A1, Oct. 31, 2003

[207] T. Dey, J. Deshpande, D. Singdeo, and P. C. Ghosh, “Study of PEM Fuel Cell End Plate Design by Structural Analysis Based on Contact Pressure,” *Journal of Energy*, vol. 2019, pp. 1–11, Jan. 2019.

[208] R. Doucet, C. L. Gardner, and M. Ternan, “Separation of hydrogen from hydrogen/ethylene mixtures using PEM fuel cell technology,” *Int J Hydrogen Energy*, vol. 34, no. 2, pp. 998–1007, Jan. 2009.

[209] T. Sakai *et al.*, “Electrochemical hydrogen pumps using Ba doped LaYbO 3 type proton conducting electrolyte,” *Int J Hydrogen Energy*, vol. 38, no. 16, pp. 6842–6847, 2013.

[210] J. Zou *et al.*, “Insights into electrochemical hydrogen compressor operating parameters and membrane electrode assembly degradation mechanisms,” *J Power Sources*, vol. 484, p. 229249, Feb. 2021.

[211] L. E. Khotseng, *Electrocatalysis and Electrocatalysts for a Cleaner Environment ... - Google Kitaplar*. 2022. Accessed: Mar. 30, 2023. [Online]. Available: https://books.google.com.tr/books?hl=tr&lr=&id=J117EAAAQBAJ&oi=fnd&pg=PA3&dq=Recent+Advances+in+Pt-Based+Binary+and+Ternary+Alloy+Electrocatalysts+for+Direct+Methanol+Fuel+Cells&ots=m_1t4i7p3L&sig=NS__rN_Lc-g-L-uR6zjIWoDSQIw&redir_esc=y#v=onepage&q=Recent

[212] T. Gu, W. K. Lee, and J. W. Van Zee, “Quantifying the ‘reverse water gas shift’ reaction inside a PEM fuel cell,” *Appl Catal B*, vol. 56, no. 1-2 SPEC. ISS., pp. 43–50, Mar. 2005.

[213] F. Zhou, S. J. Andreasen, S. K. Kær, and J. O. Park, “Experimental investigation of carbon monoxide poisoning effect on a PBI/H3PO4 high temperature polymer electrolyte membrane fuel cell: Influence of anode humidification and carbon dioxide,” *Int J Hydrogen Energy*, vol. 40, no. 43, pp. 14932–14941, Nov. 2015.

[214] H. Abe, J. Liu, and K. Ariga, “Catalytic nanoarchitectonics for environmentally compatible energy generation,” *Materials Today*, vol. 19, no. 1, pp. 12–18, Jan. 2016.

[215] E. O. Eren, N. Özkan, and Y. Devrim, “Preparation of polybenzimidazole/ZIF-8 and polybenzimidazole/UiO-66 composite membranes with enhanced proton conductivity,” *Int J Hydrogen Energy*, Nov. 2021.

[216] Y. Devrim, H. Devrim, and I. Eroglu, “Polybenzimidazole/SiO2 hybrid membranes for high temperature proton exchange membrane fuel cells,” *Int J Hydrogen Energy*, vol. 41, no. 23, pp. 10044–10052, Jun. 2016.

[217] Y. Devrim, S. Erkan, N. Baç, and I. Eroglu, “Improvement of PEMFC performance with Nafion/inorganic nanocomposite membrane electrode assembly prepared by ultrasonic coating technique,” in *International Journal of Hydrogen Energy*, Nov. 2012, pp. 16748–16758.

[218] “1. Gas Chromatography (GC) : SHIMADZU (Shimadzu Corporation).” https://www.shimadzu.com/an/service-support/technical-support/analysis-basics/fundamentals/gc2.html (accessed Apr. 06, 2023).

[219] S. S. Araya *et al.*, “A comprehensive review of PBI-based high temperature PEM fuel cells,” 2016.

[220] W. Anne Majerus, Fosca Conti, Carsten Korte and D. S. Lehnert, “Thermogravimetric and spectroscopic investigation of the interaction between polybenzimidazole and phosphoric acid,” *Abstract #1510, Honolulu PRiME 2012, © 2012 The Electrochemical Society*, 2012.

[221] Y. Devrim, A. Albostan, and H. Devrim, “Experimental investigation of CO tolerance in high temperature PEM fuel cells,” *Int J Hydrogen Energy*, vol. 43, no. 40, pp. 18672–18681, Oct. 2018.

[222] T. Gu, W. K. Lee, and J. W. van Zee, “Quantifying the ‘reverse water gas shift’ reaction inside a PEM fuel cell,” *Appl Catal B*, vol. 56, no. 1–2, pp. 43–50, Mar. 2005.

[223] M. Nordio, M. Eguaras Barain, L. Raymakers, M. Van Sint Annaland, M. Mulder, and F. Gallucci, “Effect of CO2 on the performance of an electrochemical hydrogen compressor,” *Chemical Engineering Journal*, p. 123647, Dec. 2019.

[224] Q. Li, R. He, J.-A. Gao, J. O. Jensen, and Niels. J. Bjerrum, “The CO Poisoning Effect in PEMFCs Operational at Temperatures up to 200°C,” *J Electrochem Soc*, vol. 150, no. 12, p. A1599, Nov. 2003.

[225] F. A. de Bruijn, D. C. Papageorgopoulos, E. F. Sitters, and G. J. M. Janssen, “The influence of carbon dioxide on PEM fuel cell anodes,” *J Power Sources*, vol. 110, no. 1, pp. 117–124, Jul. 2002.

[226] Q. Li, R. He, J.-A. Gao, J. O. Jensen, and Niels. J. Bjerrum, “The CO Poisoning Effect in PEMFCs Operational at Temperatures up to 200°C,” *J Electrochem Soc*, vol. 150, no. 12, p. A1599, 2003.

[227] T. Smolinka, M. Heinen, Y. X. Chen, Z. Jusys, W. Lehnert, and R. J. Behm, “CO2 reduction on Pt electrocatalysts and its impact on H 2 oxidation in CO2 containing fuel cell feed gas - A combined in situ infrared spectroscopy, mass spectrometry and fuel cell performance study,” *Electrochim Acta*, vol. 50, no. 25-26 SPEC. ISS., pp. 5189–5199, Sep. 2005.

[228] Y. Oono, T. Fukuda, A. Sounai, and M. Hori, “Influence of operating temperature on cell performance and endurance of high temperature proton exchange membrane fuel cells,” *J Power Sources*, vol. 195, no. 4, pp. 1007–1014, 2010.

[229] M. G. H. Al-Tememy and Y. Devrim, “Development of effective bimetallic catalyst for high-temperature PEM fuel cell to improve CO tolerance,” *Int J Energy Res*, vol. 45, no. 2, pp. 3343–3357, Feb. 2021.

[230] S. M. M. Ehteshami and S. H. Chan, “A review of electrocatalysts with enhanced CO tolerance and stability for polymer electrolyte membarane fuel cells,” *Electrochim Acta*, vol. 93, pp. 334–345, Mar. 2013.

[231] G. Postole and A. Auroux, “The poisoning level of Pt/C catalysts used in PEM fuel cells by the hydrogen feed gas impurities: The bonding strength,” *Int J Hydrogen Energy*, vol. 36, no. 11, pp. 6817–6825, 2011.

[232] F. Zhou, S. J. Andreasen, S. K. Kær, and J. O. Park, “Experimental investigation of carbon monoxide poisoning effect on a PBI/H3PO4 high temperature polymer electrolyte membrane fuel cell: Influence of anode humidification and carbon dioxide,” *Int J Hydrogen Energy*, vol. 40, no. 43, pp. 14932–14941, 2015.

[233] R. J. Bellows, E. P. Marucchi-Soos, and D. T. Buckley, “Analysis of Reaction Kinetics for Carbon Monoxide and Carbon Dioxide on Polycrystalline Platinum Relative to Fuel Cell Operation,” *Ind Eng Chem Res*, vol. 35, no. 4, pp. 1235–1242, 1996.

[234] V. F. Valdés-López, T. Mason, P. R. Shearing, and D. J. L. Brett, “Carbon monoxide poisoning and mitigation strategies for polymer electrolyte membrane fuel cells – A review,” *Prog Energy Combust Sci*, vol. 79, p. 100842, Jul. 2020.

[235] C. Molochas and P. Tsiakaras, “Carbon Monoxide Tolerant Pt-Based Electrocatalysts for H2-PEMFC Applications: Current Progress and Challenges,” *Catalysts 2021, Vol. 11, Page 1127*, vol. 11, no. 9, p. 1127, Sep. 2021.

[236] A. Abdulla, K. Laney, M. Padilla, S. Sundaresan, and J. Benziger, “Efficiency of hydrogen recovery from reformate with a polymer electrolyte hydrogen pump,” *AIChE Journal*, vol. 57, no. 7, pp. 1767–1779, 2011.

APPENDICES

A. TYPICAL GC CHROMATOGRAM FOR PURE H_2

SHIMADZU LabSolutions **Analysis Report**

Pure H2

uV

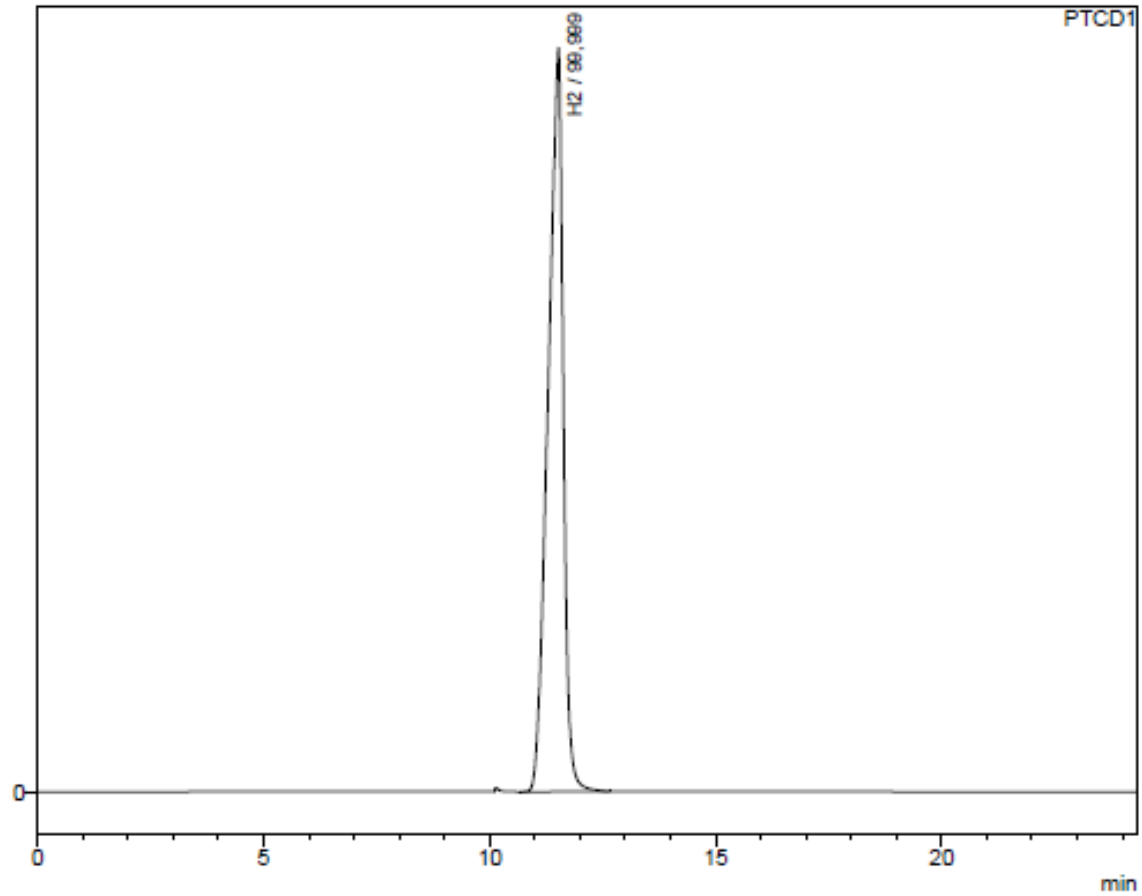

<Peak Table>

PTCD1

Peak#	Ret. Time	Area	Conc.	Unit	Name	Area%
1	11,524	2045325	99,999	%	H2	100,000
Total		2045325				100,000

B. TYPICAL GC CHROMATOGRAM FOR CO_2

SHIMADZU LabSolutions **Analysis Report**

Pure CO2

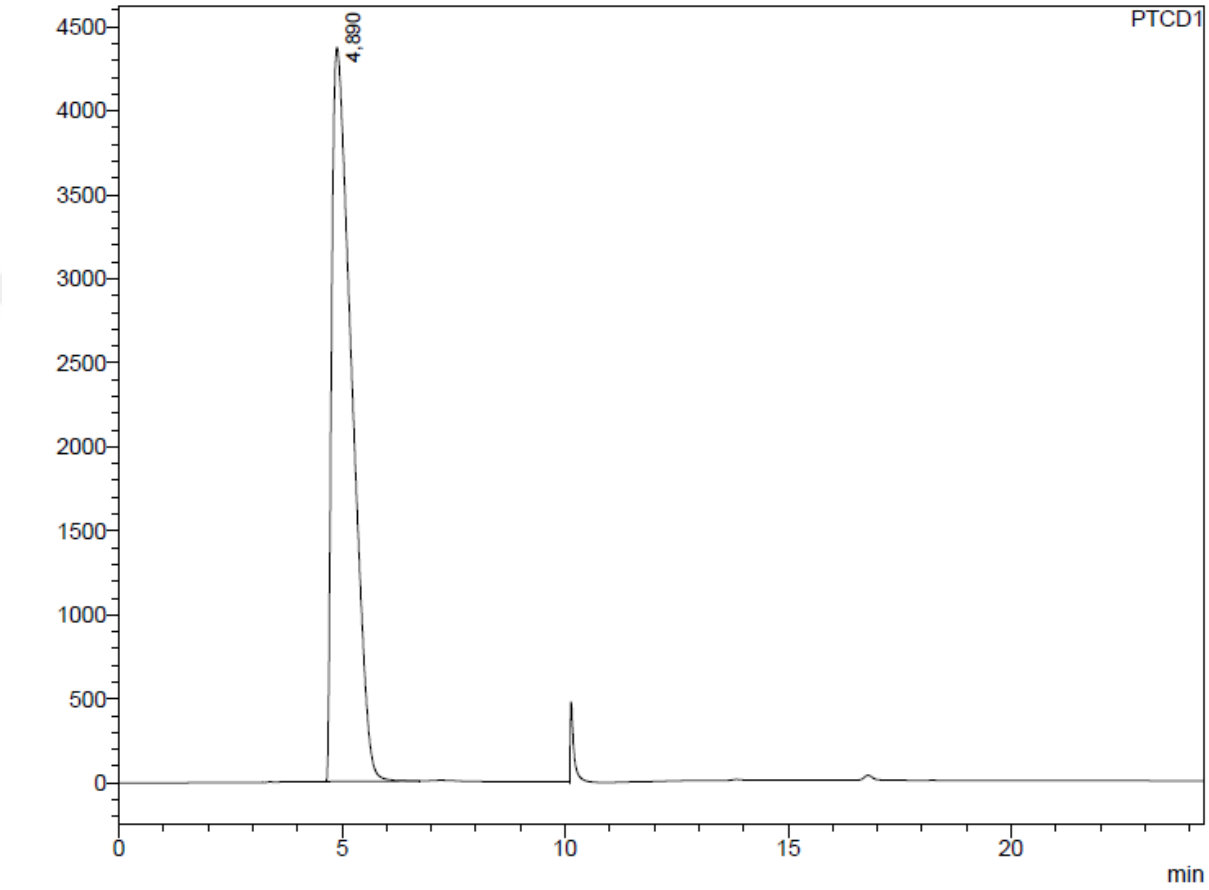

<Peak Table>

PTCD1

Peak#	Ret. Time	Area	Height	Conc.	Unit	Mark	Name
1	4,890	135204	4368	99,523	%		CO2
Total		135204	4368				

C. TYPICAL GC CHROMATOGRAM FOR CO

SHIMADZU LabSolutions **Analysis Report**

Pure CO

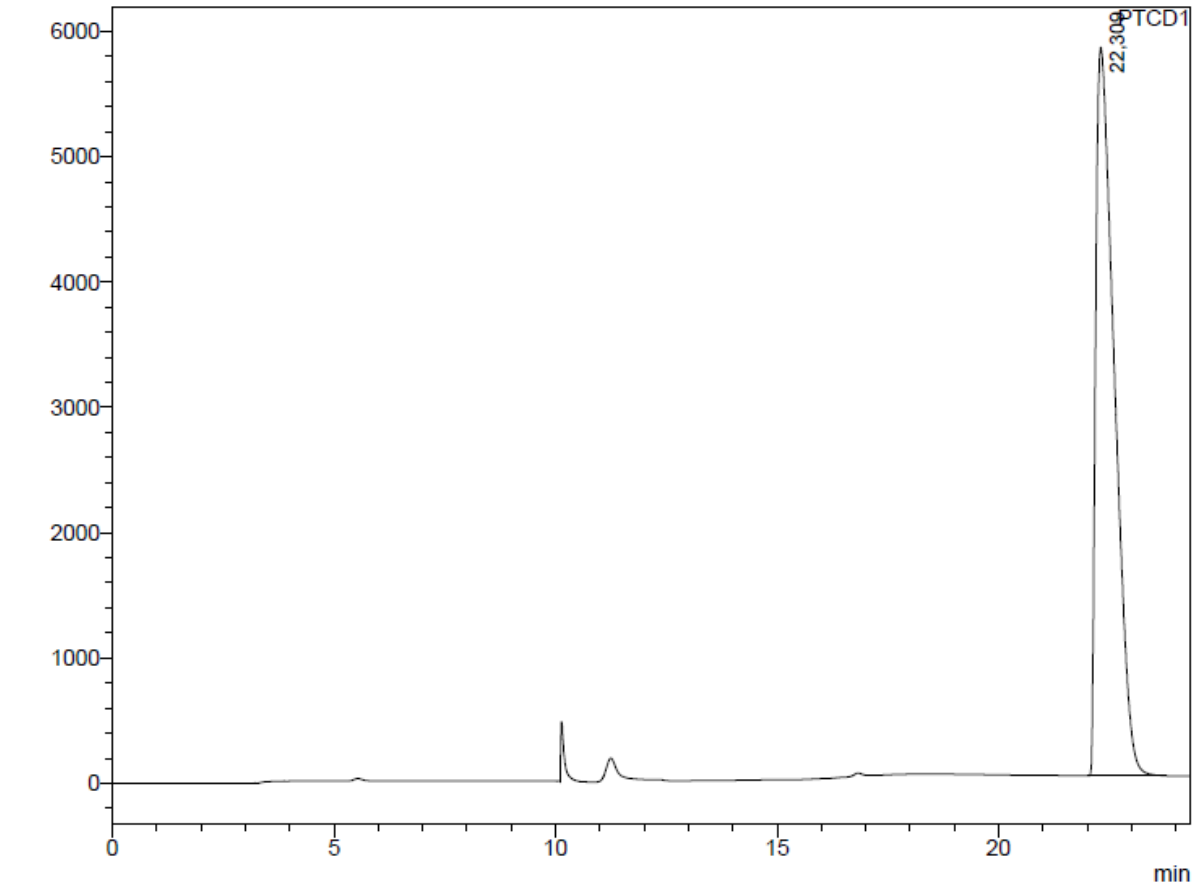

<Peak Table>

PTCD1

Peak#	Ret. Time	Area	Height	Conc.	Unit	Mark	Name
1	22,309	170428	5812	99,796	%		CO
Total		170428	5812				

D. TYPICAL GC CHROMATOGRAM FOR RG-1

SHIMADZU LabSolutions **Analysis Report**

H2 CO2 CO : 75 25 0

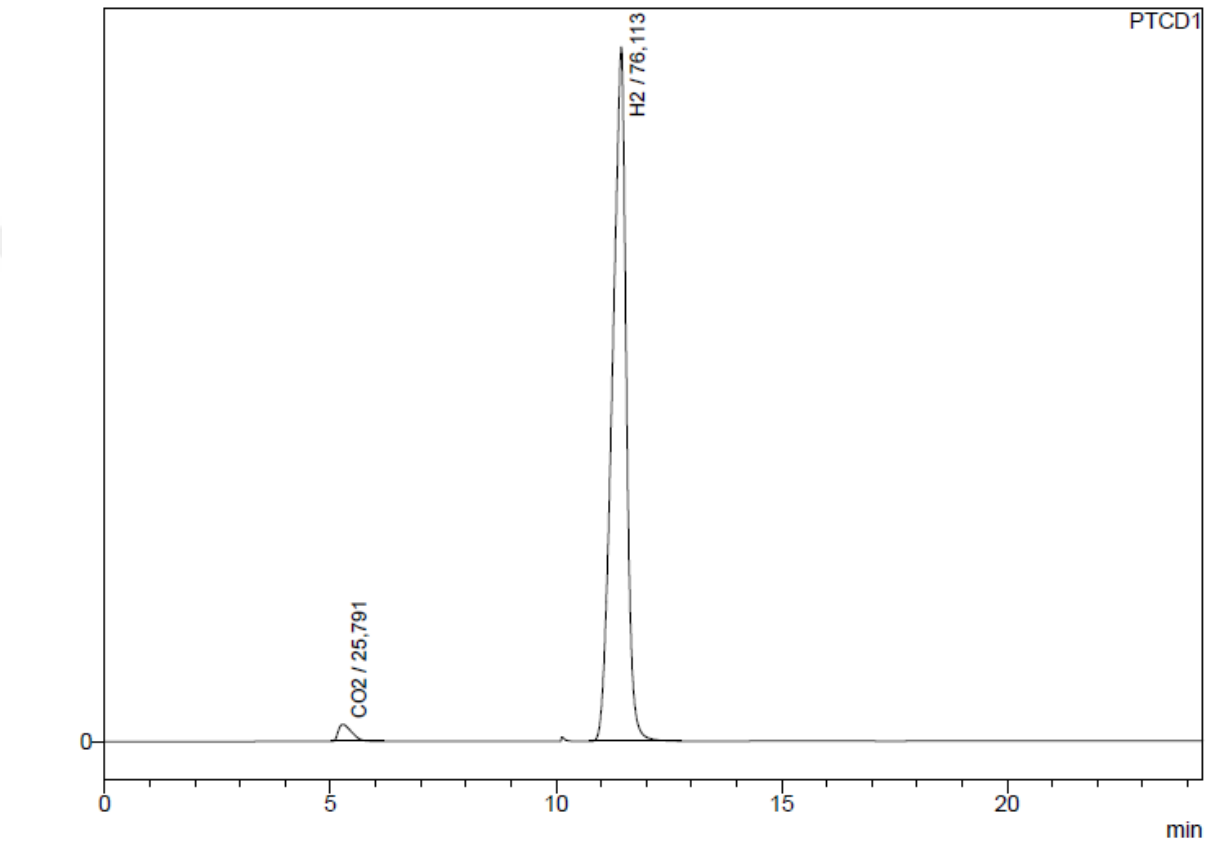

<Peak Table>

PTCD1

Peak#	Ret. Time	Area	Conc.	Unit	Name	Area%
1	5,279	35917	25,791	%	CO2	2,279
2	11,448	1540236	76,113	%	H2	97,721
Total		1576153				100,000

E. TYPICAL GC CHROMATOGRAM FOR RG-2

SHIMADZU LabSolutions **Analysis Report**

H2 CO2 CO : 72 26 2

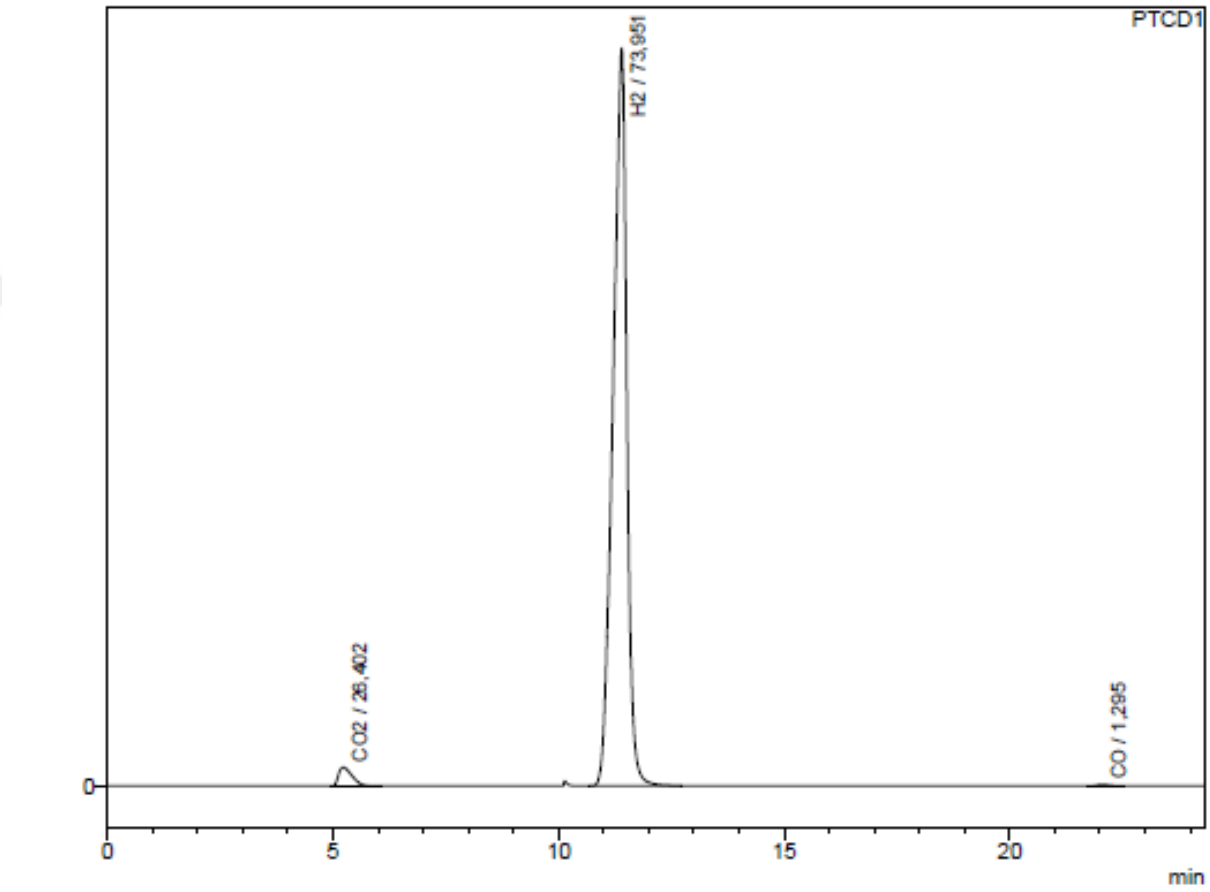

<Peak Table>

PTCD1

Peak#	Ret. Time	Area	Conc.	Unit	Name	Area%
1	5,227	36768	26,402	%	CO2	2,395
2	11,403	1496487	73,951	%	H2	97,460
3	22,061	2237	1,295	%	CO	0,146
Total		1535493				100,000

F. TYPICAL GC CHROMATOGRAM FOR RG-3

SHIMADZU LabSolutions **Analysis Report**

H2 CO2 CO : 75 22 3

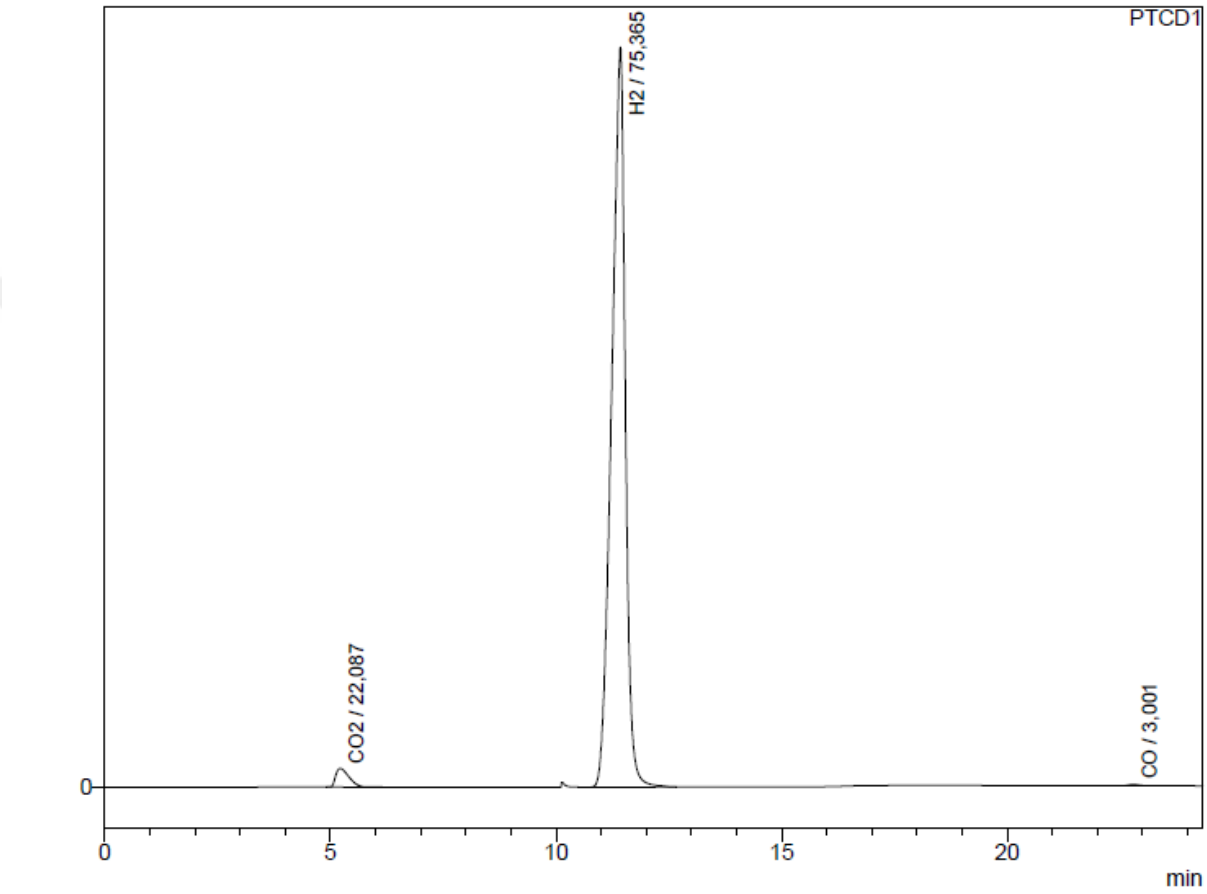

<Peak Table>

PTCD1

Peak#	Ret. Time	Area	Conc.	Unit	Name	Area%
1	5,220	36212	22,087	%	CO2	2,400
2	11,428	1470204	75,365	%	H2	97,452
3	22,796	2221	3,001	%	CO	0,147
Total		1508637				100,000

G. TYPICAL GC CHROMATOGRAM FOR RG-4

SHIMADZU LabSolutions **Analysis Report**

H2 CO2 CO : 75 20 5

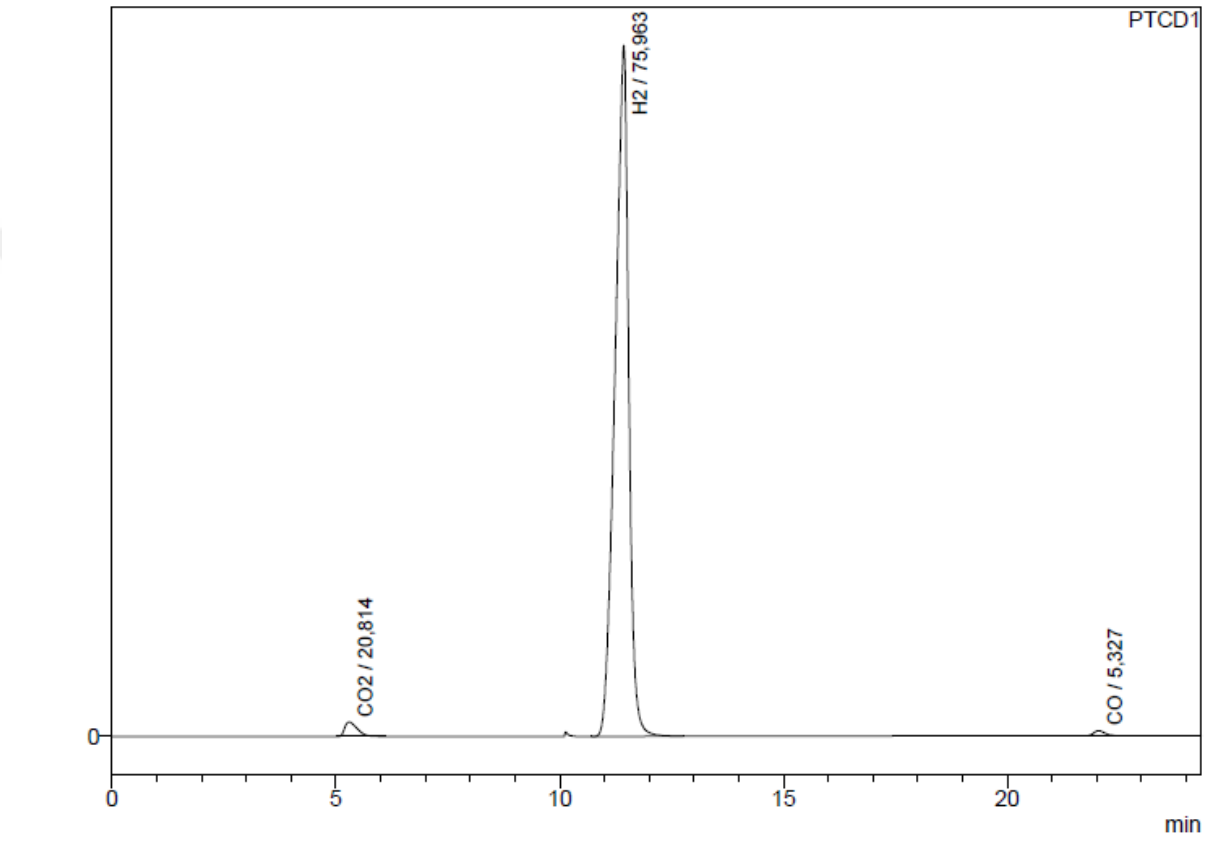

<Peak Table>

PTCD1

Peak#	Ret. Time	Area	Conc.	Unit	Name	Area%
1	5,299	28986	20,814	%	CO2	1,840
2	11,435	1537205	75,963	%	H2	97,576
3	22,042	9207	5,327	%	CO	0,584
Total		1575398				100,000

H. TYPICAL GC CHROMATOGRAM FOR RG-5

SHIMADZU LabSolutions **Analysis Report**

H2 CO2 CO : 97 0 3

uV

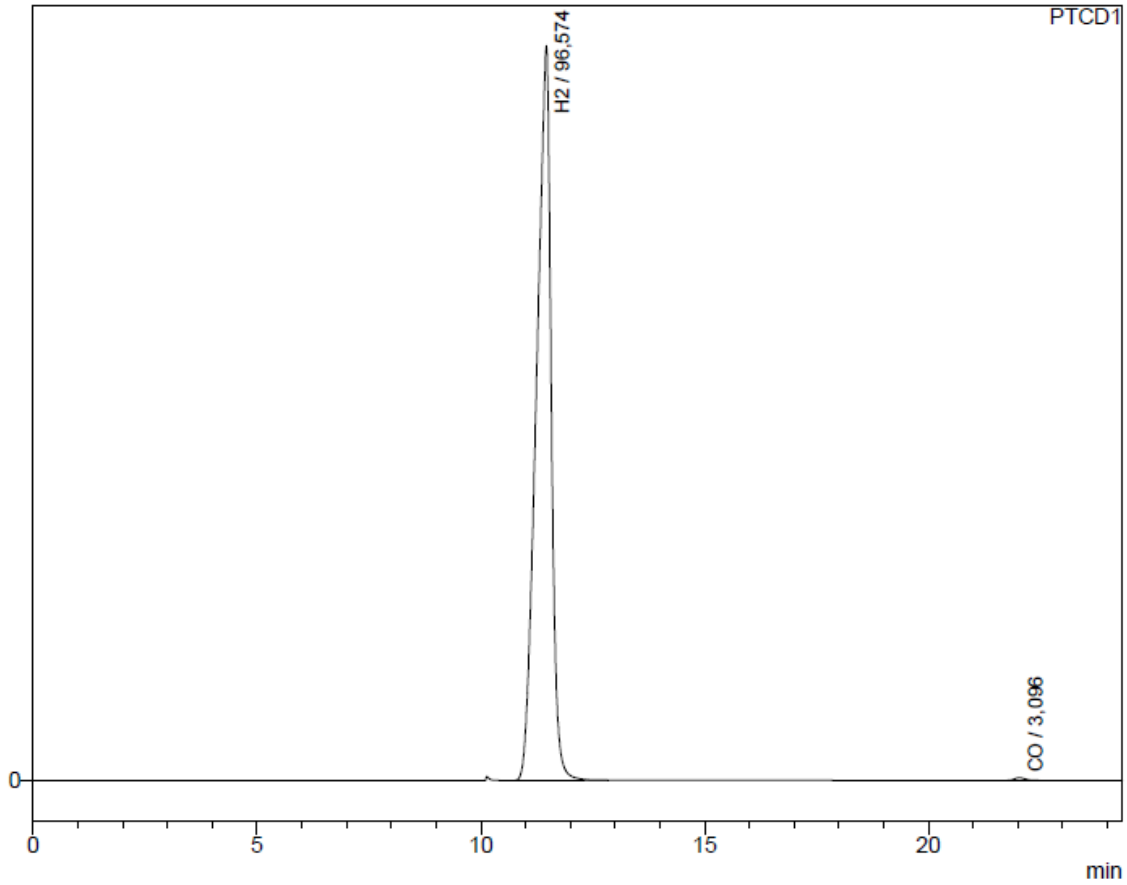

<Peak Table>

PTCD1

Peak#	Ret. Time	Area	Conc.	Unit	Name	Area%
1	11,466	1954276	96,574	%	H2	99,727
2	22,033	5350	3,096	%	CO	0,273
Total		1959626				100,000

I. TYPICAL GC CHROMATOGRAM FOR RG-6

SHIMADZU LabSolutions **Analysis Report**

H2 CO2 CO : 95 0 5

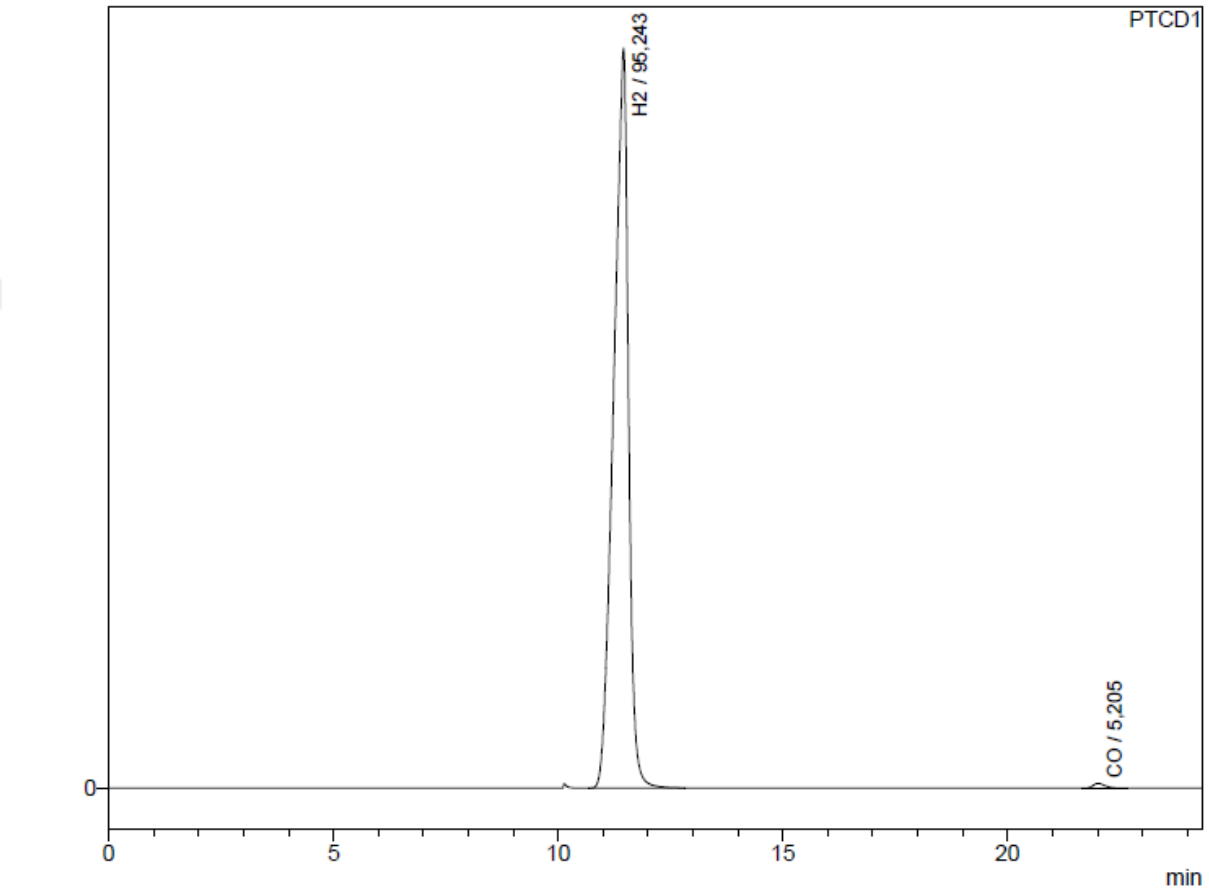

<Peak Table>

PTCD1

Peak#	Ret. Time	Area	Conc.	Unit	Name	Area%
1	11,456	1927341	95,243	%	H2	99,535
2	22,018	8996	5,205	%	CO	0,465
Total		1936337				100,000